Two-Step Overall Water-Splitting Systems Consisting of Stable Oxides

(酸化物を用いた二段階励起水分解システムの構築)

山梨大学大学院

医学工学総合教育部

博士課程学位論文

2017 年 3 月

谷川　聡

Index

1. Introduction

1.1 Background

Huge amount of energy is spent for economic activity. Energy consumption must be increase because population explosion and economic growth. After industrial revolution, energy source of human society is fossil fuel as oil, coal and gas. However, use of huge amount of energy from fossil fuel leads to some issues, air pollution from NOx and SOx and global-warming from heat-trapping gas such as CO_2. These issues are occurred in world wide scale. The oil prospect said to be depletion in 50 to 100 years. Therefore, reduce to depend of fossil fuel is required and change energy source from oil energy to renewable clean energy.

As substitute energy from fossil fuel, renewable energy; wind energy, water energy, solar energy, geothermal energy, biomass etc. is studying all over the world. Especially, solar energy has huge amount of energy. The solar energy irradiated in the earth in 1 hour exceeds the energy human being used in a year. At the same time, hydrogen is attracting a lot of attention as alternative energy of fossil fuel. Hydrogen reacts with oxygen in fuel cell then energy and water are generated. In this reaction, any environmental burden compounds are not generated. However, hydrogen is not being naturally in the earth. Therefore, hydrogen is produced by steam-reforming method or partial oxidation process etc. But these hydrogen production methods use fossil fuel, natural gas and naphtha as raw materials. To solve energy and environmental issues, fossil fuel free hydrogen production by renewable energy is ideal.

Here, photocatalytic material like titania dioxide split water to hydrogen and oxygen with photon which has enough energy to excite electron in valence band to conduction band. [1-4]. Therefore, photocatalysts are attracting attention, because these materials product hydrogen from water and solar light. [1] If these photocatalysts have enough energy harvest, these materials can offer the fundamental solution of energy and environmental issues.

1.2 Mechanism of semiconductor photocatalyst

Figure 1.1 shows the mechanism of photocatalytic reaction of titanium dioxide. [1]

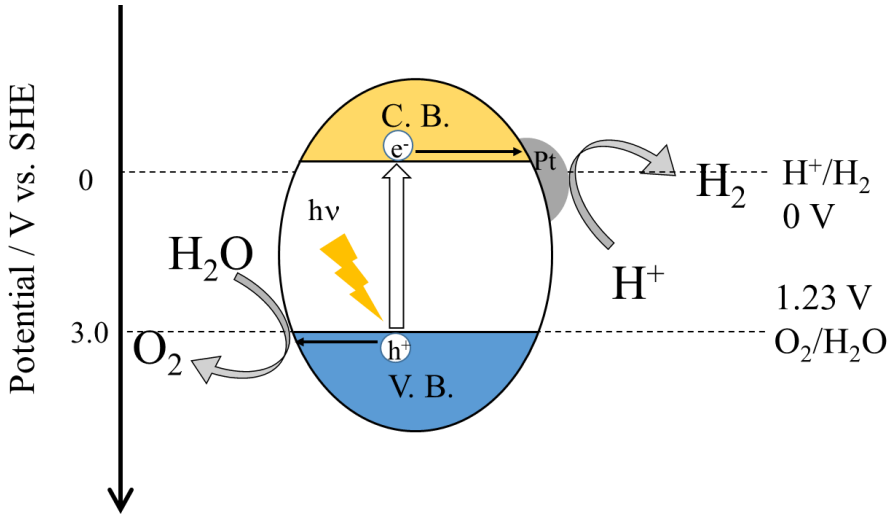

Fig.1.1 The mechanism of photocatalytic reaction of titanium dioxide

Semiconductor has conduction band and valence band these are separated by forbidden band. Electron in valence band excite to conduction band when a photon which has enough energy to over the band-gap is irradiated. Photo-generated electron in conduction band will reduce proton to hydrogen (1). In contrast, photo-generated hole in valence band oxide water to oxygen. (2) Totally photocatalyst produces hydrogen and oxygen from water. (3)

(1) $2H^+ + 2e^- \rightarrow H_2$

(2) $2H_2O \rightarrow O_2 + 4H^+ + 4e^-$

(3) $2H_2O \rightarrow O_2 + 2H_2$

This reaction occurs under these thermodynamic conditions.

1. The light which irradiated to photocatalyst has energy over the band gap.
2. Conduction band bottom is negative to H^+/H_2 oxidation reduction potential to generate hydrogen.
3. Valence band top is positive to O_2/H_2O oxidation reduction potential to generate oxygen.

In Figure 1.1, the scheme of photocatalytic water splitting is shown, and photocatalytic activity is improved by depositing platinum on surface as co-catalyst. In this case, platinum is used as electron trap. Photo-excited electron will be trapped at platinum co-catalyst and it works as reduction site, it passes electron to adsorption. Furthermore, it improves water-splitting activity by reducing backward reaction combination of photo-excited electron and photo-generated hole by trapping photo-excited electrons.

Titanium dioxide has the band gap 3.2 eV, it equals to the wavelength of around 390 nm. From the solar spectrum shown in figure 1.2, ~400 nm of solar light is a few percent of solar light. Therefore, photocatalytic hydrogen production under solar light irradiation required to be visible light sensitive for improve its efficiency.

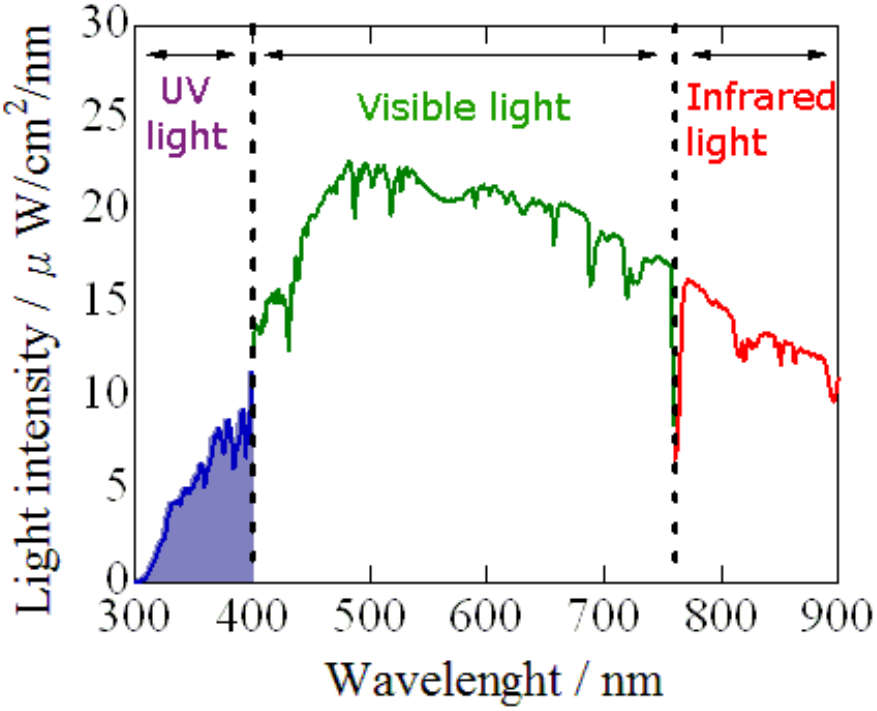

Fig.1.2 Solar spectrum

Generally, visible light is defined as the wavelength is over 400 nm. And the band gap of photocatalyst is calculated by following process.

Photon energy E (eV) is represented by the product of plank constant h and light frequency v.

$$E = h\nu \quad \cdots (1)$$

Light frequency is quotient of light speed c and wavelength λ.

$$\nu = \frac{c}{\lambda} \quad \cdots (2)$$

Equation (3) is gained by substitute equation (2) into equation (1).

$$E = \frac{ch}{\lambda} \quad \cdots (3)$$

Plank constant h is 4.14×10^{15} eVs, light speed c is 3.0×10^{-3} m/s. These constants are substituted into equation (3).

$$E = \frac{4.14\times10^{-15}\times3.0\times10^{8}}{\lambda} = \frac{1240\times10^{-9}}{\lambda} \quad \cdots (4)$$

According from equation (4), the band gap of visible light sensitive photocatalyst is ~3.1 eV.

The valence band top of oxide semiconductor constructed by oxygen 2p orbital is around 3.0 eV. [5] To generate hydrogen from water, conduction band bottom must be negative to 0 V. Therefore, the band gap of oxide photocatalyst is over 3.0 eV. That is the reason that oxide photocatalysts are difficult to use wide visible light region. In contrast, non-oxide photocatalyst is also studied and nitride, sulfide and carbide photocatalysts are developed. [6-7] However, these materials have a problem of stability. Photo-generated holes oxide themselves, then reduce their photocatalytic activities or solve them to the solution. The stability of photocatalysts must be ensured for sustainable energy production from solar light. Oxide photocatalysts are some kinds of ideal material in this regards.

1.3 Previous strategy for visible light sensitization

Two methods are already developed for visible light sensitization of photocatalysts. One is band engineering for one-step excitation, the other is Z-scheme system for two-step excitation.

1.3.1 Band engineering for one-step excitation

Band engineering is a method to control the band structure of a material. Band structure is controlled to narrow the band gap or to form an isolated mini-band in forbidden band by suitable element doping or preparing solid solution.

Valence band top of oxide semiconductor photocatalyst is located around 3.0 V. When conduction band is controlled to use visible light, hydrogen is not generated because conduction band bottom of the material is to be positive to H^+/H_2 oxidation reduction potential. Therefore, valence band control of a material is major for band engineering of oxide materials.

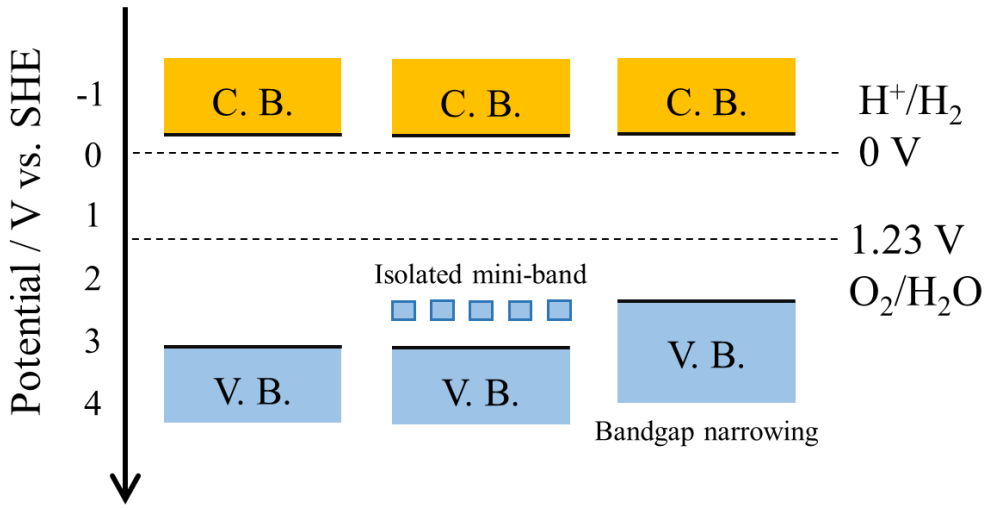

Fig.1.3 Valence band control for visible light sensitization

As for specific method of band structure control

1. Doping a suitable element into a photocatalyst which form an isolated donor mini-band in forbidden band above valence band, or to shift the valence band top to narrow the band gap by constructing mixture orbital with O 2p orbital.
2. Developing a material which have suitable valence band to replace O 2p orbital.

In case 1, it is reported that doping some element which has closed-shell electronic structure like N^{3-}, Ag^{+}, Pb^{2+} form isolated donor mini-band or narrow the band gap. [6, 8] Doping makes photocatalyst absorb wider wavelength light, however, dopant works as recombination center of photo-generated electron and hole. Therefore, suitable amount of doping is required to improve photocatalytic activity.

In case 2, study of developing a material which has suitable valence band is carried out and some materials are developed, for example $BiVO_4$ or $AgNbO_3$ etc. In $BiVO_4$, Bi 6s orbital hybrid to O 2p orbital, then valence band top is shifted to negative. Ag 4d orbital also hybrid to O 2p orbital in $AgNbO_3$, then valence band is shifted and narrowed band gap. [8-9]

Many visible light sensitive photocatalysts are developed and the study of band structure control of photocatalyst is doing hard. However, the number of overall water splitting photocatalyst under visible light irradiation, e.g. GaN-ZnO solid solution, $NiO/AgTa_{0.7}Nb_{0.3}O_3$, $RuO_2/BiYWO_6$, C nano-dot/C_3N_4, and IrO_2/Rh, Sb-$SrTiO_3$, is limited. [2, 10-15]

1.3.2 Z-scheme system for two-step excitation

Conduction band bottom of visible light sensitive oxide photocatalyst is positive to proton reduction potential, because valence band top of oxide semiconductor is located around 3.0 V. Therefore, valence band of photocatalyst which can split water with UV light is controlled to sensitive to visible light in above section. However in a Z-scheme system, a material which cannot generate hydrogen since its positive potential of conduction band bottom compared to hydrogen reduction potential can be used as a part of Z-scheme system. The mechanism of Z-scheme system is shown in Figure 1.4.

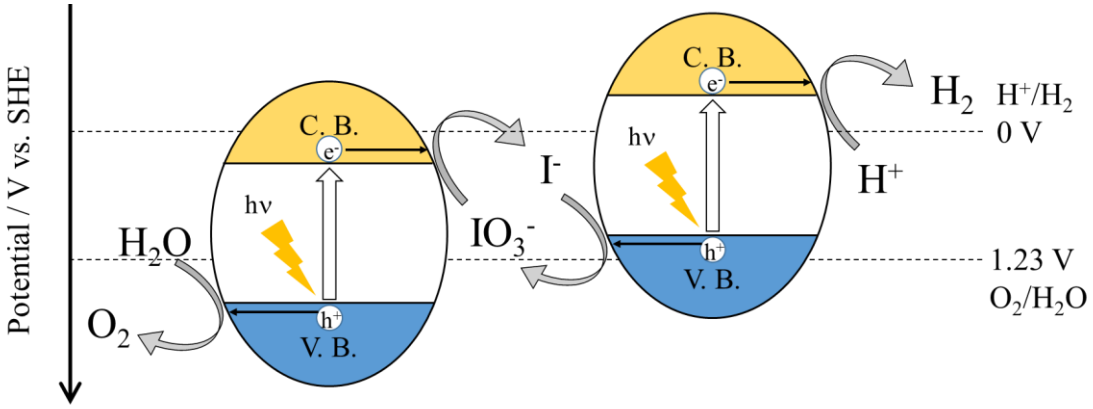

Fig.1.4 Z-scheme system

In a Z-scheme system, oxygen evolution photocatalyst and hydrogen evolution photocatalyst are combined with redox-mediator. Photo-generated hole in oxygen evolution photocatalyst oxidize water to oxygen, and photo-generated electron reduce redox mediator. Reduced redox mediator is oxidized by photo-generated hole in hydrogen evolution photocatalyst. And photo-generated electron in hydrogen evolution photocatalyst reduce proton to hydrogen. Then this system works catalytically. In oxygen evolution photocatalyst, the conduction band bottom potential doesn't have to be negative to proton reduction potential, but the valence band top potential has to be positive to water oxidation potential. In contrast, the valence band top doesn't have to be positive to water oxidation potential, but the conduction band bottom has to be negative to the proton reduction potential in hydrogen evolution photocatalyst. Therefore, photocatalyst with small band gap can be able to use. However, the potential of redox mediator required to be between the potential of conduction band bottom of oxygen evolution photocatalyst and the potential of valence band top of hydrogen evolution photocatalyst. Therefore, Fe^{3+}/Fe^{2+} (0.77 V) and IO_3^-/I^- (0.67 V) are widely used as redox mediator for their redox potential. [16-19]

Merit of this system is can be able to use a photocatalyst which has only hydrogen evolution activity or oxygen evolution activity, therefore wider range of photocatalysts can be employed for water splitting reaction. For example, overall water splitting was

carried out by platinum deposited tungsten oxide (Pt/WO_3) as oxygen evolution photocatalyst and platinum deposited chromium and tantalum co-doped strontium titanate ($Pt/Cr,Ta\text{-}SrTiO_3$) as hydrogen evolution photocatalyst with I^-/IO_3^- redox mediator. [16] However, poor charge transfer efficiency of redox mediator proceeding backward reactions, reduction redox mediator on hydrogen evolution photocatalyst, oxidation redox mediator on oxygen evolution photocatalyst, and recombination of photo-generated electron and hole, is an example of demerit.

1.4 Objective of this study

The objective of this study is constructing Z-scheme system using stable oxides under visible light irradiation. To archive this objective, band structure control and Z-scheme system mechanism were employed. First, band structures of stable oxides were controlled to be sensitive to visible light then visible light sensitive hydrogen evolution photocatalyst and oxygen evolution photocatalyst were prepared. Next, construct Z-scheme system by these band-controlled stable oxide-based photocatalysts to split water under visible light irradiation. (Figure 1.5)

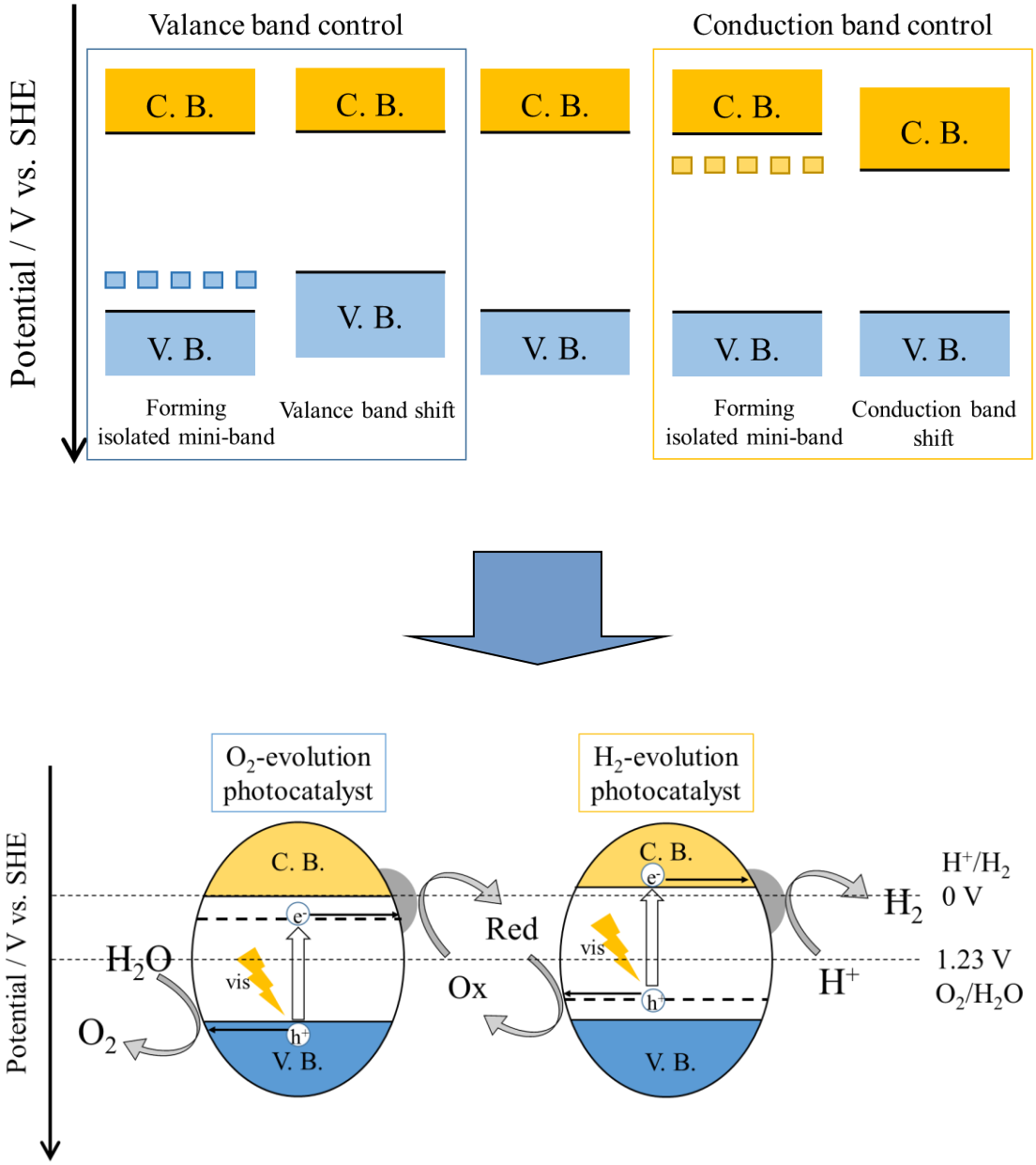

Fig.1.5 Band structure control and construct Z-scheme system

As base material, titanium dioxide was employed because this material was well known as its stability, naturally abundant and high activity. Strontium titanate was also well known as almost same properties. In this study first titanium dioxide was employed as base materials for constructing Z-scheme system.

References

[1] A. Fujishima, K. Honda, *Nature*, **238**, 37 (1972)

[2] K. Maeda, K. Teramura, D. Lu, T. Takata, N. Saito, Y. Inoue, K. Domen, *Nature*, **295**, 440 (2006)

[3] H. Yoneyama, M. Koizumi, H. Tamura, *Bull. Chem. Soc. Jpn*., **52**, 3449 (1979)

[4] H. Kato, K. Asakura, A. Kudo, *J. Am. Chem. Soc.*, **125**, 3082 (2003)

[5] H. Kato, A. Kudo, *J. Phys. Chem. B*, **106**, 5029 (2002)

[6] R. Asahi, T. Morikawa, T. Ohwaki, K. Aoki, Y. Taga, *Science*, **293**, 269 (2001)

[7] T. Umebayashi, T. Yamaki, S. Tanaka, K. Asai, *Chem. Lett.*, **32**, 330 (2003)

[8] H. Kato, H. Kobayashi, A. Kudo, *J. Phys. Chem. B*, **106**, 12441 (2002)

[9] A. Kudo, K. Omori, H. Kato, *J. Am. Chem. Soc.*, **121**, 11459 (1999)

[10] K. Maeda, K. Teramura, T. Takata, M. Hara, N. Saito, K. Toda, Y. Inoue, H. Kobayashi, K. Domen, *J. Phys. Chem. B.*, **109**, 20504 (2005)

[11] K. Maeda, T. Takata, M. Hara, N. Saito, Y. Inoue, H. Kobayashi, K. Domen, *J. Am. Chem. Soc.*, **127**, 8286 (2005)

[12]H. Liu, J. Juan, W. Whangguan, Y. Teraoka, *J. Phys. Chem. C*, **112**, 8521 (2008)

[13]J. Liu, Y. Liu, N. Liu, Y. Han, X. Zhang, H. Huang, Y. Lifshitz, S. T. Lee, J. Zhong. Z. Kang, *Science*, **347**, 970 (2015)

[14] N. Lei, M. Tanabe, H. Irie, *Chem. Comm.*, **49**, 10094 (2013)

[15] R. Asahi, H. Nemoto, Q. Jia, K. Saito, A. Iwase, A. Kudo, *Chem. Comm.*, **50**, 2543 (2014)

[16] K. Sayama, K. Mukasa, R. Abe, Y. Abe, H. Arakawa, *J. Photo. Photo. A*, **148**, 71 (2002)

[17] H. Kato, Y. Sakai, A. Iwase, A. Kudo, *Bull. Chem. Soc. Jpn.*, **80**, 2457 (2007)

[18] S. Hara, M. Yoshimizu, S. Tanigawa, L. Ni, B. Ohtani, H. Irie, *J. Phys. Chem. C*, **116**, 17458 (2012)

[19] K. Maeda, R. Abe, K. Domen, *J. Phys. Chem. Lett.*, **115**, 3057 (2011)

2. Titanium dioxide based Z-scheme system

2.1 Band-structure control of titanium dioxide

In this chapter, the objective is constructing titanium dioxide based Z-scheme system and split water under visible light irradiation. However, titanium dioxide was well known photocatalyst, it only works under UV-light irradiation. Therefore to split water under visible light irradiation, titanium dioxide needs to introduce visible light sensitivity. In this study band structure was controlled by doping foreign element to base material, titanium dioxide.

2.1.1 Preparation of doped titanium dioxide samples

Doped titanium dioxide was prepared by hydrothermal synthesis method. Commercial $Ti(SO_4)_2$ (24.0% purity, Kanto Kagaku) and doping materials as starting materials were mixed and stirred in distilled water for 30 minutes using magnetic stirrer. Then, the solutions were treated hydrothermally in an autoclave at 140 °C for 12 h, and the resulting mixtures were washed with sufficient distilled water, collected by centrifugation, and dried at 80 °C overnight. The dried samples were calcined at 600 ^oC for 12 h in muffle furnace to obtain anatase titanium dioxide, or calcined at 900 ^oC for 24 h to obtain rutile titanium dioxide. At last, obtained samples were thoroughly ground using a mortar and pestle. As a reference, non-doped anatase titanium dioxide (TiO_2(A)) and non-doped rutile titanium dioxide (TiO_2(R)) were prepared under identical conditions using only $Ti(SO_4)_2$.

Basic condition is required for sample preparation in V, In doped titanium dioxide sample and W, Ga doped titanium dioxide sample. Basic condition hydrothermal synthesis method is described in below. [1]

$NaHCO_3$ was dissolved into distilled water to prepare basic solution. Then, $Ti(SO_4)_2$ and dopant materials were added into this solution and stirred 30 minutes using magnetic stirrer. The solution was poured into autoclave, then, heated at 140 ^oC for 12 h. Next, the resulting mixture was stirred in HCl solution to remove Na. After that, the samples were washed with sufficient distilled water, collected by centrifugation, and dried at 80 °C overnight. Then, the sample was calcined at 600 ^oC for 12 h or at 900 ^oC

for 24 h in muffle furnace. At last, obtained samples were thoroughly ground using a mortar and pestle.

2.1.2 Preparation of $(Ti_{1-2x}V_xGa_x)O_2$

$(Ti_{1-2x}V_xGa_x)O_2$ was prepared by hydrothermal synthesis method.

As dopant, $VOSO_4$（Kanto Kagaku）and $Ga(NO_3)_3$（Wako）were weighed these molar ratio is to be stoichiometry. Then, $(Ti_{1-2x}V_xGa_x)O_2$ was prepared by hydrothermal synthesis method. This sample was calcined at 600 ^oC for 12 h and anatase titanium dioxide based sample was obtained. Here Ga was employed as counter dopant to keep charge neutrality.

2.1.3 Preparation of $(Ti_{1-2x}V_xIn_x)O_2$

$(Ti_{1-2x}V_xIn_x)O_2$ was prepared by hydrothermal synthesis method.

As dopant, $VOSO_4$（Kanto Kagaku）and $InCl_3 \cdot 4H_2O$（Kanto Kagaku） were weighted these molar ratio is to be stoichiometry. Then, $(Ti_{1-2x}V_xIn_x)O_2$ was prepared by hydrothermal synthesis method in basic condition. This sample was calcined at 600 ^oC for 12 h and anatase titanium dioxide based sample was obtained. Here In was employed as counter dopant to keep charge neutrality.

2.1.4 Preparation of $(Ti_{1-3x}W_xGa_{2x})O_2$

$(Ti_{1-3x}W_xGa_{2x})O_2$ was prepared by hydrothermal synthesis method.

As dopant, $Na_2WO_4 \cdot nH_2O$ and $Ga(NO_3)_3$ (Wako) were weighted these molar ratio is to be stoichiometry. Then, $(Ti_{1-3x}W_xGa_{2x})O_2$ was prepared by hydrothermal synthesis method in basic condition. This sample was calcined at 900 ^oC for 24 h and rutile titanium dioxide based sample was obtained. Here Ga was employed as counter dopant to keep charge neutrality.

2.1.5 Preparation of $(Ti_{1-2x}Ta_xCr_x)O_2$

$(Ti_{1-2x}Ta_xCr_x)O_2$ was prepared by hydrothermal synthesis method.

As dopant, $TaCl_5$（Kanto Kagaku）and $CrCl_3 \cdot 6H_2O$（Kanto Kagaku）were weighed these molar ratio is to be stoichiometry. Then, $(Ti_{1-2x}Ta_xCr_x)O_2$ was prepared by hydrothermal synthesis method. This sample was calcined at 600 ^oC for 12 h or 900 ^oC for 24 h, then anatase titanium dioxide based sample or rutile titanium dioxide based sample was obtained. Here Ta was employed as counter dopant to keep charge neutrality.

2.1.6 Preparation of $(Ti_{1-x}Rh_x)O_2$

$(Ti_{1-x}Rh_x)O_2$ was prepared by hydrothermal synthesis method.

As dopant, $Rh(NO_3)_3$（Kanto Kagaku）was weighed. Then, $(Ti_{1-x}Rh_x)O_2$ was prepared by hydrothermal synthesis method. This sample was calcined at 600 ^oC for 12 h or 900 ^oC for 24 h, then anatase titanium dioxide based sample or rutile titanium dioxide based sample was obtained.

2.2 Deposition of platinum co-catalyst

$H_2PtCl_6 \cdot 6H_2O$（Kanto Kagaku） was employed as platinum source. First, platinum was weighed to the weighed to give a weight fraction of Pt relative to band structure controlled titanium dioxide sample of 1×10^{-3}. Sample powder was first dispersed in 100 mL methanol solution (20 vol%) as a hole scavenger. The weighed $H_2PtCl_6 \cdot 6H_2O$ was added to the aqueous suspension in which either photocataslyst was dispersed, and then the suspension was sufficiently deaerated using liquid nitrogen (N_2). While deaerating, a xenon lamp (LA-251 Xe; Hayashi Tokei) with an optical filter (Y-44, Hoya) was employed for light irradiation of the suspension for 4 h. The suspension was then

centrifuged and washed with distilled water. The resulting residues were dried at 80 ^{o}C overnight and then ground into a fine powder using an agate mortar.

2.3 Characterization

Prepared samples were characterized by X-Ray Diffraction (XRD) (Panalytical, PW-1700 system) and UV-vis diffuse reflectance spectroscopy (UV-vis DRS) (JASCO, V-650). Photocatalytic activities of these samples were measured using a gas-closed-circulation system (Makuhari glass, CLS-1370-PSWG). Figure 2.1 shows a picture of that system. Several samples were also characterized by Scanning Electronic Microscopy (SEM) (JEOL, JSM-6500F), X-Ray Fluorescence (XRF) (Rigaku, ZSXP PrimusII system), and Brunauer-Emmett-Teller (BET) surface areas which determined using a nitrogen adsorption apparatus (Micromeritics, TriStar 3000; Shimadzu). Laser flash photolysis (Quantel, Brilliant B) was carried out with the help of Leibnitz University of Hannover.

In the gas-closed-circulation system, light was irradiated into sample container and water splitting reaction was carried out at (1), generated gases were pumped and diffused to circulation system (2), then analyzed by gas chromatography (Shimadzu, GC-8A) from sample gas inlet (3). Experimental condition of photocatalytic reaction is kept same condition, sample amount 60 mg, solution 10 mL, Ar gas was filled in circulation system after deaeration. The solution dispersed sample was evacuated air by vacuuming before light irradiation. The solution was kept stirring during experimental. 300W Xe lamp (LA-251 Xe; Hayashi Tokei) equipped with an optimal filter (Y-44, Hoya) and light-emitting-diode (LED) lamp with a wavelength 420nm (LED 420 nm, LEDH60-420, Hamamatsu Photonics) were employed as light source, and these light intensities are shown in Figure 2.2.

Sometimes when we performed water splitting experiments, a different amount of nitrogen (N_2) was detected. The gas-closed-circulation system, however, repeatedly deaerated to a final pressure of 2.5 Pa and then introduced argon gas into the system in the same way. From these reasons, the detected N_2 was originated from the intruded air

from outside, and the effect of residual O_2 and N_2 in water was possibly excluded. [2-4] Therefore, when N_2 was unexpectedly observed, O_2 amount was calculated using the following equation.

$$O_2 = obs.O_2 - obs.N_2 \times \frac{0.21}{0.78}$$

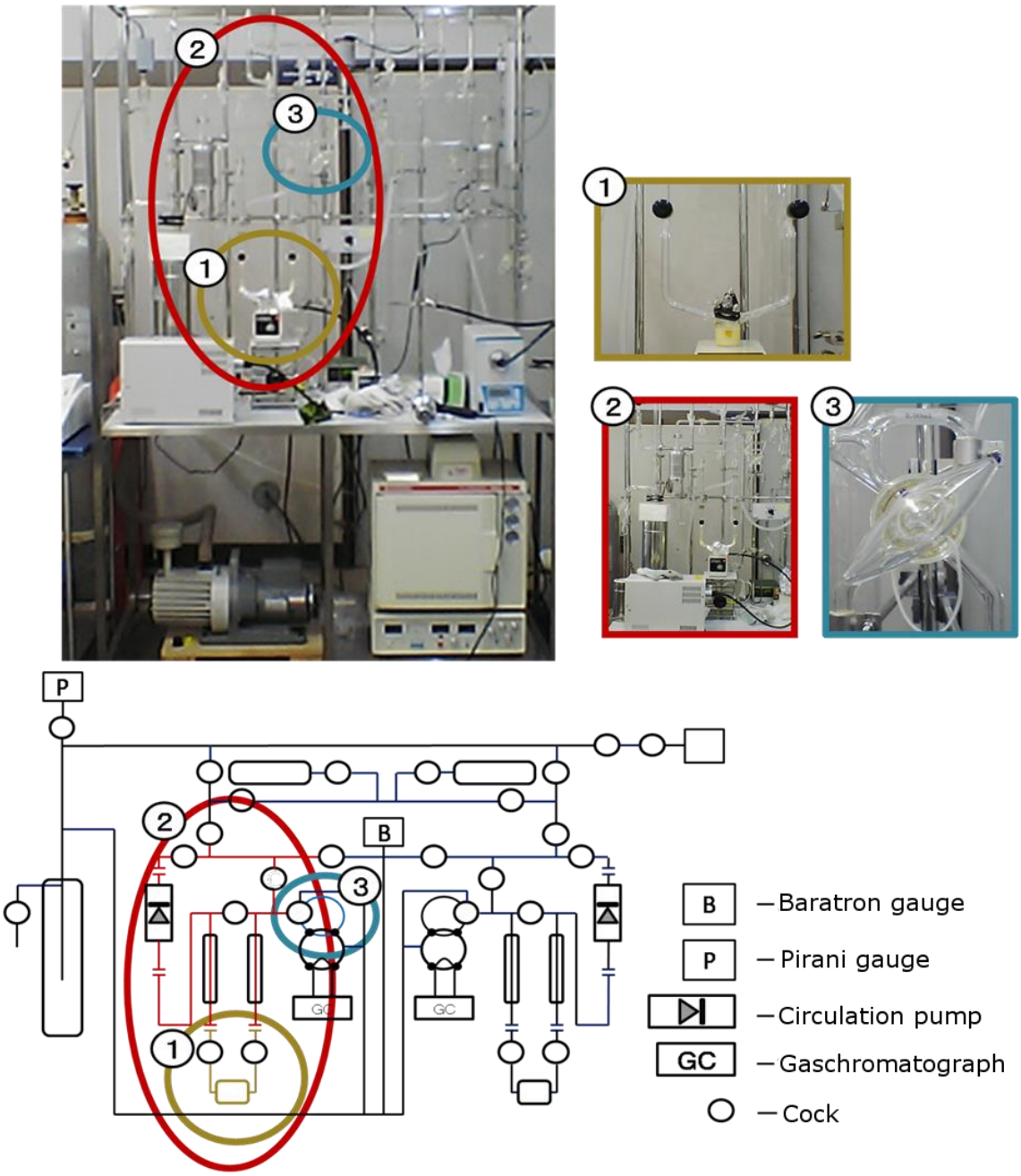

Fig.2.1 Gas-closed-circulation system

(1) Reaction container、(2) Circulation system、 (3) Sample gas inlet

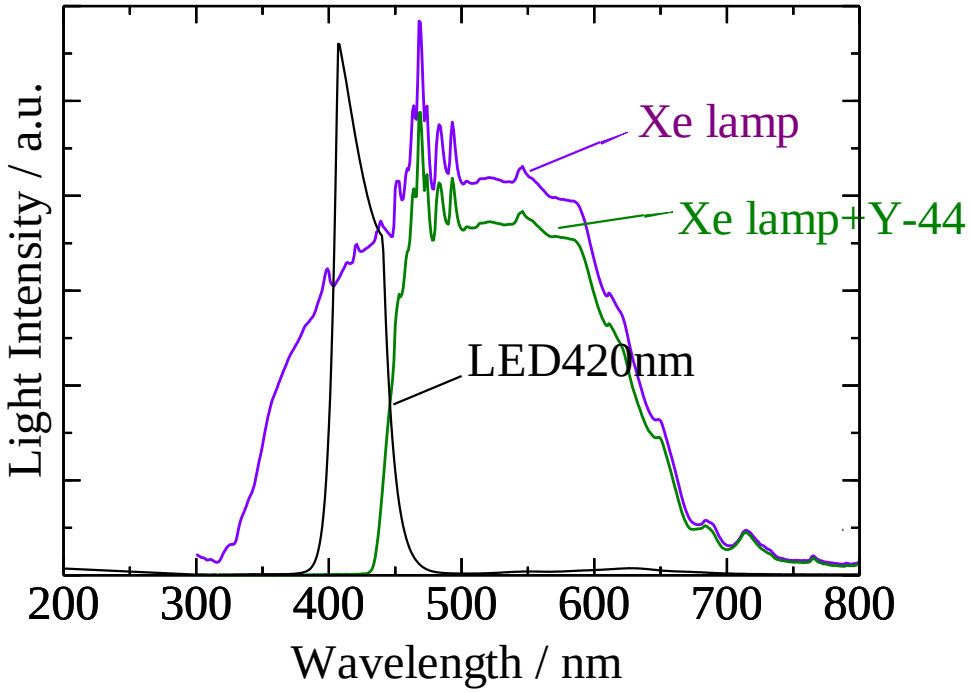

Fig.2.2　Spectrum of Xe lamp and LED420nm.

※In vertical scale, a.u. is employed because the light intensity of Xe lamp can be controlled up to 100 mW/cm^2.

2.4 Results and discussion

2.4.1 X-ray diffraction

The crystal structures of these prepared samples are shown in Figure 2.3.

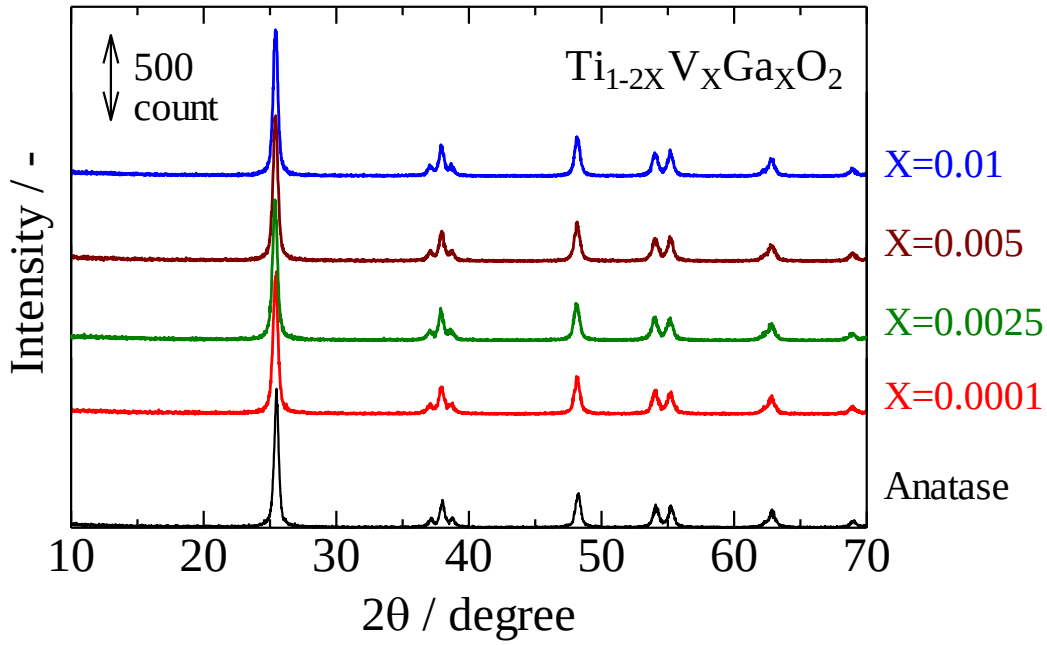

(a) XRD patterns of $(Ti_{1-2x}V_xGa_x)O_2$

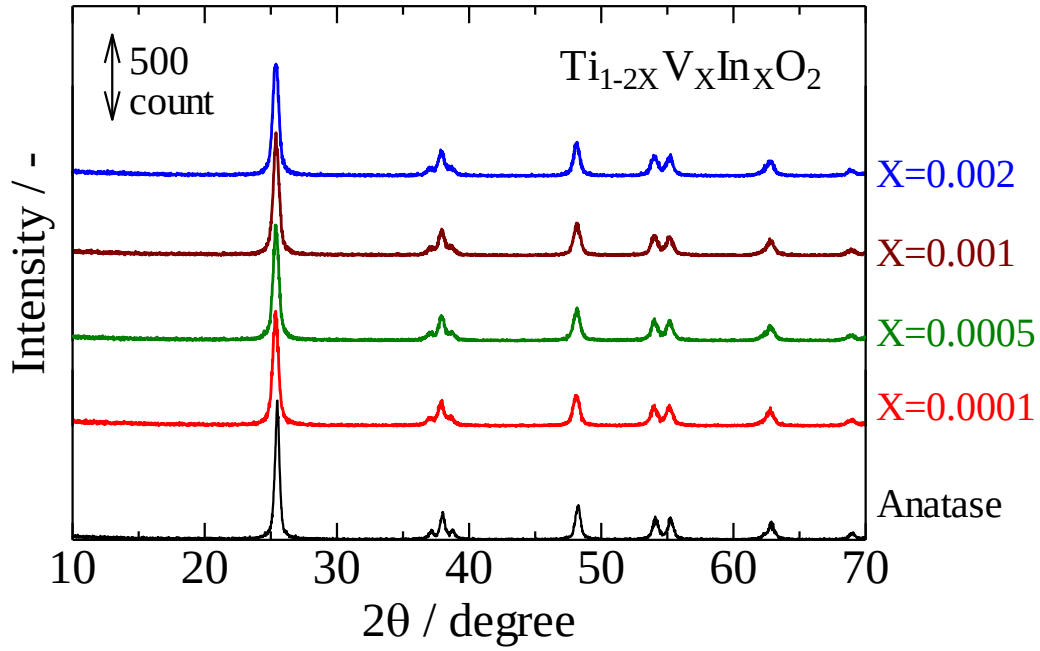

(b) XRD pattern of $(Ti_{1-2x}V_xIn_x)O_2$

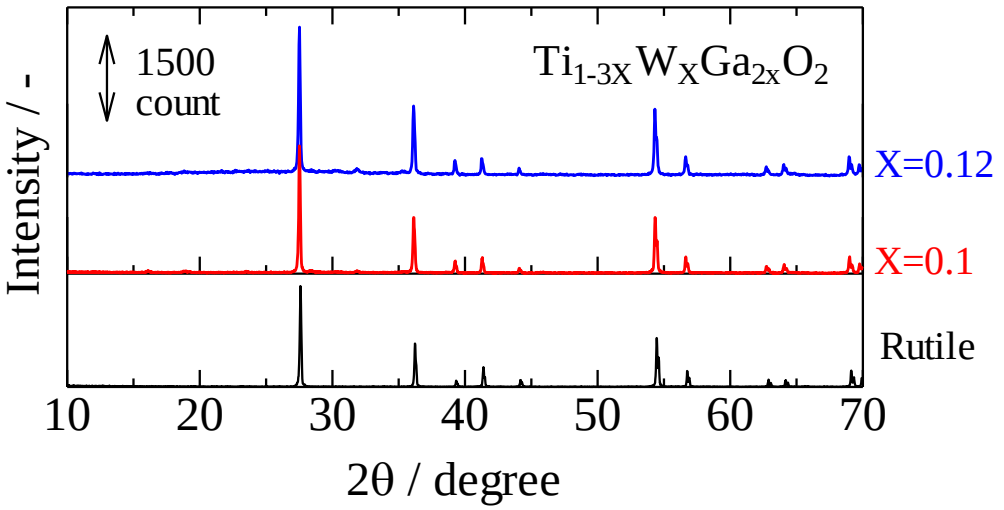

(c) XRD pattern of $(Ti_{1-2x}W_xGa_x)O_2$

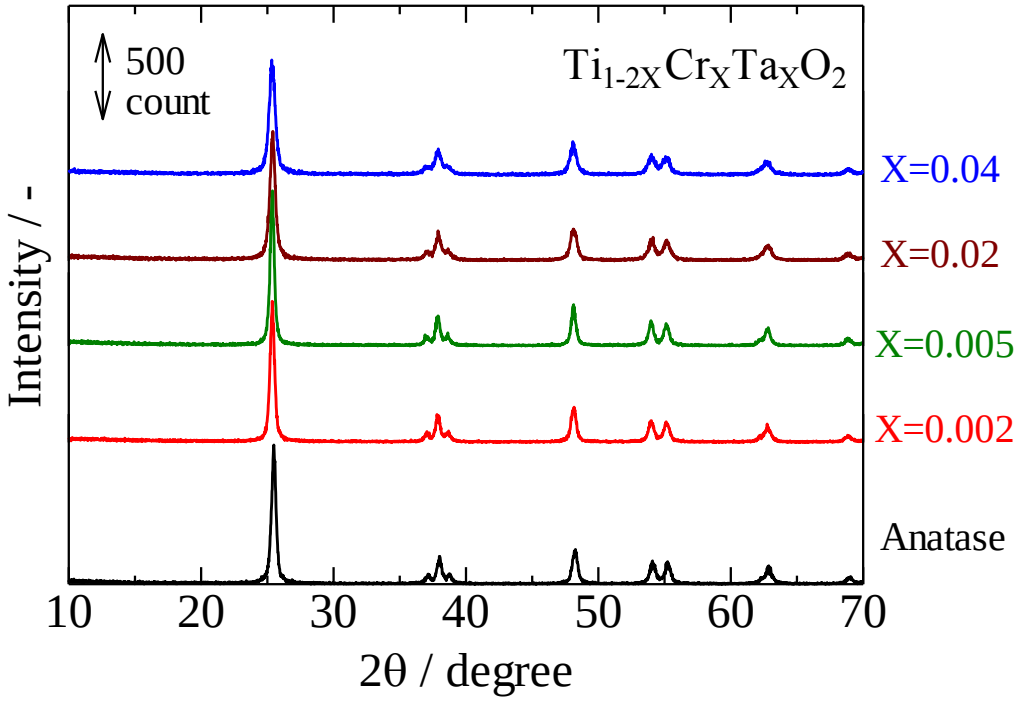

(d) XRD pattern of $(Ti_{1-2x}Cr_xTa_x)O_2$

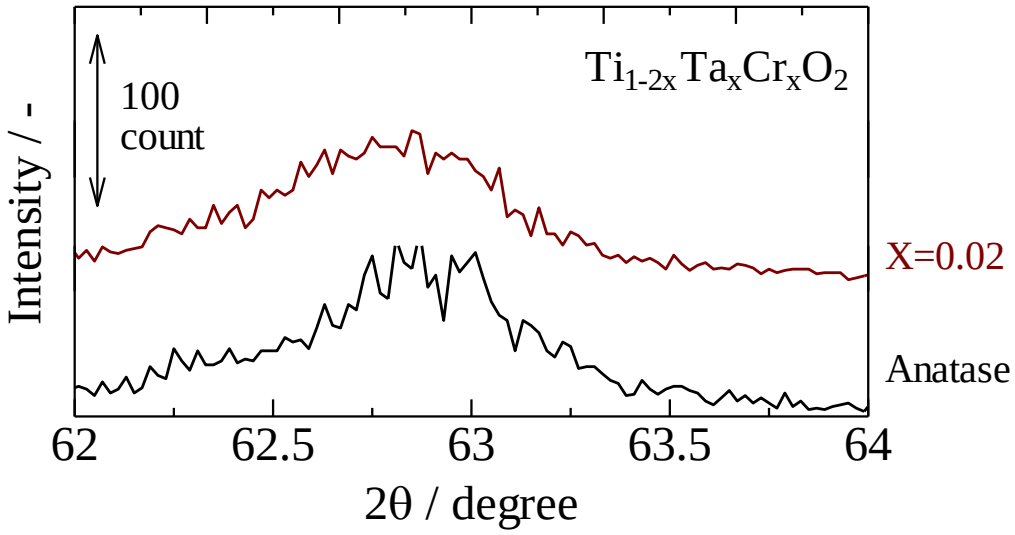

(e) Enlarged XRD pattern of $(Ti_{1-2x}Cr_xTa_x)O_2$

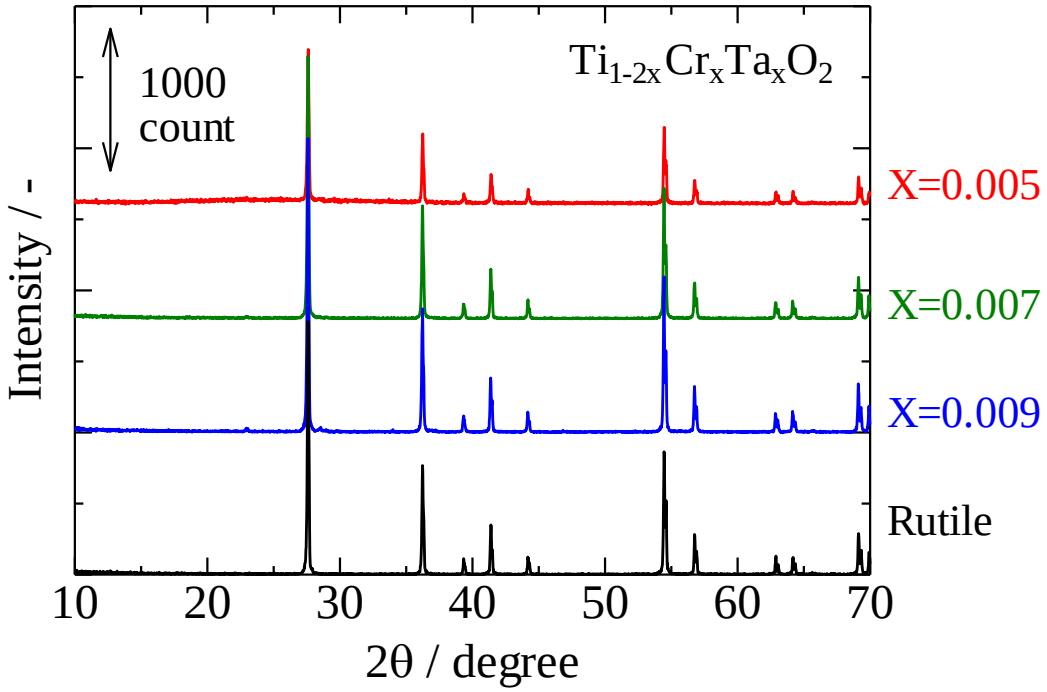

(f) XRD pattern of $(Ti_{1-2x}Cr_xTa_x)O_2$

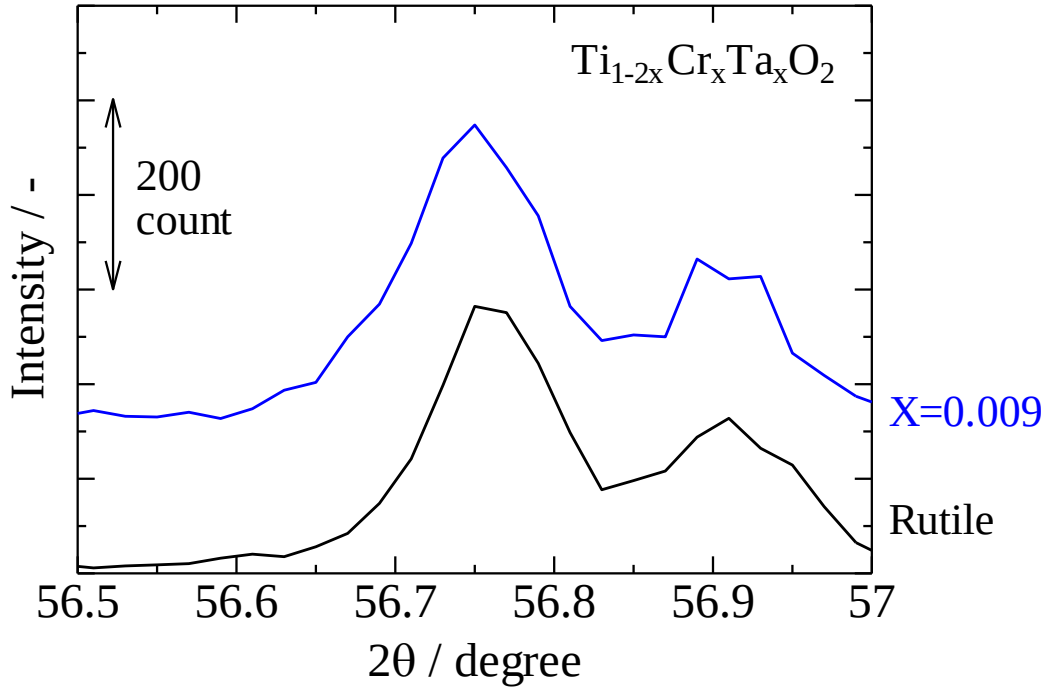

(g) Enlarged XRD pattern of $(Ti_{1-2x}Cr_xTa_x)O_2$

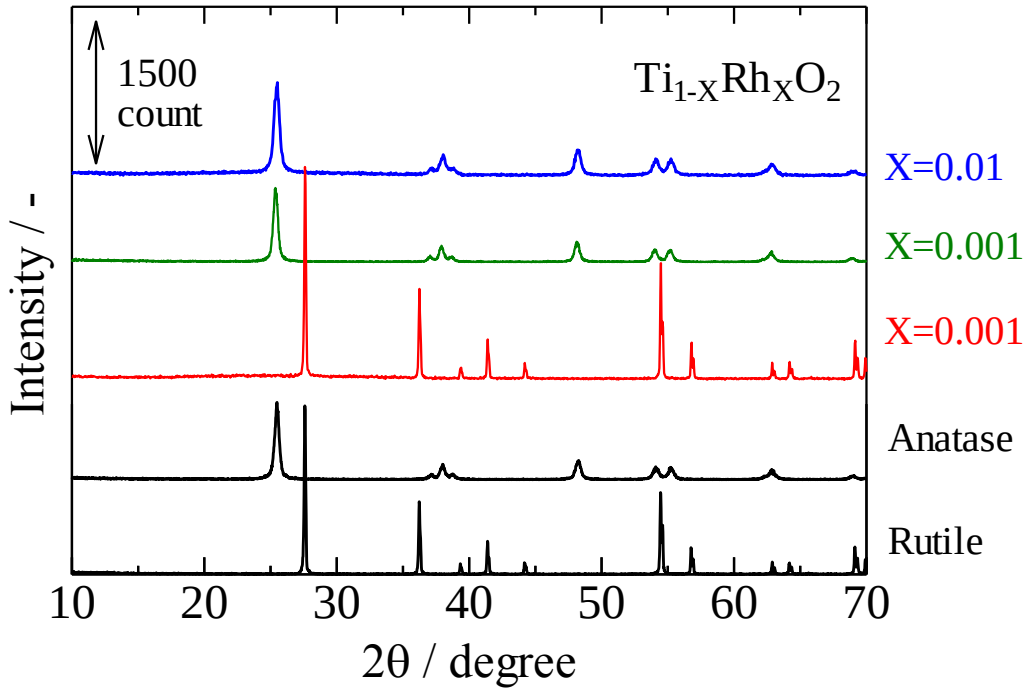

(h) XRD pattern of $(Ti_{1-x}Rh_x)O_2$

Fig.2.3 (a)-(h) XRD pattern of prepared samples

From these results of XRD, all prepared samples have anatase titanium dioxide or

rutile titanium dioxide single phase. $(Ti_{1-2x}Cr_xTa_x)O_2$ anatase and $(Ti_{1-2x}Cr_xTa_x)O_2$ rutile, these were employed as hydrogen- and oxygen-evolution photocatalyst according to following chapter, show peak shift to lower angle compared to non-doped reference anatase titanium dioxide and non-doped reference rutile titanium dioxide. These results are reasonable when one considers that the effective ionic radii of Ti^{4+}, Cr^{3+}, and Ta^{5+} (six-coordination) are 0.0605, 0.0615, and 0.064 nm, respectively [5]. Thus, in both the anatase and rutile forms of the titanium dioxide photocatalysts, Cr and Ta ions were likely incorporated at Ti sites.

2.4.2 UV-vis diffuse reflectance spectroscopy

UV-vis spectra of prepared samples are shown in figure 2.4.

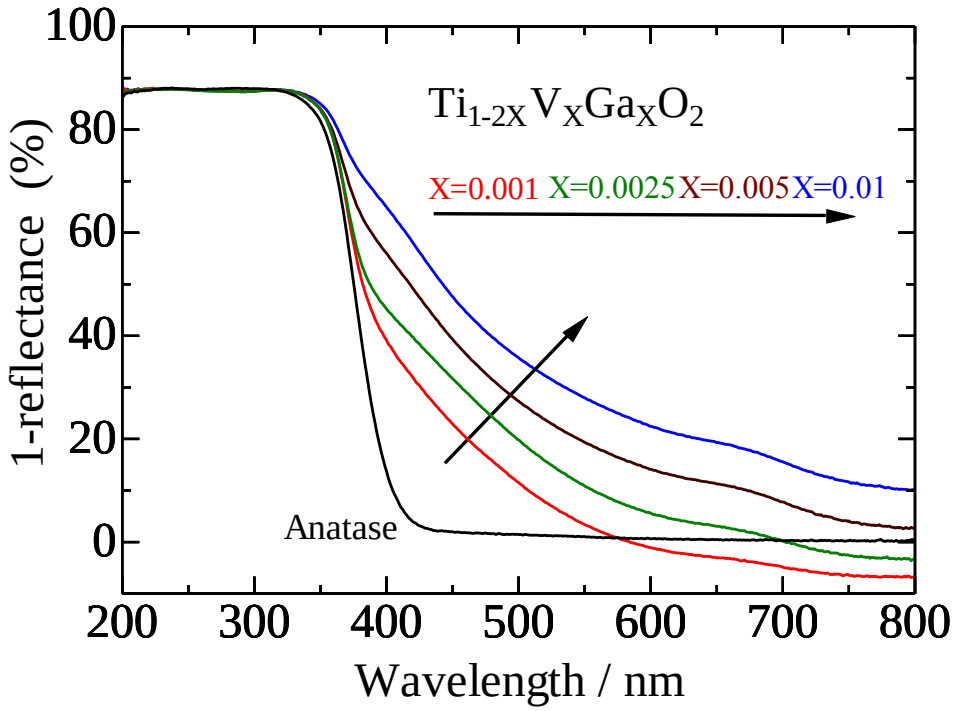

(a) UV-vis spectra of $(Ti_{1-2x}V_xGa_x)O_2$

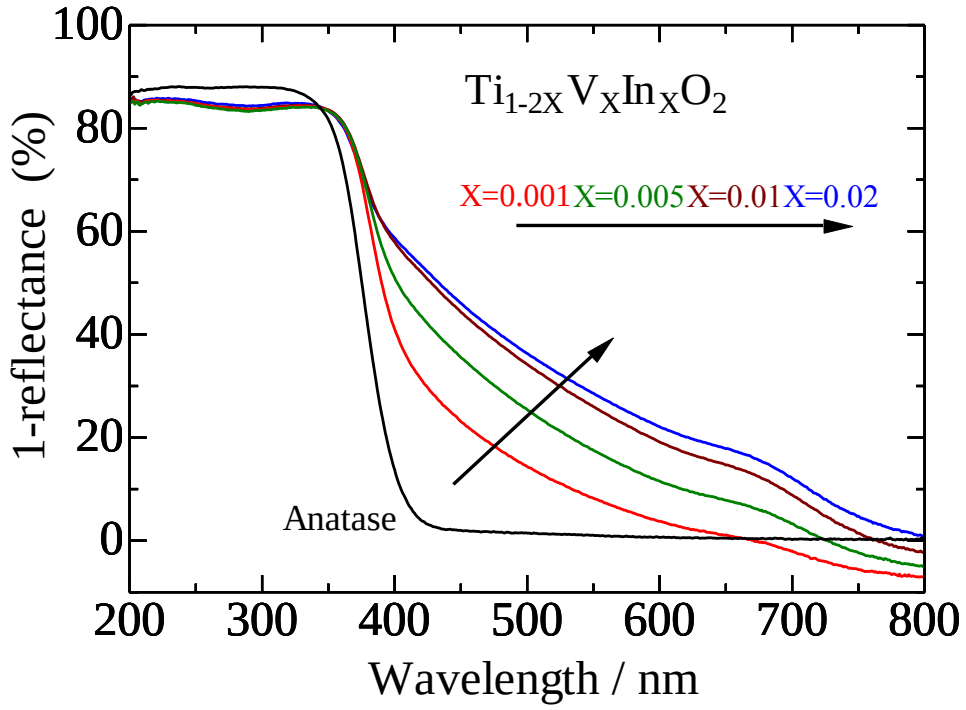

(b) UV-vis spectra of $(Ti_{1-2x}V_xIn_x)O_2$

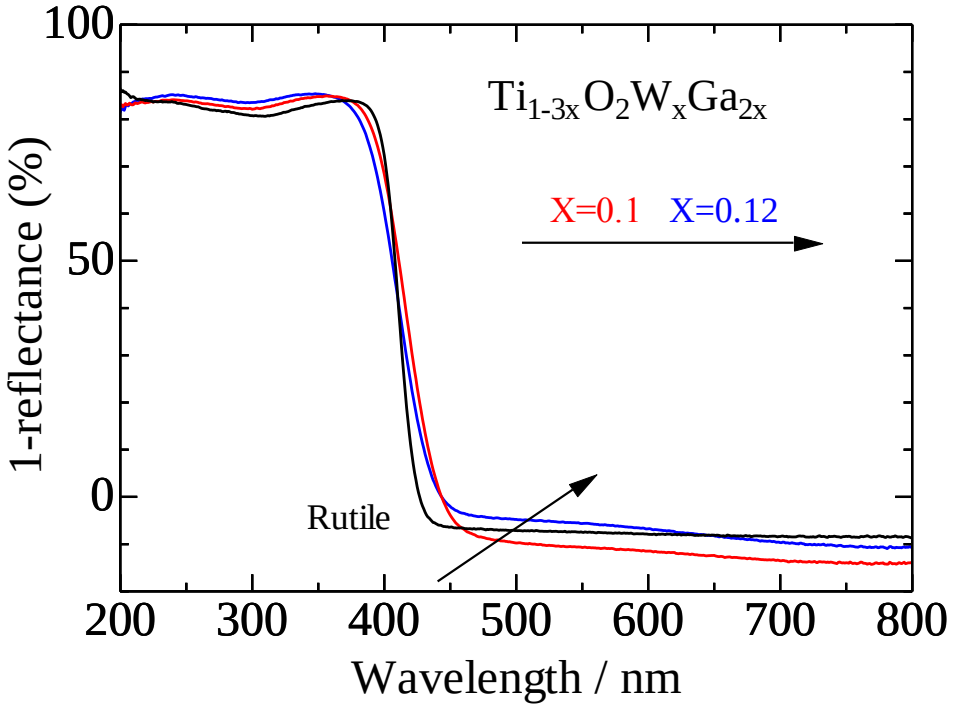

(c) UV-vis spectra of $(Ti_{1-2x}W_xGa_x)O_2$

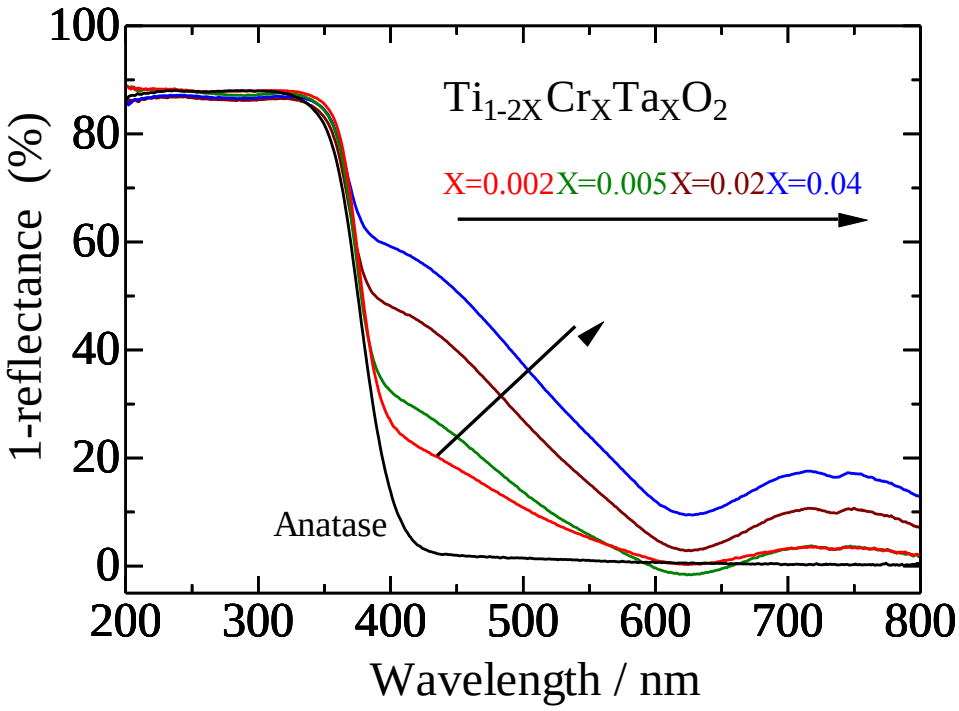

(d) UV-vis spectra of $(Ti_{1-2x}Cr_xTa_x)O_2$(A)

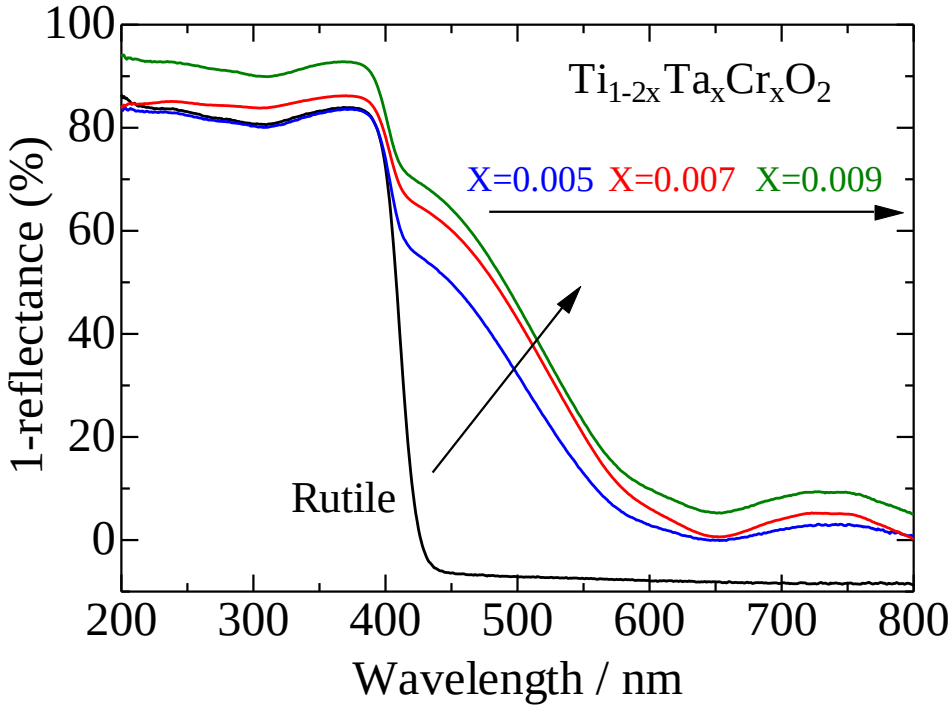

(e) UV-vis spectra of $(Ti_{1-2x}Cr_xTa_x)O_2$(R)

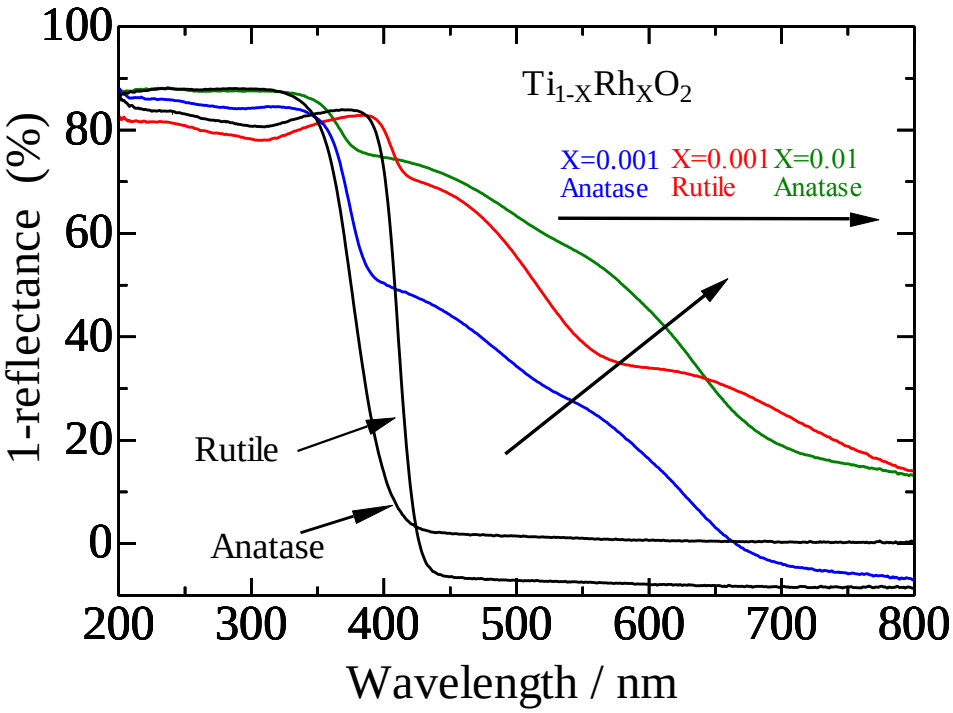

(f) UV-vis spectra of $(Ti_{1-x}Rh_x)O_2$

Fig.2.4 (a)-(f) UV-vis spectra of prepared samples

$(Ti_{1-2x}V_xGa_x)O_2$, $(Ti_{1-2x}V_xIn_x)O_2$, $(Ti_{1-2x}Cr_xTa_x)O_2$(A), $(Ti_{1-2x}Cr_xTa_x)O_2$(R), and $(Ti_{1-x}Rh_x)O_2$ have new absorption shoulder in visible light region. In contrast, $(Ti_{1-2x}W_xGa_x)O_2$ shows slightly shift absorption edge to visible light side. According to these results and previous studies, V 3d orbital formed isolated mini-band below conduction band in $(Ti_{1-2x}V_xGa_x)O_2$ and $(Ti_{1-2x}V_xIn_x)O_2$ samples, Rh 4d orbital formed isolated mini-band above valence band in $(Ti_{1-x}Rh_x)O_2$ samples. [6-7] Cr 3d orbital in anatase titanium dioxide formed isolated mini-band above valence band. In contrast, Cr 3d orbital formed isolated mini-band below conduction band in rutile titanium dioxide. [8-9] In $(Ti_{1-2x}W_xGa_x)O_2$ samples, W 5d orbital formed mixture band with Ti 3d orbital then conduction band bottom shifted to positive. [1] Then, the band structures of these materials are estimated and shown in Figure 2.5.

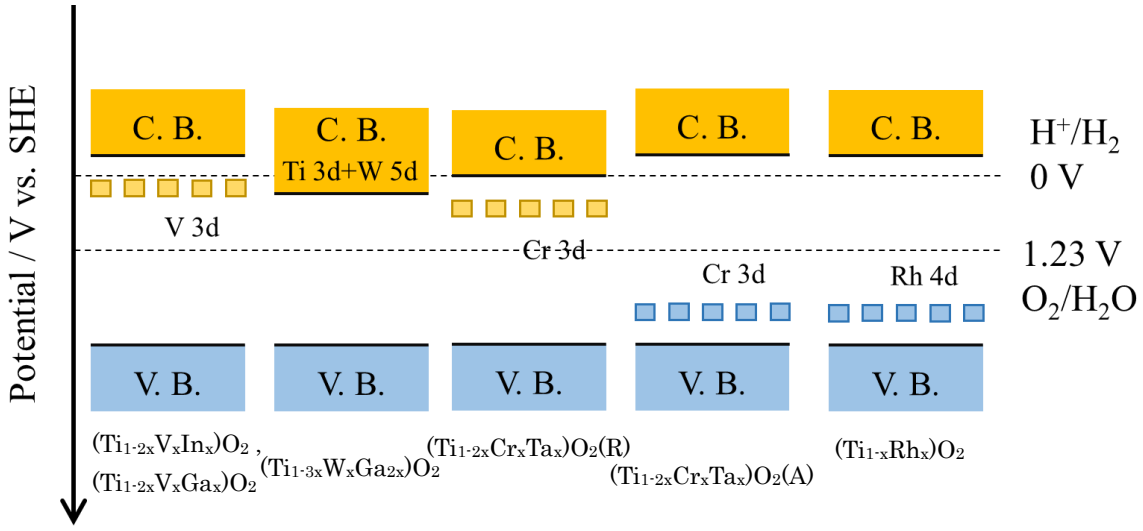

Fig.2.5 Band structure of $(Ti_{1-2x}V_xIn_x)O_2$, $(Ti_{1-2x}V_xGa_x)O_2$, $(Ti_{1-3x}W_xGa_{2x})O_2$, $(Ti_{1-2x}Cr_xTa_x)O_2$(A), $(Ti_{1-2x}Cr_xTa_x)O_2$(R), and $(Ti_{1-x}Rh_x)O_2$

Bandgaps of these prepared samples were calculated by Kubelka-Munk conversion, it sometimes called Tauc plot. This conversion method was developed by Tauc, Davis, and Mott. The conversion equation is shown below.

$$[F(R_\infty)h\nu]^{\frac{1}{n}} = A(h\nu E_g)$$

Here, $F(R_\infty)$is Kubelka-Munk equation、$F(R_\infty)=(1- R_\infty)^2 /2 R_\infty$. R_∞ is a reflectance of the sample. $h\nu$ is a photon energy (eV), A is a constant, E_g is a band gap. n is decided by transition mode of photo excitation. In titanium dioxide, n=2 for indirect transition. Plot this equation $h\nu$ vs $[F(R_\infty)h\nu]^{1/2}$ and extrapolate to $[F(R_\infty)h\nu]^{1/2}$ zero. The point of intersection is the band gap of that material.

Tauc plots of $(Ti_{1-2x}Cr_xTa_x)O_2$ x=0.02 Anatase (Cr,Ta-TiO_2 (A) x=0.02) and $(Ti_{1-2x}Cr_xTa_x)O_2$ x=0.009 Rutile (Cr,Ta-TiO_2 (R) x=0.009), they were employed as hydrogen- and oxygen-evolution photocatalyst, are shown in Figure 2.6.

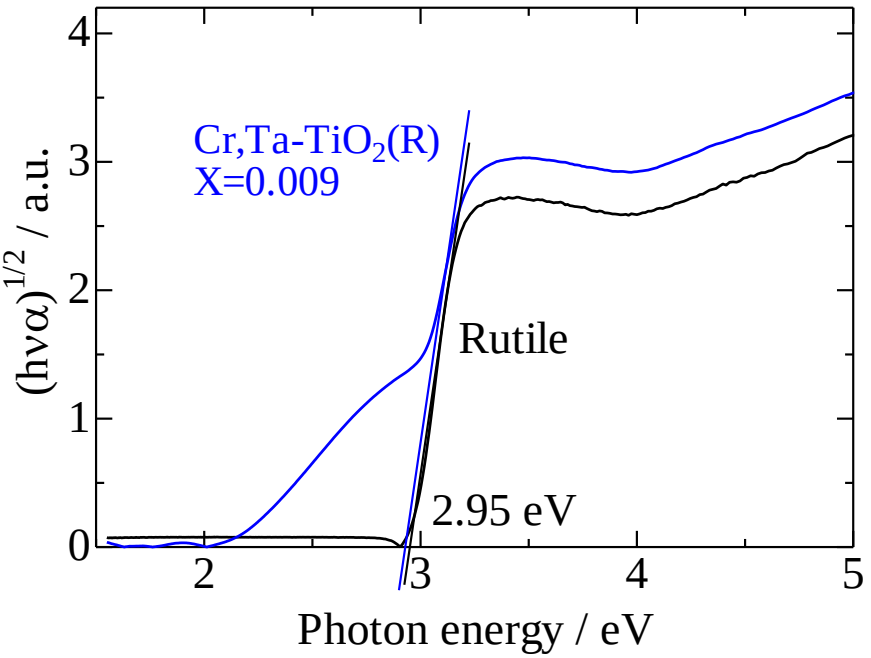

(a) Tauc plot of Cr,Ta-TiO_2(R)

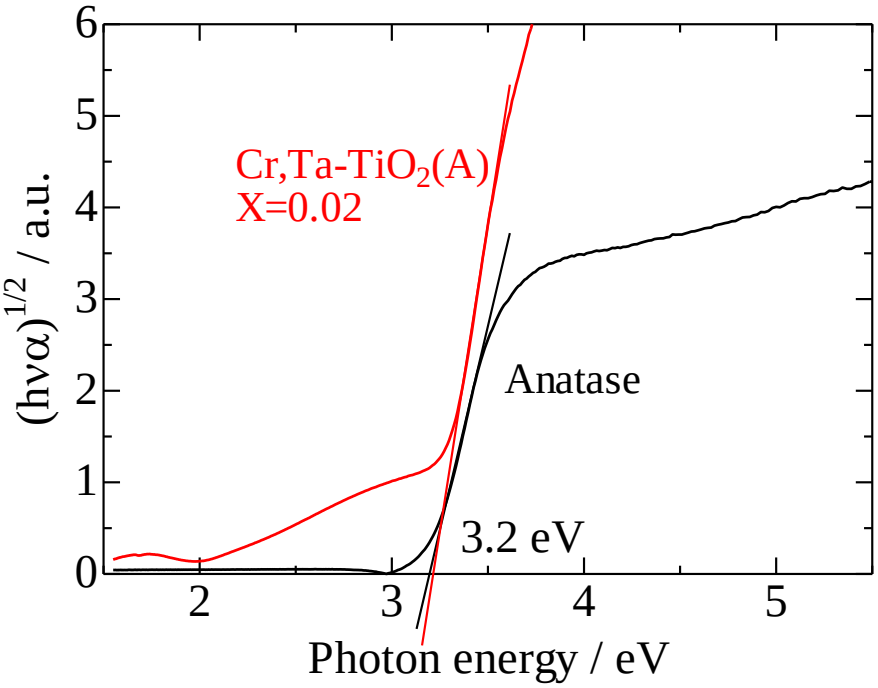

(b) Tauc plot of Cr,Ta-TiO_2(A)

Fig.2.6 Tauc plot of (a)$(Ti_{1-2x}Cr_xTa_x)O_2$ (R) x=0.009 and (b)$(Ti_{1-2x}Cr_xTa_x)O_2$ (A) x=0.02

From these figures, anatase sample has the band gap of 3.2 eV, rutile sample has the

band gap of around 3.0 eV. These results indicate their band gaps were not changed. Therefore, band structures of these samples were estimated to be forming an isolated mini-band in forbidden band.

2.4.3 Scanning electron microscopy

SEM images of $(Ti_{1-2x}Cr_xTa_x)O_2$ (R) x=0.009 and $(Ti_{1-2x}Cr_xTa_x)O_2$ (A) x=0.02 are shown in Figure 2.7.

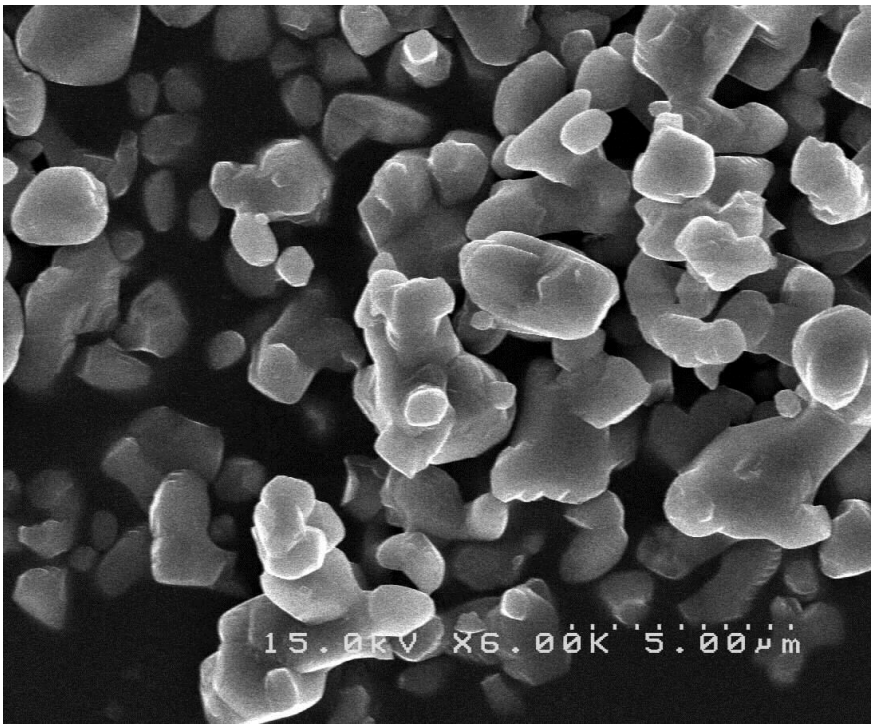

(a) $(Ti_{1-2x}Cr_xTa_x)O_2$ (R) x=0.009

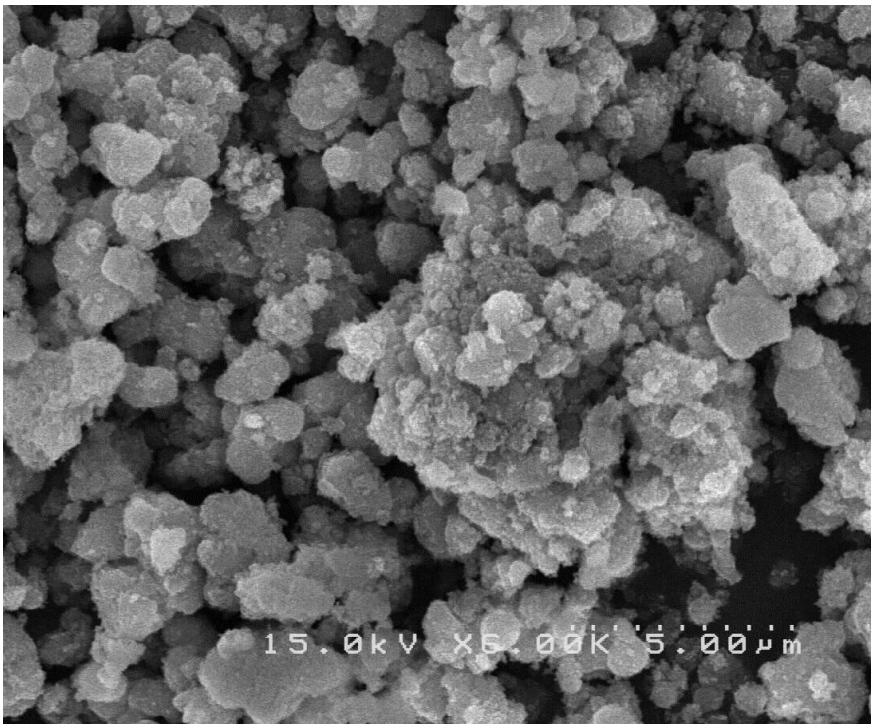

(b) $(Ti_{1-2x}Cr_xTa_x)O_2$ (A) x=0.02

Fig.2.7 SEM images of (a) $(Ti_{1-2x}Cr_xTa_x)O_2$ (R) x=0.009

and (b) $(Ti_{1-2x}Cr_xTa_x)O_2$ (A) x=0.02

Both Cr,Ta-TiO_2(A) and Cr,Ta-TiO_2(R) particles were connected with each other. That was observed due to rather high calcination temperature and long calcination time (900°C for 24 h and 600°C for 12 h).

Particle connection reduce surface area, however it doesn't mean bad effect for photocatalytic activities. D. W. Bahneman et al., reported the network of nano-crystalline mesoporous titanium dioxide improve photo-generated electron diffusion. Therefore particle connection of these samples could behavior as electron diffusion path. [10]

2.4.4 Brunauer-Emmett-Teller specific surface area

BET specific surface areas of $(Ti_{1-2x}Cr_xTa_x)O_2$ (R) x=0.009 and $(Ti_{1-2x}Cr_xTa_x)O_2$ (A) x=0.02 were determined using a nitrogen adsorption apparatus. The equations which used to calculate specific surface area were shown in below.

$$\frac{1}{Q\left[\left(\frac{P_o}{P}\right)-1\right]} = \frac{C-1}{Q_m C}\left[\frac{P}{P_o}\right] + \frac{1}{Q_m C}$$

P and P_o are the equilibrium and the saturation pressure of adsorbates at the temperature of adsorption, Q is the adsorbed gas quantity, and Q_m is the monolayer adsorbed gas quantity. C is the *BET constant*,

$$C = \exp\left(\frac{E_1 - E_2}{RT}\right)$$

E_1 is the heat of adsorption for the first layer, and E_2 is that for the second and higher layers and is equal to the heat of liquefaction.

A BET plot with $1/(Q[(P_o/P)-1])$ vs P/P_o according to experimental results was plotted. A BET plot of $(Ti_{1-2x}Cr_xTa_x)O_2$ (A) x=0.005 is shown in figure 2.8.

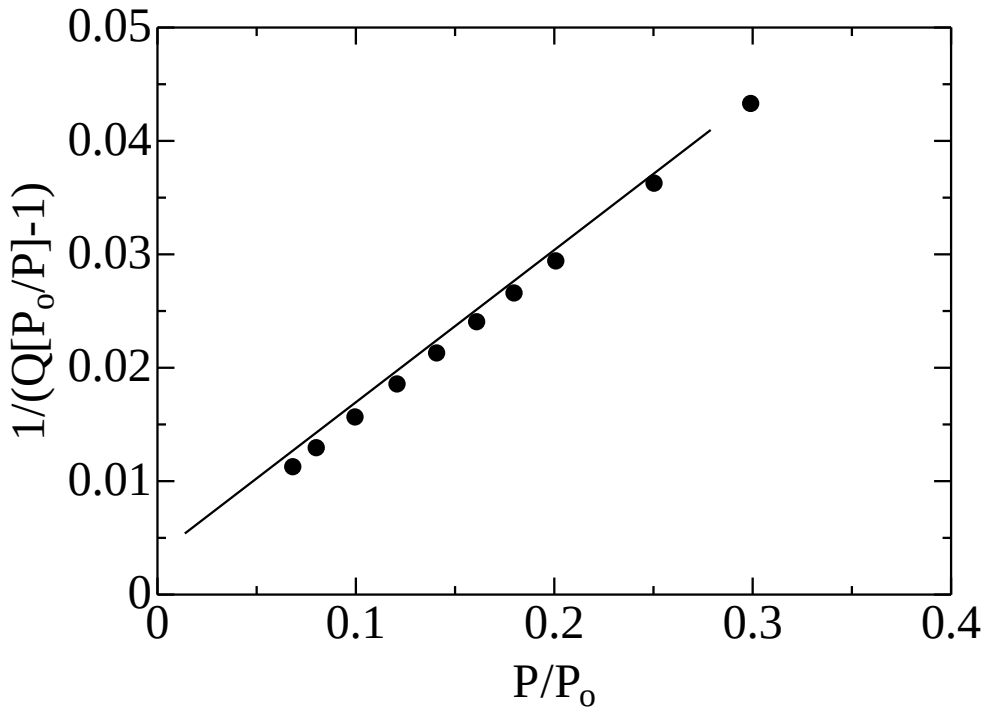

Fig.2.8 BET plot of $(Ti_{1-2x}Cr_xTa_x)O_2$ (A) x=0.005

The value of the slope s and the y-intercept l of the line were used to calculate the monolayer adsorbed gas quantity Q_m and the BET constant C by following equations.

$$Q_m = \frac{1}{s+l}$$

$$C = \frac{s}{l} + 1$$

Then, the total surface area S_{total} and the specific surface area S were calculated from

following equations.

$$S_{total} = \frac{Q_m N A_{cs}}{M}$$

$$S = \frac{S_{total}}{w}$$

Q_m is in units of volume which are also the units of the monolayer volume of the adsorbate gas, N is Avogadro's number, A_{cs} the adsorption cross section of the adsorbing species, M the molar volume of the adsorbate gas, and w the mass of the sample.

From these equations and experiments, BET specific surface areas of $(Ti_{1-2x}Cr_xTa_x)O_2$ (R) x=0.009 and $(Ti_{1-2x}Cr_xTa_x)O_2$ (A) x=0.02 were calculated to 1.68 m^2/g and 31.17 m^2/g, respectively. These surface areas were reasonable to the pictures of SEM, the size of $(Ti_{1-2x}Cr_xTa_x)O_2$ (R) x=0.009 particles were lager than that of $(Ti_{1-2x}Cr_xTa_x)O_2$ (A) x=0.02.

2.4.5 X-ray fluorescence

XRF of $(Ti_{1-2x}Cr_xTa_x)O_2$ (A) x=0.02 and $(Ti_{1-2x}Cr_xTa_x)O_2$ (R) x=0.009 were measured, and the results are shown in figure 2.9.

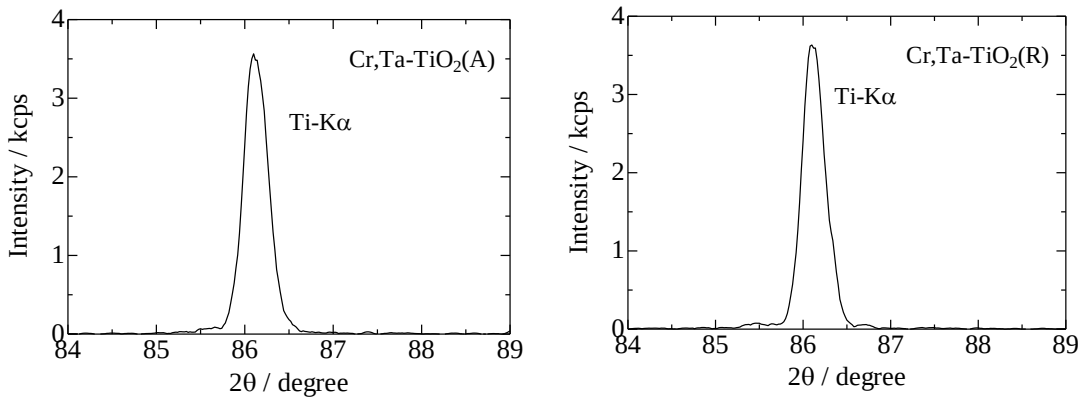

(a) (b)

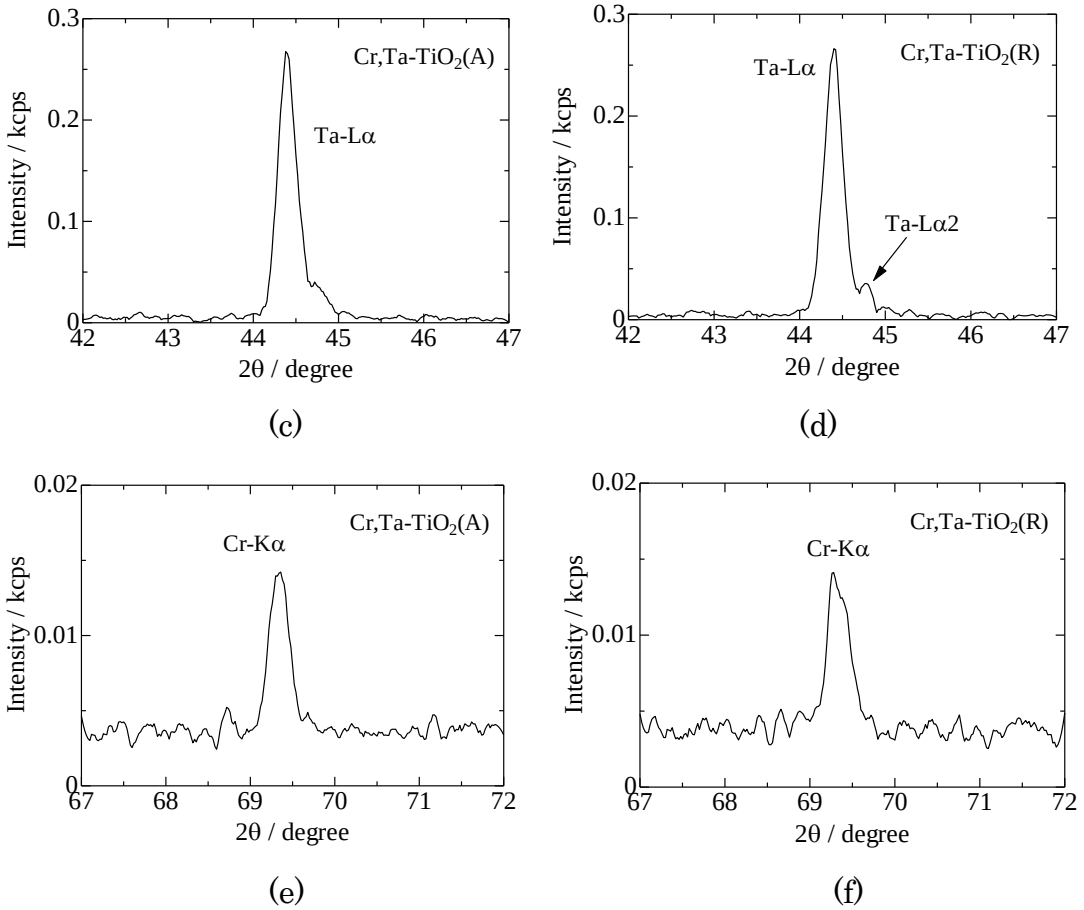

Fig.2.9 XRF peaks of (a) (c) (e) $(Ti_{1-2x}Cr_xTa_x)O_2$ (A) x=0.02 and (b) (d) (f) $(Ti_{1-2x}Cr_xTa_x)O_2$ (R) x=0.009

According to the quantitative analyses, the molar ratio of Ti: Ta: Cr was 0.982 : 0.014 : 0.004 in CrTa-TiO_2(A)x=0.02 and the molar ratio of Ti: Ta: Cr was 0.992 : 0.006 : 0.002 in CrTa-TiO_2(R)x=0.009. Those molar ratios are not consistent with the starting ratios used in the preparation of the photocatalyst. This discrepancy was attributed to differences in the solubility of Ti, Cr and Ta in aqueous solution under hydrothermal conditions. However, in both samples, Ta and Cr peaks were clearly observed, therefore these results supported to succeed of Ta and Cr doping to titanium dioxide.

2.4.6 Half reaction of oxygen evolution photocatalyst

A mechanism of half reaction of oxygen evolution photocatalyst which formed isolated mini-band below conduction band is shown in Figure 2.10. Photo-generated hole oxidize water to oxygen, and photo-generated electron reduce sacrificial agent like IO_3^-

and Ag^{+}.

Oxygen evolution activities of prepared samples are shown in Figure 2.11.

Here, oxygen evolution reaction of V,Ga-TiO_2 and V,In-TiO_2 were used $AgNO_{3aq}$ as sacrificial agent. Oxygen evolution reaction of W,Ga-TiO_2 was used Fe_3^{+} as sacrificial agent. Other oxygen evolution reactions were used IO_3^{-} as sacrificial agent. The pH of Fe_3^{+} solution was adjusted to pH 2, the other was not adjusted.

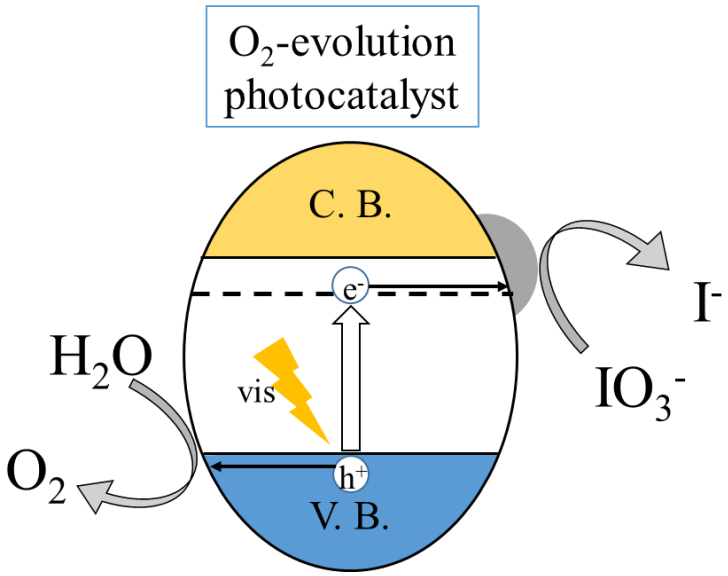

Fig.2.10 Mechanism of half reaction of oxygen evolution photocatalyst

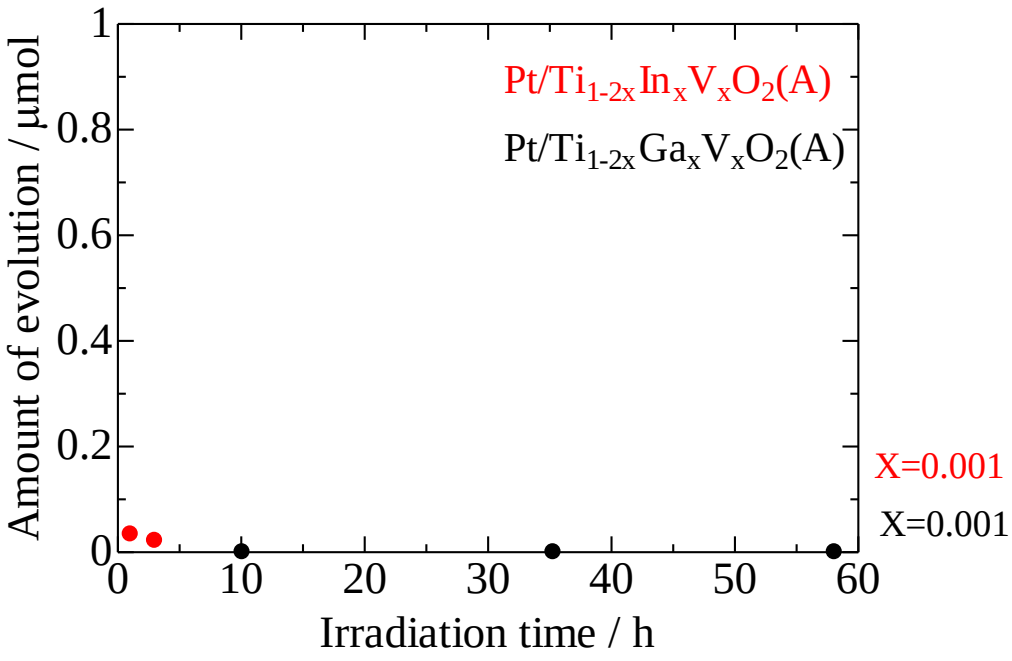

(a) Half reactions in $AgNO_{3aq}$ solution with Pt/$Ti_{1-2x}In_xV_xO_2$(A) or

$Pt/Ti_{1-2x}Ga_xV_xO_2$(A).

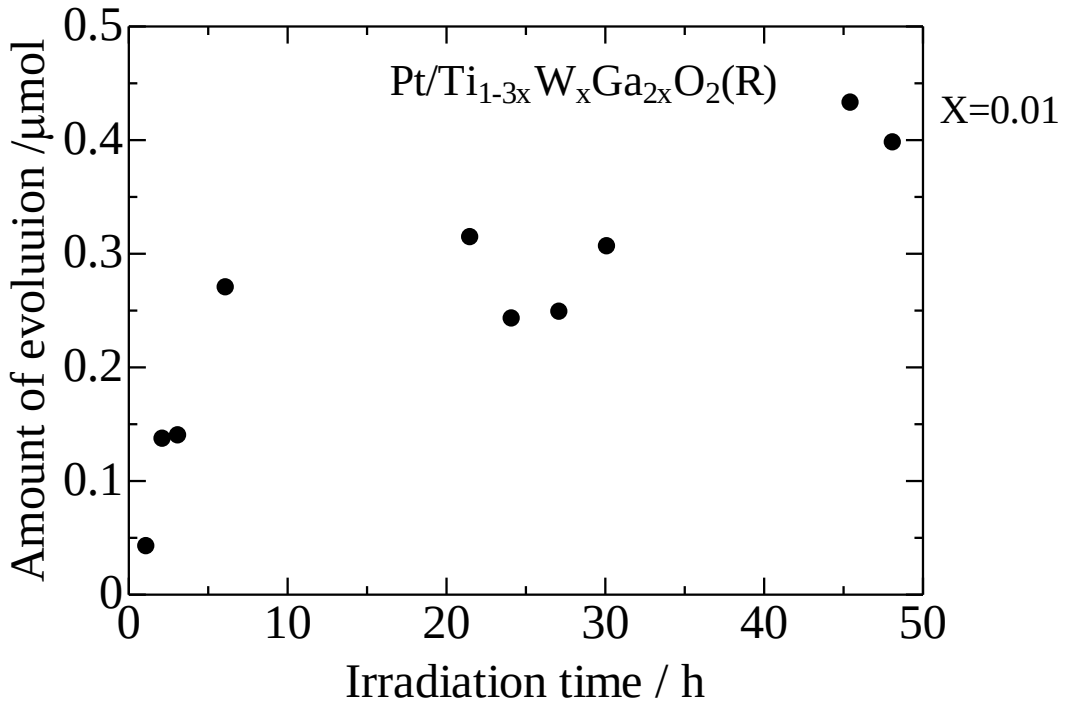

(b) Half reactions in $FeCl_3 \cdot 6H_2O_{aq}$ solution with $Pt/Ti_{1-3x}W_xGa_{2x}O_2$(R).

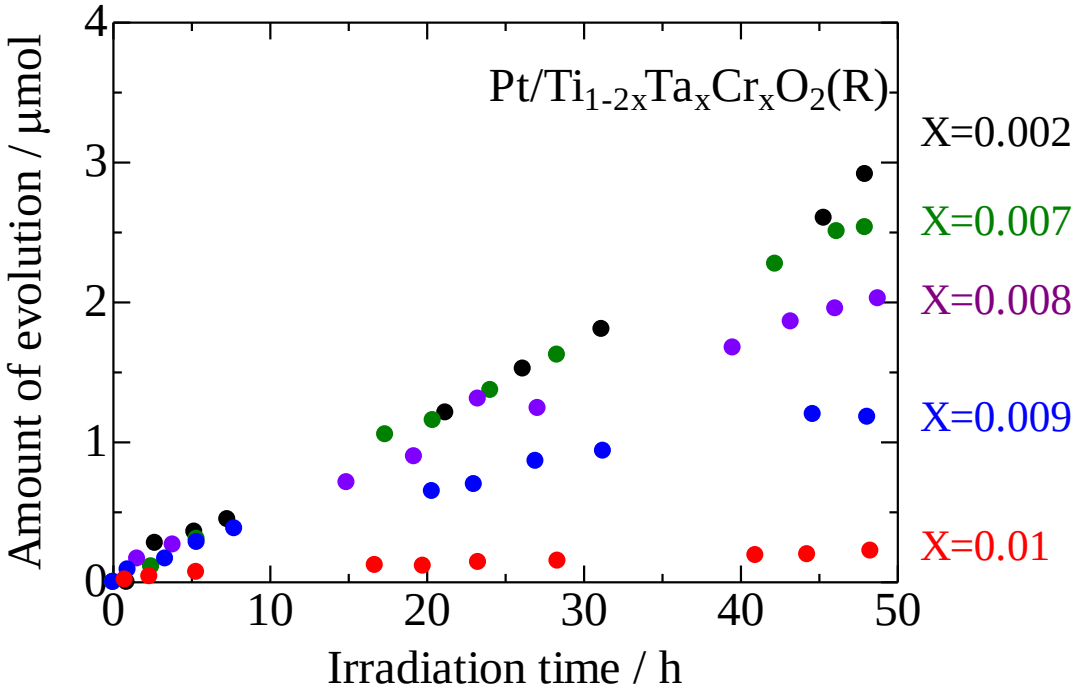

(c) Half reactions in $NaIO_{3aq}$ solution with $Pt/Ti_{1-2x}Ta_xCr_xO_2$(R).

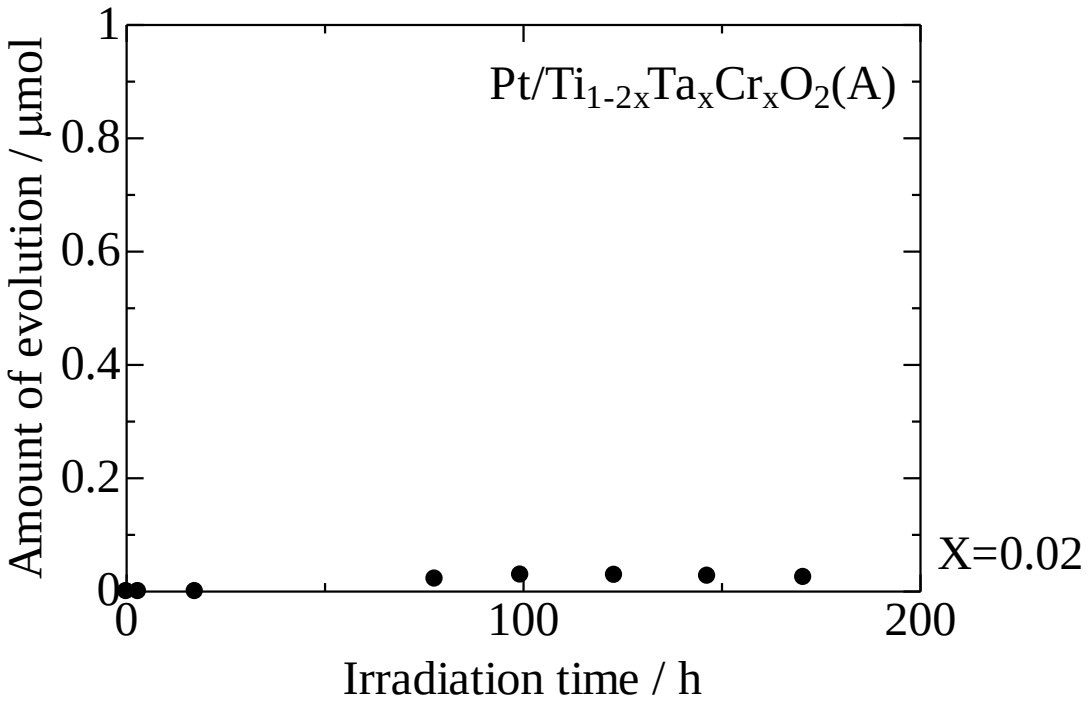

(d) Half reactions in $NaIO_{3aq}$ solution with $Pt/Ti_{1-2x}Ta_xCr_xO_2(A)$

Fig.2.11　Half reaction activities of oxygen evolution

(a)$Pt/Ti_{1-2x}In_xV_xO_2(A)$ or $Pt/Ti_{1-2x}Ga_xV_xO_2(A)$ in $AgNO_{3aq}$ solution

(b)$Pt/Ti_{1-3x}W_xGa_{2x}O_2(R)$ in $FeCl_3 \cdot 6H_2O_{aq}$ solution (c)$Pt/Ti_{1-2x}Ta_xCr_xO_2(R)$ in $NaIO_{3aq}$ solution (d) $Pt/Ti_{1-2x}Ta_xCr_xO_2(A)$ in $NaIO_{3aq}$ solution

Figure2.11 shows $Pt/Ti_{1-2x}In_xV_xO_2(A)$, $Pt/Ti_{1-2x}Ga_xV_xO_2(A)$, and $Pt/Ti_{1-2x}Ta_xCr_xO_2(A)$ have negligible oxygen evolution activities, $Pt/Ti_{1-3x}W_xGa_{2x}O_2(R)$ has poor oxygen evolution activity, and $Pt/Ti_{1-2x}Ta_xCr_xO_2(R)$ has good oxygen evolution activity.

From these results, $Pt/Ti_{1-2x}Ta_xCr_xO_2(R)$ x=0.009 was employed as oxygen evolution photocatalyst for their higher oxygen evolution activities and near activity to hydrogen evolution photocatalyst. Hydrogen evolution activity of oxygen evolution photocatalyst was described in following chapter 2.4.7 and no hydrogen was detected. Therefore, we succeed to prepare oxygen evolution photocatalyst from rutile titanium dioxide, which has only oxygen evolution photocatalytic activity under visible light irradiation. Additionally, oxygen evolution activity of $Pt/Ti_{1-2x}Ta_xCr_xO_2(A)$ x=0.02, which employed as hydrogen evolution photocatalyst detail was described following chapter, was determined and negligible amount of oxygen was detected.

2.4.7 Half reaction of hydrogen evolution photocatalyst

A mechanism of half reaction of hydrogen evolution photocatalyst which formed isolated mini-band above balance band is shown in Figure 2.12. Photo-generated electron reduce proton to hydrogen, and photo-generated hole oxidize sacrificial agent like I^- and methanol.

The results of hydrogen evolution half reactions using I^- sacrificial agent are shown in Figure 2.13.

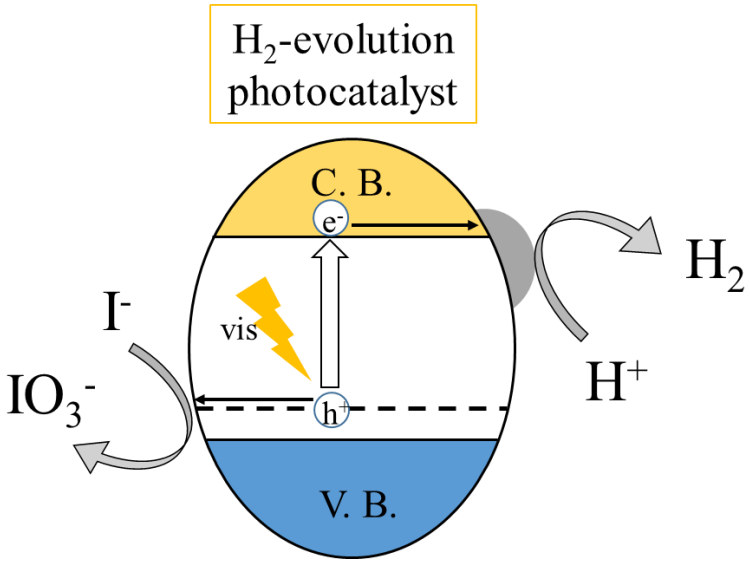

Fig2.12 Mechanism of half reaction of hydrogen evolution photocatalyst

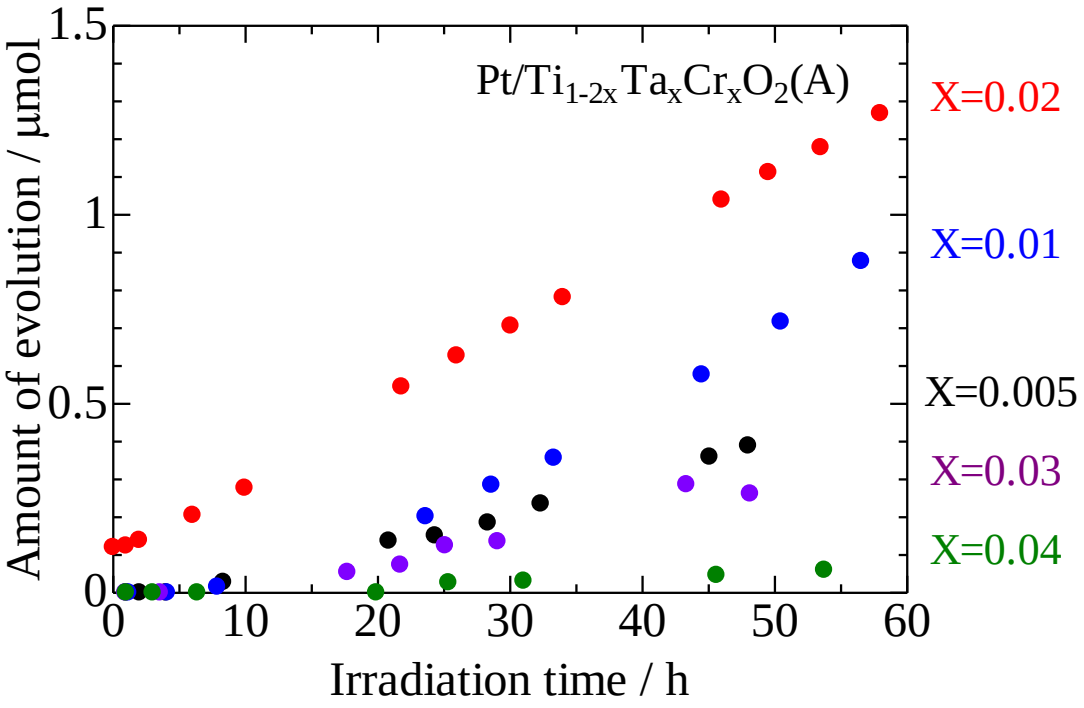

(a) Half reactions in NaI_{aq} solutions with $Pt/Ti_{1-2x}Ta_xCr_xO_2(A)$

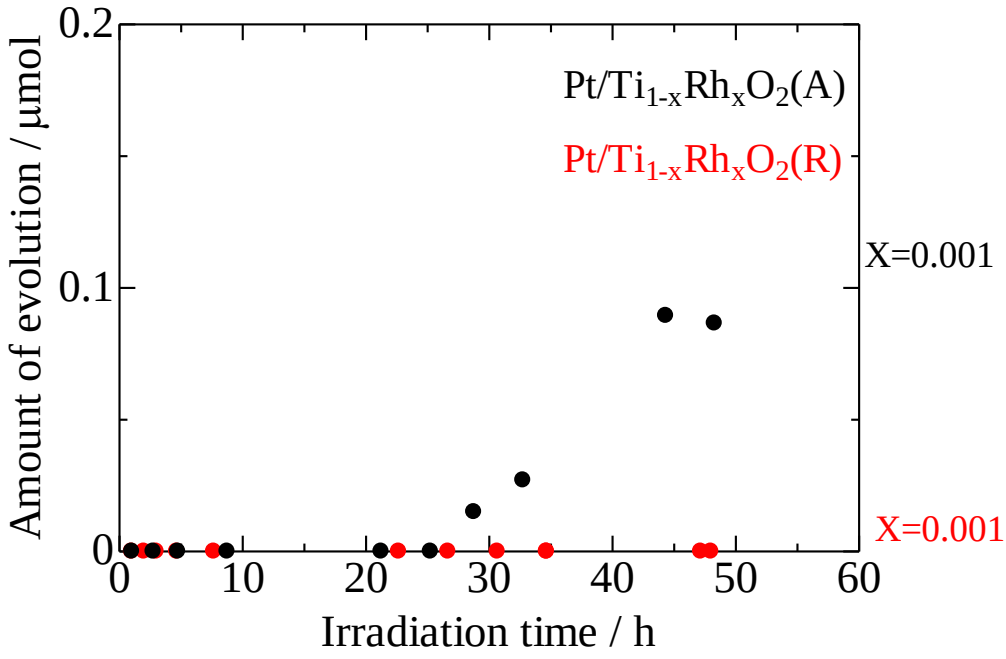

(b) Half reactions in NaI_{aq} solutions with $Pt/Ti_{1-x}Rh_xO_2(A)$ or $Pt/Ti_{1-x}Rh_xO_2(R)$

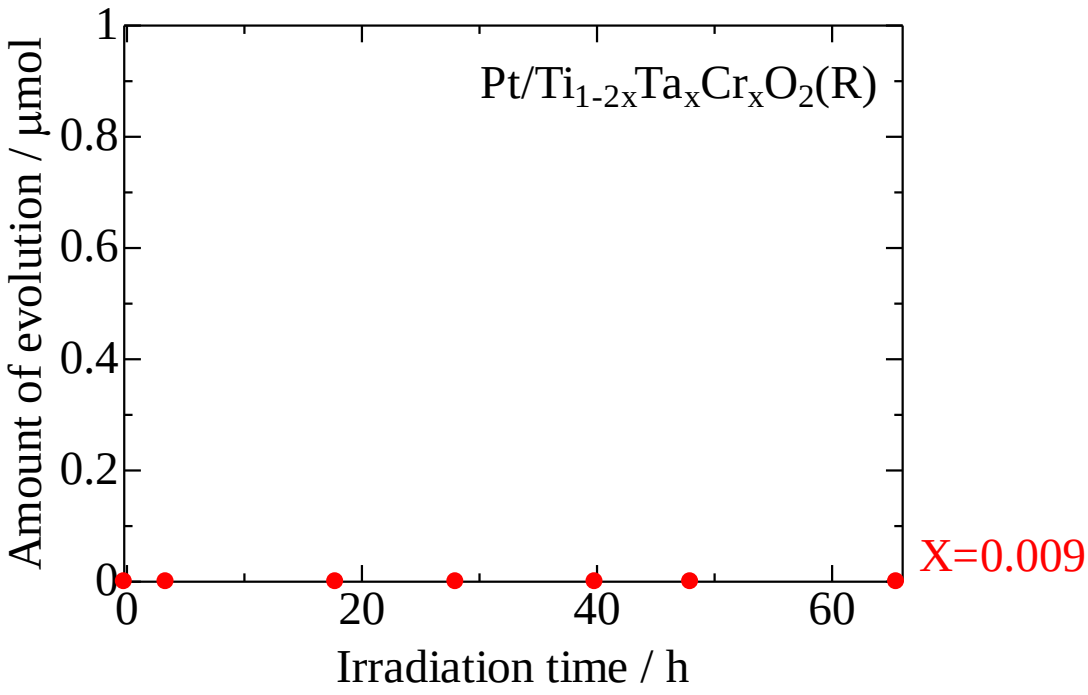

(c) Half reaction in NaI_{aq} solution with $Pt/Ti_{1-2x}Ta_xCr_xO_2(R)$

Fig2.13 Half reactions of hydrogen evolution

(a)(b)(c) $Pt/Ti_{1-2x}Ta_xCr_xO_2(A)$, $Pt/Ti_{1-2x}Ta_xCr_xO_2(R)$, $Pt/Ti_{1-x}Rh_xO_2(A)$ or $Pt/Ti_{1-x}Rh_xO_2(R)$ in NaI_{aq} solutions

From Figure 2.13, $Pt/Ti_{1-2x}Ta_xCr_xO_2(A)$ and $Pt/Ti_{1-x}Rh_xO_2(A)$ show hydrogen evolution activities. However, $Pt/Ti_{1-x}Rh_xO_2(R)$ doesn't shows hydrogen evolution activity. The reason was estimated to the position of conduction band bottom of $Pt/Ti_{1-x}Rh_xO_2(R)$. Conduction band bottom of rutile titanium dioxide is 0 V and proton reduction position is 0 V, therefore it can but it's difficult to reduce proton to hydrogen in rutile titanium dioxide sample.

From these results, as hydrogen evolution photocatalyst Pt/Cr,Ta-TiO_2 (A) x=0.02 was employed for the highest hydrogen evolution activity. Oxygen evolution reaction of hydrogen evolution photocatalyst, Pt/Cr,Ta-TiO_2 (A) x=0.02, was also carried out and the result is shown in figure 2.11(d) and negligible amount of oxygen was detected. Therefore, $Pt/Ti_{1-2x}Ta_xCr_xO_2(A)$ x=0.02 has only hydrogen evolution activity, that mean we succeed to prepare hydrogen evolution photocatalyst from anatase titanium dioxide under visible light irradiation.

Figure 2.13 also shows the result of hydrogen evolution reaction of Pt/Cr,Ta-TiO_2 (R) x=0.009 which employed as oxygen evolution photocatalyst, and hydrogen didn't detected.

2.4.8 Laser flash photolysis

Laser flash photolysis for detecting trapped photo-excited electron was carried out. The results Pt/CrTa-TiO_2(A) x=0.02, CrTa-TiO_2(A) x=0.02, Pt/CrTa-TiO_2(R) x=0.009 , and CrTa-TiO_2(R) x=0.009 of time variation is shown in figure 2.14.

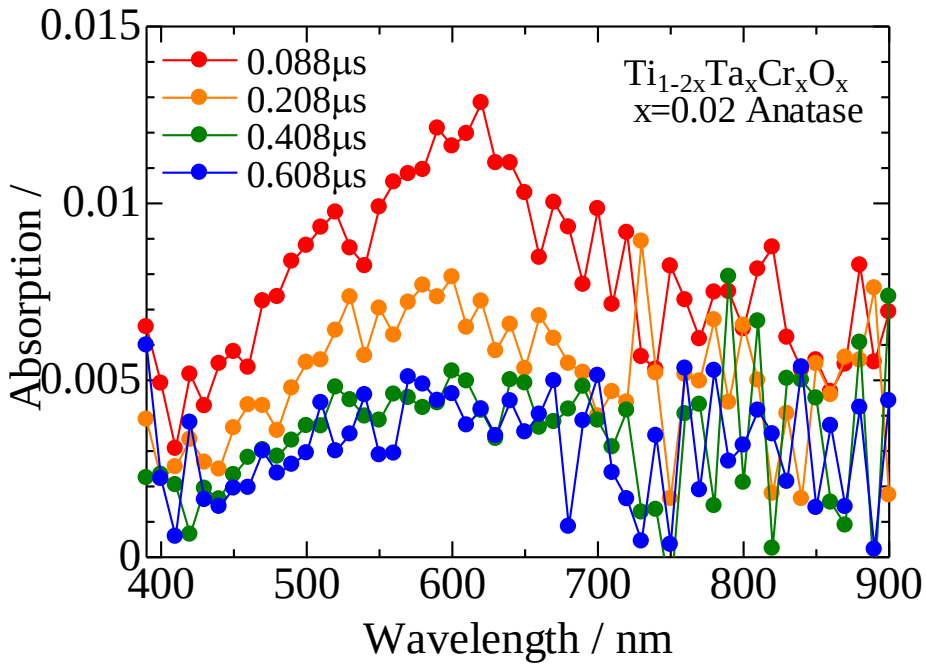

(a) Light absorption of CrTa-TiO_2(A) x=0.02

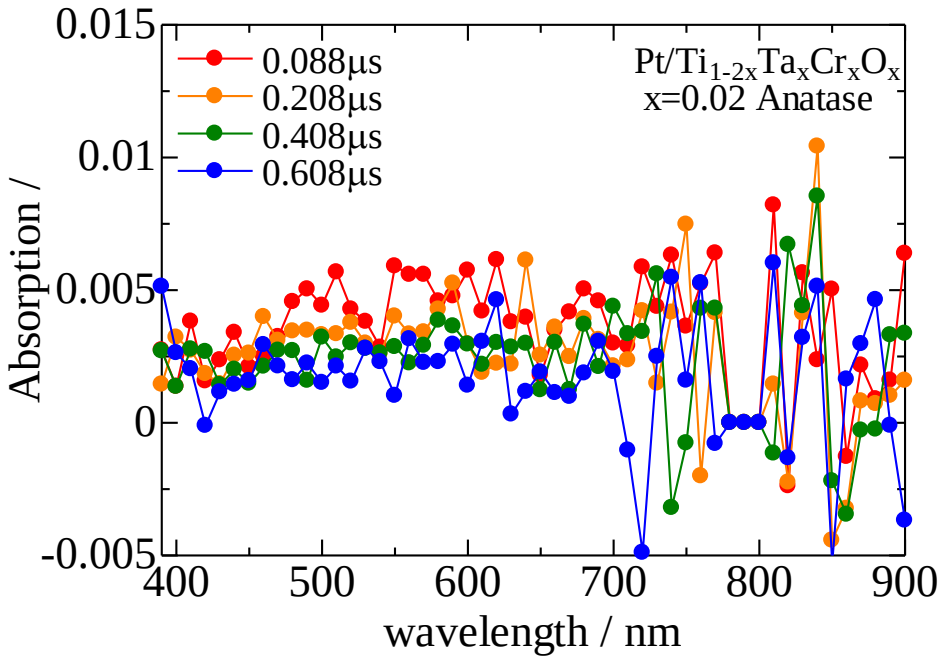

(b) Light absorption of Pt/CrTa-TiO_2(A) x=0.02

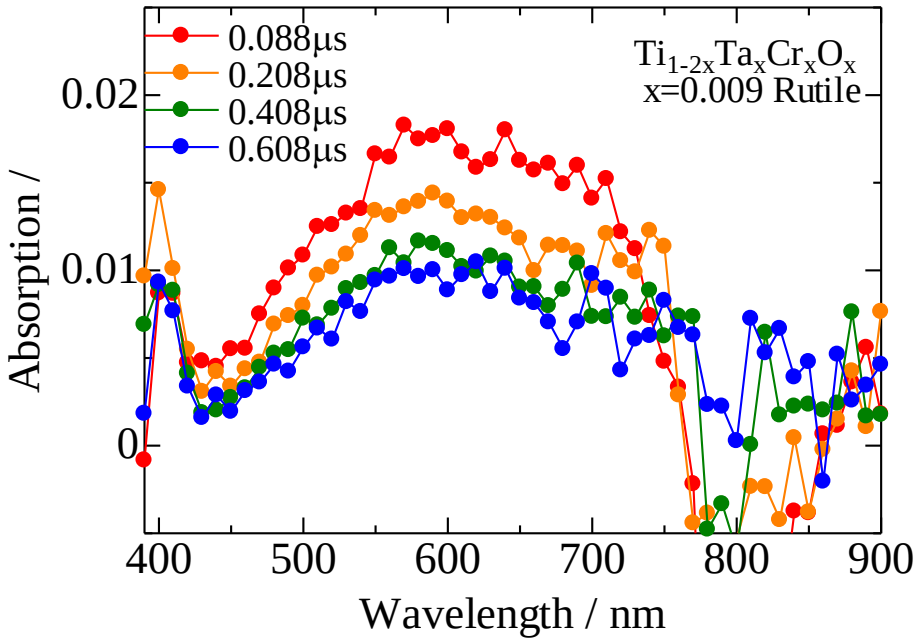

(c) Light absorption of CrTa-TiO_2(R) x=0.009

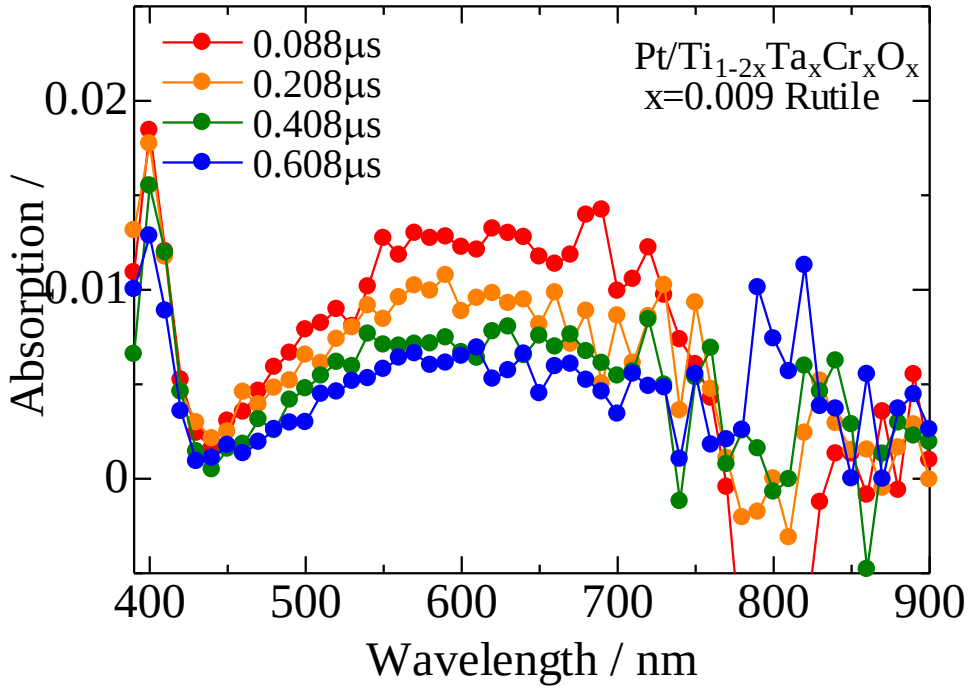

(d) Light absorption of Pt/CrTa-TiO_2(R) x=0.009

Fig.2.14 (a)-(d) time variation of light absorption

From these results of time variation of light absorption, photo-generated electron in Cr,Ta-TiO_2(A), hydrogen evolution photocatalyst, estimated to trapped at platinum deposited on sample surface. In contrast, photo-generated electron in Cr,Ta-TiO_2(R), oxygen evolution photocatalyst, estimated to trapped at shallow trapping site. The different behavior of electron can be considered from the difference of photocatalytic activity, hydrogen evolution photocatalyst and oxygen evolution photocatalyst.

2.4.9 Action spectrum

Wavelength dependence of photocatalytic reaction was measured and the results are shown in figure 2.15. Hg-Xe lamp with spectroscope was employed as light source. Experimental condition of this reaction was written in below. Sample amount; 60 mg, sacrificial agent; $AgNO_{3aq}$ (0.01M) 10 mL or methanol (20 vol%) 10 mL.

Apparent quantum efficiency (AQE) was calculated by following equation.

$$\text{AQE (\%)} = \frac{2 \times H_2 evolution\ rate}{incident\ photon\ rate} \times 100$$

$$\text{AQE (\%)} = \frac{4 \times O_2 evolution\ rate}{incident\ photon\ rate} \times 100$$

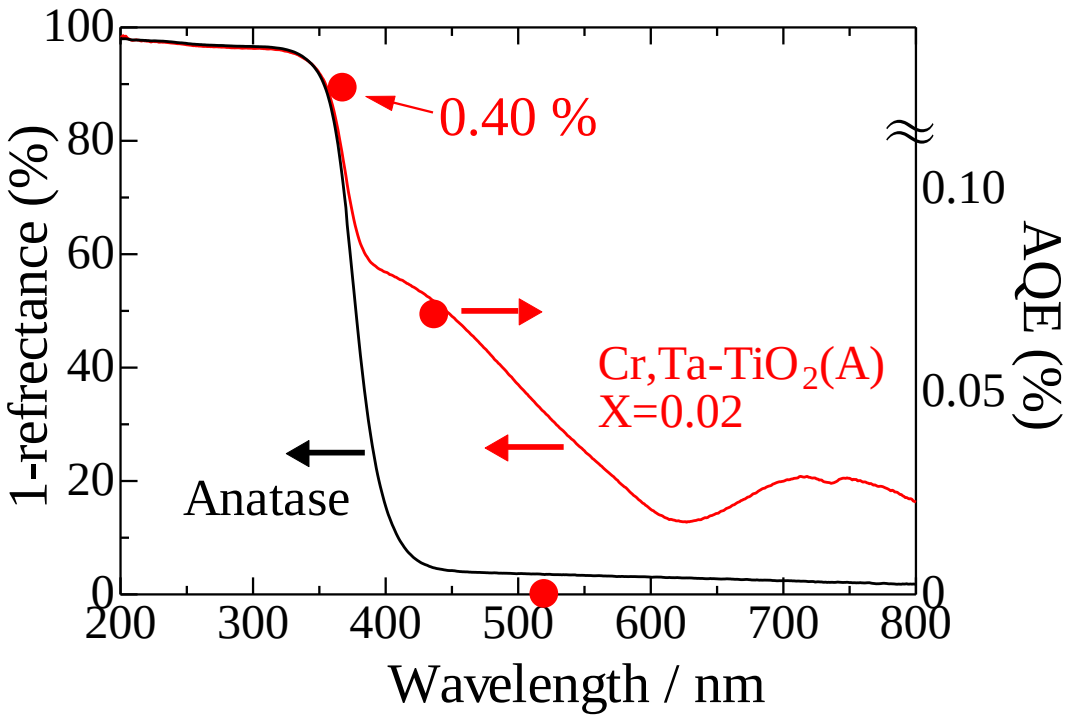

(a) Action spectrum of hydrogen evolution photocatalyst

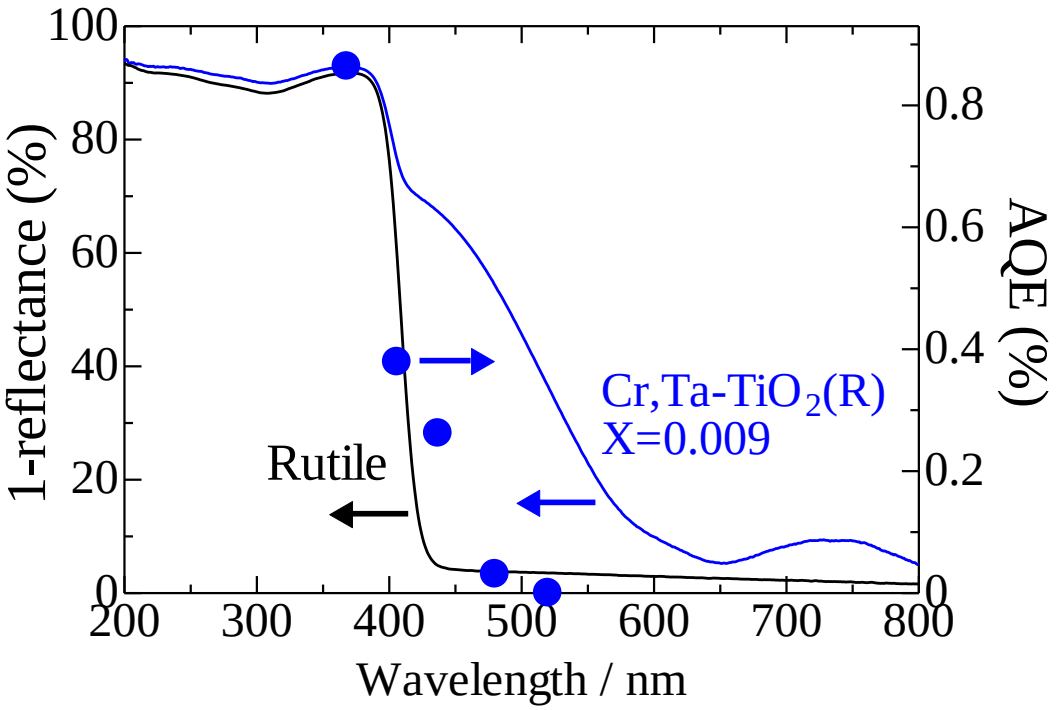

(b) Action spectrum of oxygen evolution phtocatalyst

Fig2.15 Action spectrum of (a) hydrogen evolution photocatalyst and (b) oxygen evolution photocatalyst

According to the results, both samples can be able to visible light up to around 520 nm. However, for formation of isolated mini-band, AQE of these samples don't fit with absorption spectrum. In addition, for rich amount of doping in oxygen evolution photocatalyst, AQE in visible light region also don't fit with the absorption spectrum.

2.4.10 Water splitting reaction

The results of water splitting reaction of constructed Z-scheme system using Pt/Cr,Ta-TiO_2 (A) x=0.02 and Pt/Cr,Ta-TiO_2 (R) x=0.009 are shown below. Xe-lamp with an optimal filter was employed in Figure 2.16 and LED lamp was employed in Figure 2.17.

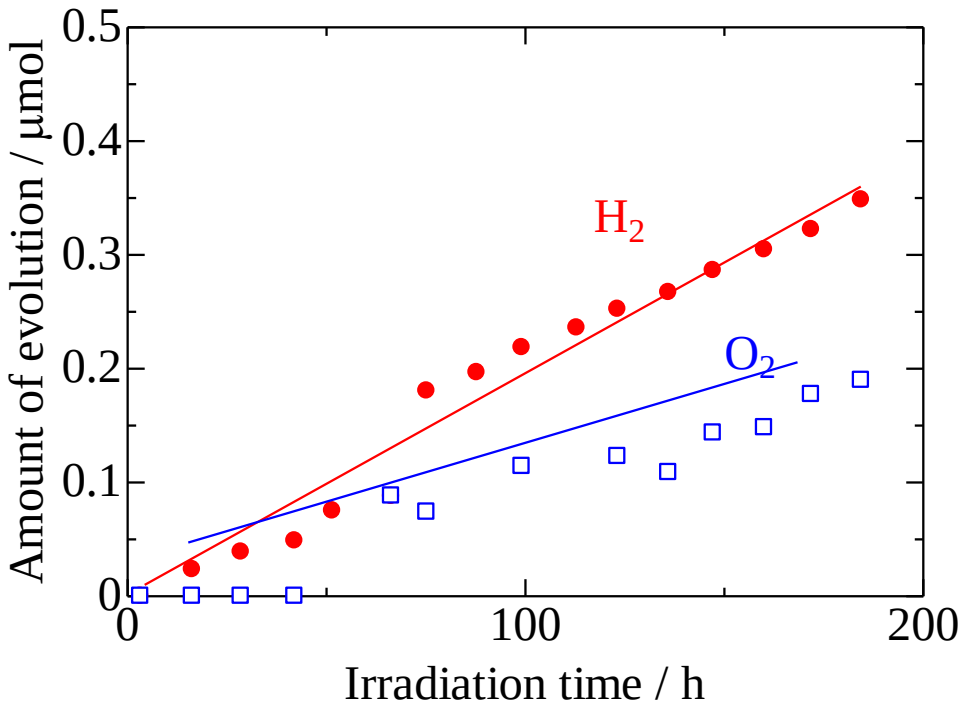

Fig.2.16 water splitting reaction

Experimental condition; H_2-evolution sample: Pt/Cr,Ta-TiO_2 (A) x=0.02 80 mg, O_2-evolution sample: Pt/Cr,Ta-TiO_2 (R) x=0.009 20 mg, redox solution: I-/IO_3-, light source: Xe lamp + Y-44 optimal filter.

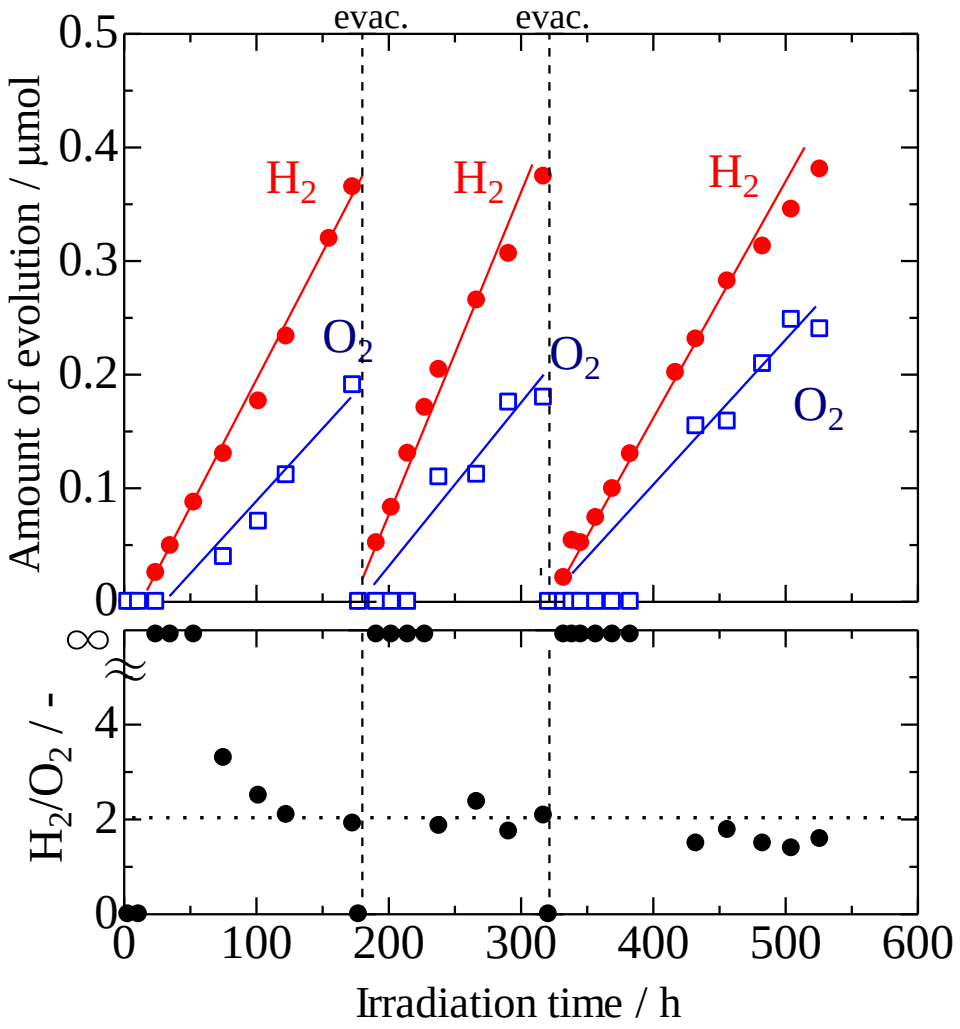

Fig.2.17 water splitting reaction

Experimental condition; H_2-evolution sample: Pt/Cr,Ta-TiO_2 (A) x=0.02 90 mg, O_2-evolution sample: Pt/Cr,Ta-TiO_2 (R) x=0.009 10 mg, redox solution: I-/IO_3-, Light source: LED420 nm

Those figures indicate hydrogen and oxygen were generated simultaneously and stoichiometry from the constructed Z-scheme system under visible light irradiation. The difference of sample amounts of hydrogen evolution photocatalyst and oxygen evolution photocatalyst is according to the poor AQE of hydrogen evolution photocatalyst.

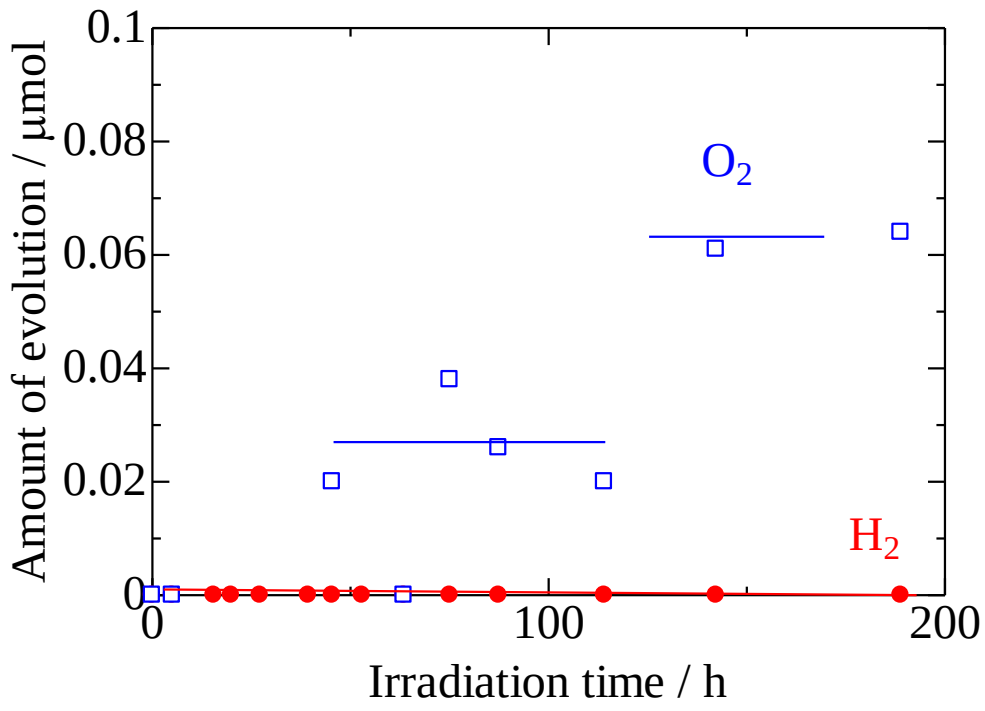

Fig.2.18 water splitting reaction

Experimental condition; H_2-evolution sample: Cr,Ta-TiO_2 (A) x=0.02 90 mg, O_2-evolution sample: Pt/Cr,Ta-TiO_2 (R) x=0.009 10 mg, redox solution: I-/IO_3-, Light source: LED420 nm

Water splitting reaction without platinum co-catalyst on hydrogen evolution photocatalyst was also investigated. According to the result, no hydrogen was detected and little oxygen was detected. That means water splitting reaction in this Z-scheme system did not worked well.

Turn over number (TON) of the reaction shown in figure 2.17 was calculated with below equation. Here, from the result of water splitting reaction of Cr,Ta-TiO2(A) and Pt/Cr,Ta-TiO2(R), figure 2.18, platinum works as hydrogen evolution site. Therefore TON was calculated from hydrogen generated amount and platinum amount on hydrogen evolution photocatalyst. From the result, the number was over 1, this mean the water splitting reaction proceeding catalytically.

$$\mathrm{TON} = \frac{product\ amount}{reaction\ site} = \frac{hydrogen\ evolution\ amount}{platinum\ amount} \cong 1.1$$

2.4.11 Isotope labelled water splitting

Photocatalytic overall water-splitting tests were also conducted with the Pt/Cr,Ta-TiO_2(A) and Pt/Cr,Ta-TiO_2(R) powders suspended in 10 mL of I^-/IO_3^- solutions containing 30% isotopic water ($H_2{}^{18}O$, Sigma-Aldrich, purity 97atom% ^{18}O) under the same conditions as the reaction which archived overall water splitting using LED420 nm. Evolved gas was detected by a gas chromatograph mass spectrometer (GCMS, GCMS-QP 2010 Ultra, Shimadzu) operated in selective-ion mode to monitor for 28 (N_2), 32 ($^{16}O^{16}O$), 34 ($^{16}O^{18}O$), 36($^{18}O^{18}O$) ions. Natural isotopic compositions of ^{16}O, ^{17}O, and ^{18}O are 99.757, 0.038, and 0.205 atm%, respectively [11]. Then, the compositions of $^{32}O_2$ ($^{16}O^{16}O$), $^{34}O_2$ ($^{16}O^{18}O$, $^{17}O^{17}O$), and $^{36}O_2$ ($^{18}O^{18}O$) in the atmospheric condition are calculated to be 99.515, 0.409, and 0.000420 atm%, respectively. We plotted the calculated $^{16}O^{18}O$ and $^{18}O^{18}O$ values using the following equation provided that the $^{14}N^{14}N$ was observed as the result of air contamination from outside as mentioned above.

$$^{16}O^{18}O = obs.{}^{16}O^{18}O - \left(obs.N_2 \times \frac{0.21}{0.78}\right) \times 0.409 \times 10^{-2}$$

$$^{18}O^{18}O = obs.{}^{18}O^{18}O - \left(obs.N_2 \times \frac{0.21}{0.78}\right) \times 0.000420 \times 10^{-2}$$

In fact, $^{18}O^{18}O$ was considered to be equal to obs.$^{18}O^{18}O$ due to the extremely small value of 0.000420×10^{-2}.

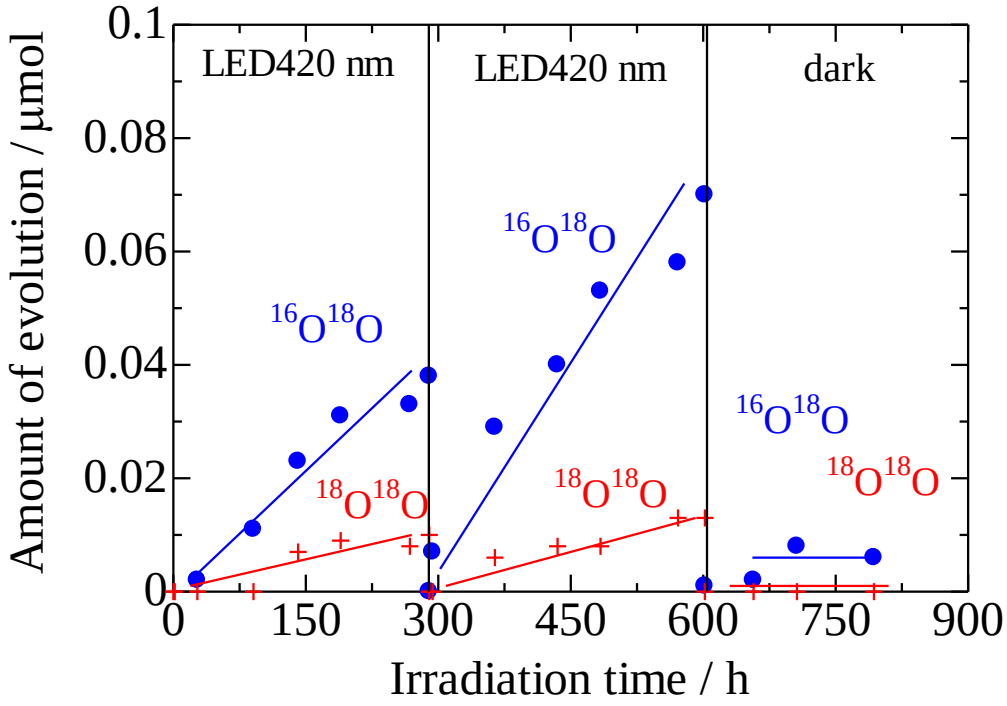

Fig.2.19 Isotope labelled water splitting

For air commingling, $^{16}O^{16}O$ was not measured correctly. Therefore $^{16}O^{16}O$ was removed from this figure. In contrast, $^{16}O^{18}O$ and $^{18}O^{18}O$ were detected with the ratio of 4:1 this mean isotopic oxygen was generated from isotopic water. Because, the ratio of $^{16}O^{16}O$: $^{16}O^{18}O$: $^{18}O^{18}O$ generated from 30 % of isotopic water was calculated to 5 : 4: 1. Therefore, this result also indicates overall water splitting of this Z-scheme system was proceeding under visible light irradiation.

2.5 short summary

Titanium dioxide based hydrogen evolution photocatalyst and titanium dioxide based oxygen evolution photocatalyst were prepared. Z-scheme system constructed of these samples split water to hydrogen and oxygen under visible light irradiation with redox mediator. Therefore we succeeded to prepare titanium dioxide based Z-scheme system and archived overall water splitting under visible light irradiation. The water splitting reaction is estimated to proceed to the scheme shown in figure 2.20.

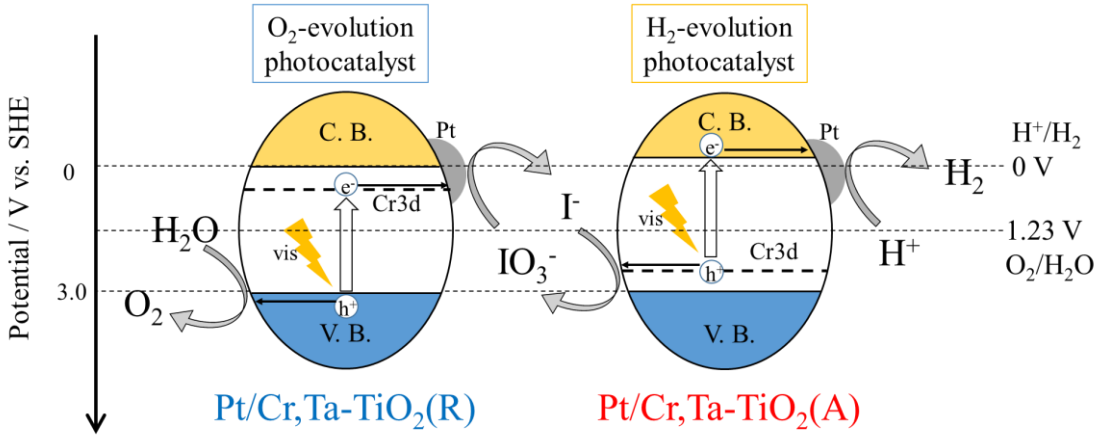

Fig.2.20 water splitting mechanism

References

[1] N. Lei, T. Kitta, N. Kumagai, B. Ohtani, K. Hashimoto, H. Irie, *J. Ceram. Soc. Jpn.*, **121**, 563 (2013)

[2] S. Hara, M. Yoshimizu, S. Tanigawa, L. Ni, B. Ohtani, H. Irie, *J. Phys. Chem. C*, **116**, 17458 (2012)

[3] S. Tanigawa, H. Irie, *App. Catal. B*, **180**, 1 (2016)

[4] N. Lei, M. Tanabe, H. Irie, *Chem. Comm.*, **49**, 10094 (2013)

[5] R.D. Shannon, C.T. Prewitt, *Acta Crystallogr. Sect. B*, **25**, 925 (1969)

[6] S. Klosek, D. Raftery, *J. Phys. Chem. B*, **105**, 2815 (2001)

[7] R. Niishiro, R. Konta, H. Kato, W.J. Chun, K. Asakura, A. Kudo, *J. Phys. Chem. C*, **111**, 17420 (2007)

[8] T. Umebayashi, T. Yamaki, H. Itoh, K. Asai, *J. Phys. Chem. Solids*, **63**, 1909 (2002)

[9] C.D. Valentin, G. Pacchioni, H. Onishi, A. Kudo, *Chem. Phys. Lett.*, **469**, 166 (2009)

[10] A.A. Ismail, D.W. Bahnemann, I. Bannat, M. Wark, *J. Phys. Chem. C*, **113**, 7429 (2009)

[11] K.J.R Rosman, P.J.P. Taylor, *Pure Appl. Chem.*, **70**, 217 (1998)

3. Z-scheme system consisted of TiO_2 and $SrTiO_3$

3.1 Sample preparation

In this section, new hydrogen evolution photocatalyst, rhodium doped strontium titanate ($SrTi_{0.99}Rh_{0.01}O_3$ (Rh-STO)) was employed. [1-2] As oxygen evolution photocatalyst chromium tantalum co-doped titanium dioxide rutile, ($Ti_{0.986}Cr_{0.007}Ta_{0.007}O_2$Rutile (Cr,Ta-$TiO_2$(R)) which has one of the highest oxygen evolution activity in chapter 2 was employed. [3-4] Using these stable oxide photocatalysts, we set out to split water under visible light irradiation and improve water splitting activity.

Band structure of chromium and tantalum co-doped titanium dioxide was controlled to form Cr 3d isolated mini-band below conduction band. In contrast, band structure of rhodium doped strontium titanate was controlled the valence band top shift to be negative, by forming mixture orbital of O 2p and Rh 3d. The image of band structure and water splitting scheme is shown in Figure 3.1. And it will work as the same to the titanium dioxide based Z-scheme system.

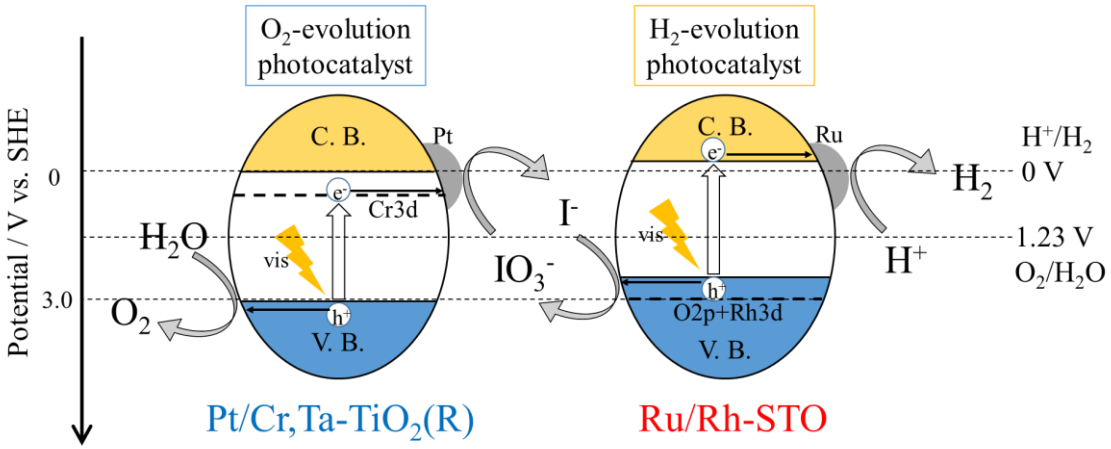

Fig.3.1 water splitting mechanism

3.1.1 Preparation of doped titanium dioxide sample

Chromium and tantalum co-doped titanium dioxide ($Ti_{0.986}Cr_{0.007}Ta_{0.007}O_2$Rutile (Cr,Ta-$TiO_2$(R)) was prepared by hydrothermal synthesis method. Commercial $Ti(SO_4)_2$ (purity 24.0%, Kanto Kagaku), $CrCl_3 \cdot 6H_2O$ (purity 93.0%, Kanto Kagaku),

and $TaCl_5$ (Kanto Kagaku) as starting materials were mixed and stirred in distilled water for 30 minutes using magnetic stirrer. Then, the solutions were poured into an autoclave and treated hydrothermally at 140 °C for 12 h, and the resulting mixtures were washed with sufficient distilled water, collected by centrifugation, and dried at 80 °C overnight. The dried samples were calcined at 900 ^{o}C for 24 h to obtain rutile titanium dioxide. At last, obtained samples were thoroughly ground using a mortar and pestle. As a reference, non-doped rutile (TiO_2(R)) was prepared under identical conditions using only $Ti(SO_4)_2$.

3.1.2 Preparation of doped strontium titanate sample

Rhodium doped strontium titanate ($SrTi_{0.99}Rh_{0.01}O_3$ (Rh-STO)) was prepared by conventional solid state reaction. [2] Commercial $SrCO_3$ (Kanto Kagaku, purity 99.9%), TiO_2 (High Purity Chemicals, purity 99.99%), and rhodium oxide (Rh_2O_3, Kanto Kagaku, purity 99.9%) powders were used as the starting materials. Stoichiometric amounts of the starting materials for Rh-STO were wet-ball milled identically. The resulting mixture was calcined at 1000 °C for 10 h and then thoroughly ground to obtain Rh-STO powder. As a reference, non-doped $SrTiO_3$ was prepared under identical conditions using only $SrCO_3$ and TiO_2.

3.2 Deposition of co-catalyst

Deposition of platinum or ruthenium co-catalyst onto prepared photocatalyst was performed by a photo-deposition method. 0.5 g of sample powder was first dispersed in 100 mL methanol solution (20 vol%) as a hole scavenger. $H_2PtCl_6 \cdot 6H_2O$ (purity 98.5 %, Kanto Kagaku) as the source of Pt was then weighed to give a weight fraction of Pt relative to the sample of 1×10^{-3}. Ruthenium chloride ($RuCl_3 \cdot nH_2O$, n was assumed to be 3), which served as the source of Ru, was then weighed to give a weight fraction of Ru relative to Rh-STO of 7×10^{-3}. The weighed $H_2PtCl_6 \cdot 6H_2O$ or $RuCl_3 \cdot nH_2O$ was added to the aqueous suspension in which either photocatalyst was dispersed, and then the

suspension was sufficiently deaerated using liquid nitrogen (N_2). While deaerating, a xenon lamp (LA-251 Xe; Hayashi Tokei) with an optical filter (Y-44, Hoya) was employed for light irradiation of the suspension for 4 h. The suspension was then centrifuged and washed with distilled water. The resulting residues were dried at 80 ^oC overnight and then ground into a fine powder using an agate mortar. Finally, Pt-deposited Cr,Ta-TiO_2(R) (Pt/Cr,Ta-TiO_2(R)) and Ru-deposited Rh-STO (Ru/ Rh-STO) photocatalyst powders were obtained.

3.3 Characterization

Prepared samples were characterized by X-Ray Diffraction (XRD) (Panalytical, PW-1700 system) to measure the crystal structure and UV-vis diffuse reflectance spectroscopy (UV-vis DRS) (JASCO, V-650) to measure the absorbance of sample. Samples were also characterized by Scanning Electronic Microscopy (SEM) (JEOL, JSM-6500F) and scanning transmission electron microscope (STEM, Tecnai Osiris, FEI) to check the sample shape. Brunauer-Emmett-Teller (BET) surface areas were determined using a nitrogen adsorption apparatus (Micromeritics, TriStar 3000; Shimadzu). The valency of the constituent elements was measured by X-ray photoelectron spectroscopy (XPS) (Shimadzu, Axis-Ultra). Quantitative analyses were also performed by X-ray Fluorescence (XRF) using a ZSXP PrimusII system (Rigaku). Photocatalytic activities of these samples were measured using a gas-closed-circulation system (Makuhari glass, CLS-1370-PSWG).

3.4 Results and discussion

3.4.1 X-ray diffraction

The crystal structures of prepared samples are shown in Figure 3.2.

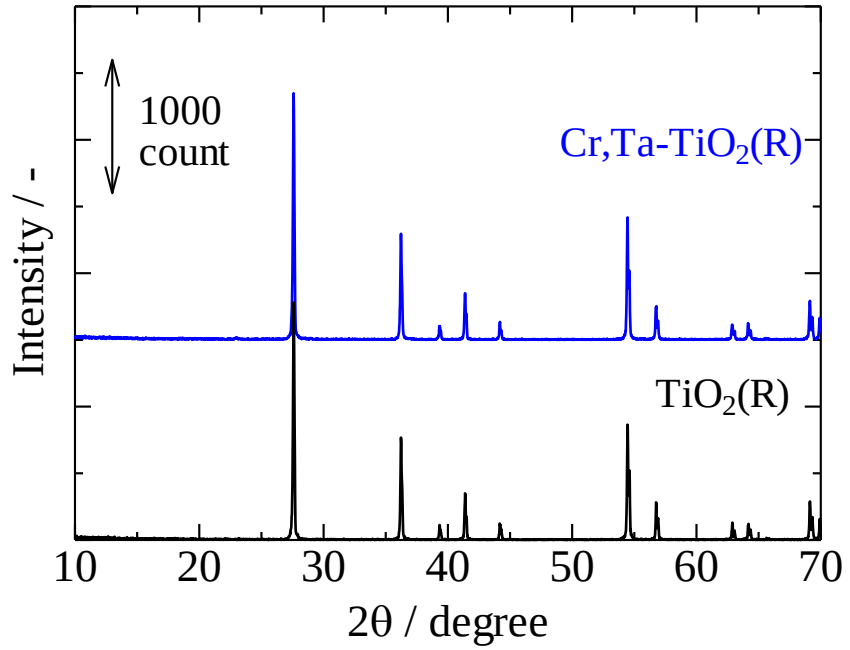

(a) XRD patterns of Cr,Ta-TiO_2

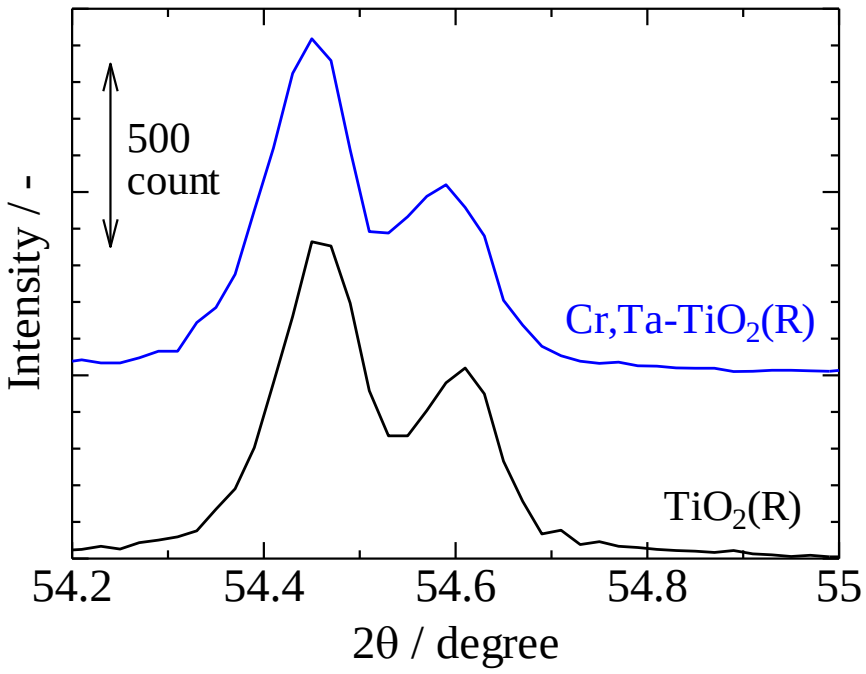

(b) Enlarged figure of (a)

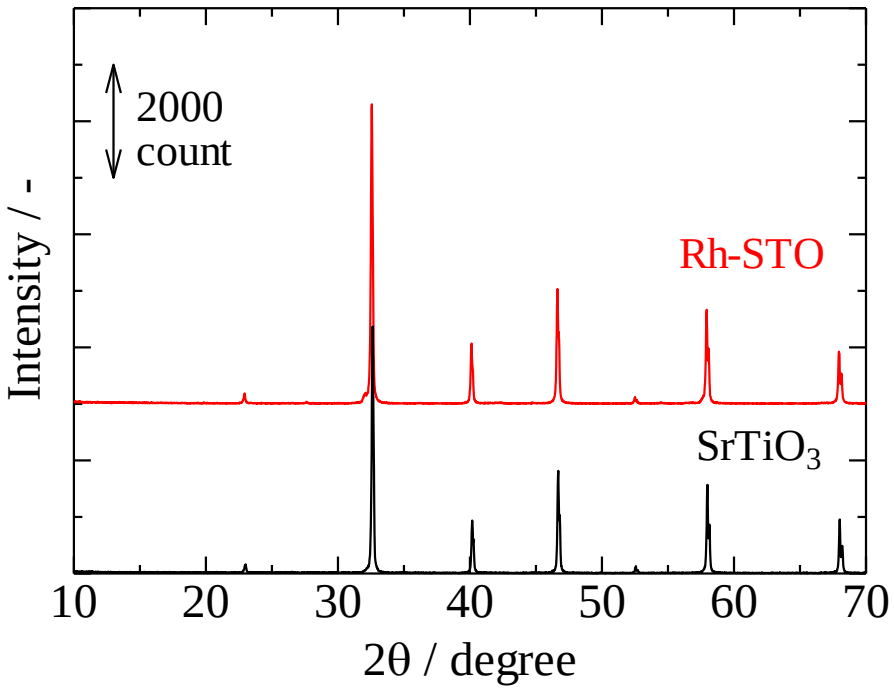

(c) XRD patterns of Rh-STO

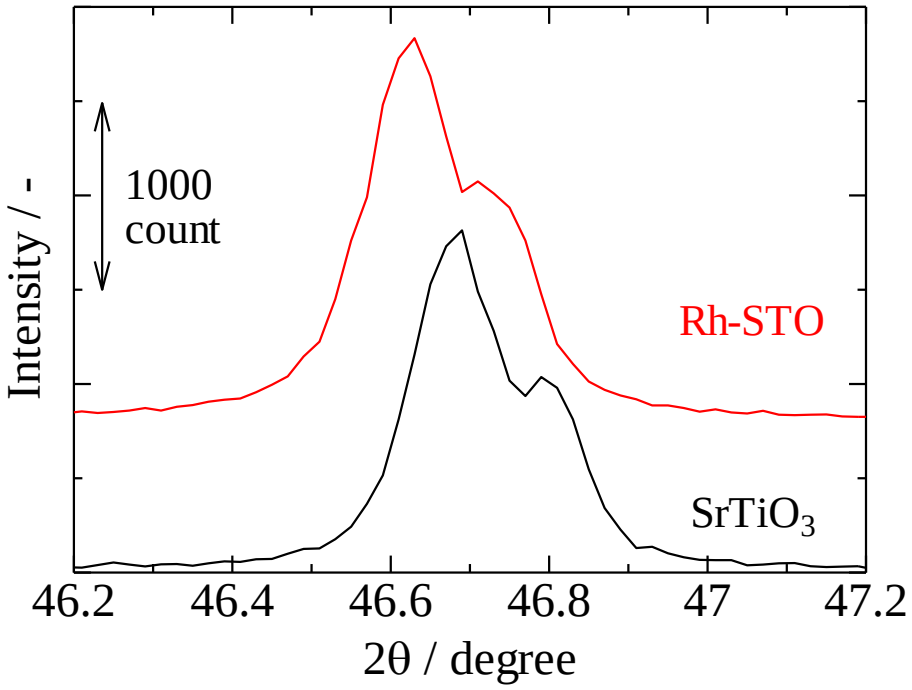

(d) Enlarged figure of (c)

Fig.3.2 XRD patterns of (a), (b) Cr,Ta-TiO_2(R) and (c), (d) Rh-STO

From the results, Cr,Ta-TiO_2 and Rh-STO have TiO_2 Rutile or $SrTiO_3$ single phase

according to their reference samples.

Figure 3.2 (b) and (d) show close upped XRD peaks of these samples. Doping of these samples was succeeded because XRD peak of these samples were shifted to lower angle. The effective ionic radii of Ti^{4+}, Cr^{3+}, and Ta^{5+} (six-coordination) are 0.0605, 0.0615 and 0.064 nm, respectively.[5] Therefore, we excluded that Cr and Ta ions were incorporated at Ti sites. According to Konda *et al*. [1], two different species of Rh (Rh^{3+} and a Rh species with a higher oxidation state than Rh^{3+}, such as Rh^{4+}) replaced Ti sites as dopants. Thus, we considered that Rh ions were incorporated at Ti sites in $SrTiO_3$.

3.4.2 UV-vis diffuse reflectance spectroscopy

UV-vis spectra of prepared samples are shown in Figure 3.3.

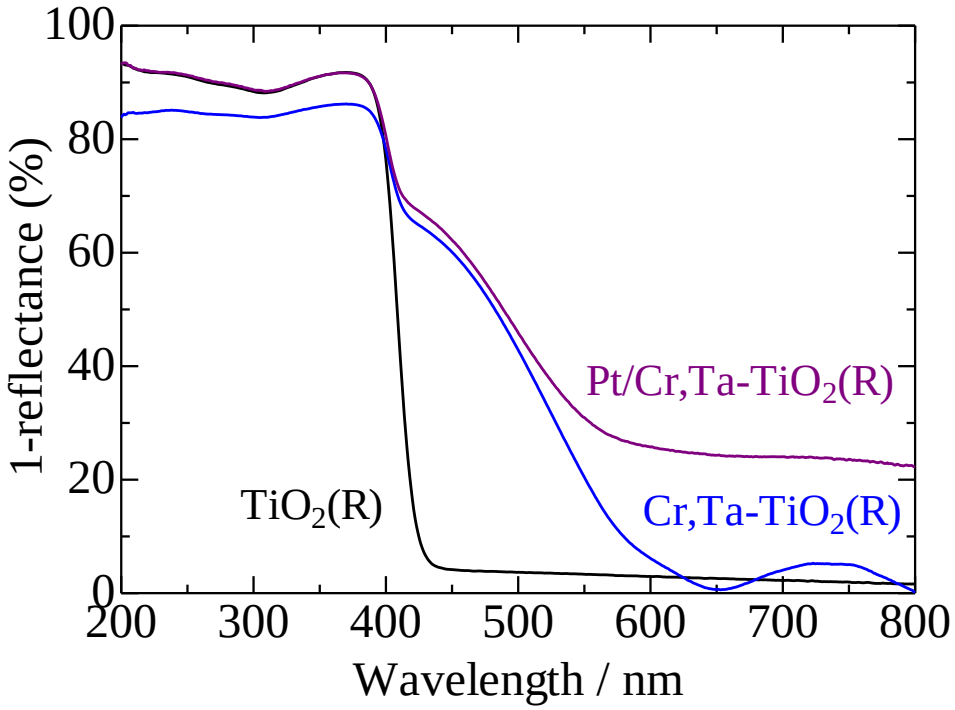

(a) UV-vis spectra of Cr,Ta-TiO_2

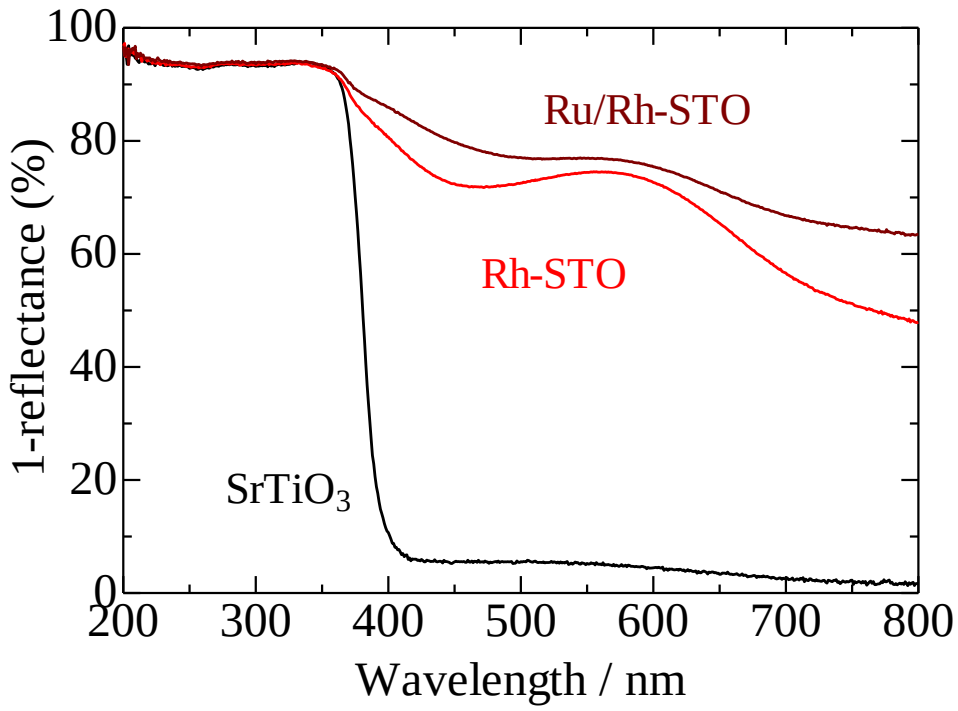

(b) UV-vis spectra of Rh-STO

Fig.3.3 UV-vis spectra of (a) TiO_2(R), Cr,Ta-TiO_2(R), and Pt/Cr,Ta-TiO_2(R) and (b) $SrTiO_3$, Rh-STO, and Ru/Rh-STO

Cr,Ta-TiO_2(R) have new absorption shoulder in visible light region. According to the results of chapter 2, Cr 3d isolated mini band was formed above valence band in forbidden band. Rh-STO shifted absorption edge to visible light region. According to these results and previous study [2], band gap of Rh-STO was estimated to be narrowed.

3.4.3 Scanning electron microscope

SEM images of prepared samples are shown in Figure 3.4.

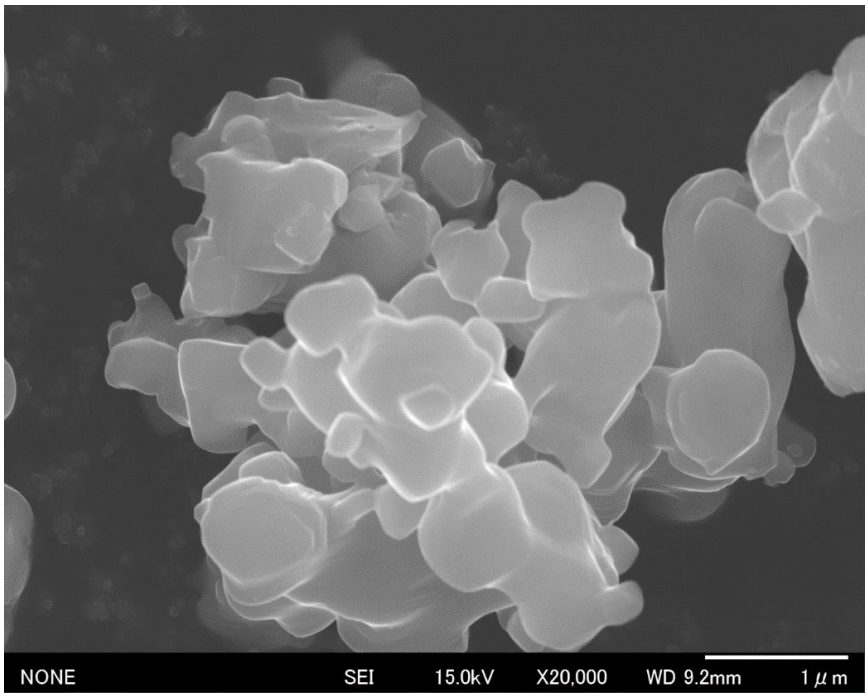

(a) Pt/Cr,Ta-TiO_2(R)

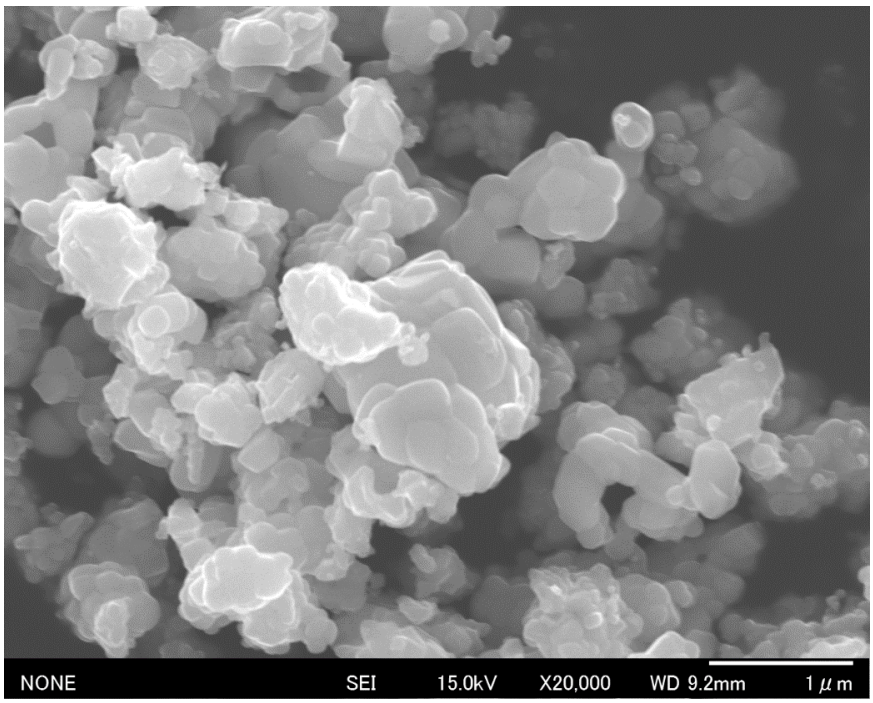

(b) Ru/Rh-STO

Fig.3.4 SEM images of (a) Pt/Cr,Ta-TiO_2 and (b) Ru/Rh-STO.

From the images of SEM, the particle sizes of Cr,Ta-TiO_2 and Rh-STO were estimated to have sizes of ~100 nm and ~50 nm, respectively. Additionally, both Cr,Ta-TiO_2 and Rh-STO particles were connected with each other, i.e ., "necking growth" was observed due to rather high calcination temperature and long calcination time (900°C for 24 h and 1000°C for 10 h).

3.4.4 Scanning transmission electron microscopy

STEM was carried out to observe co-catalysts on these prepared samples. These STEM images are shown in figure 3.5.

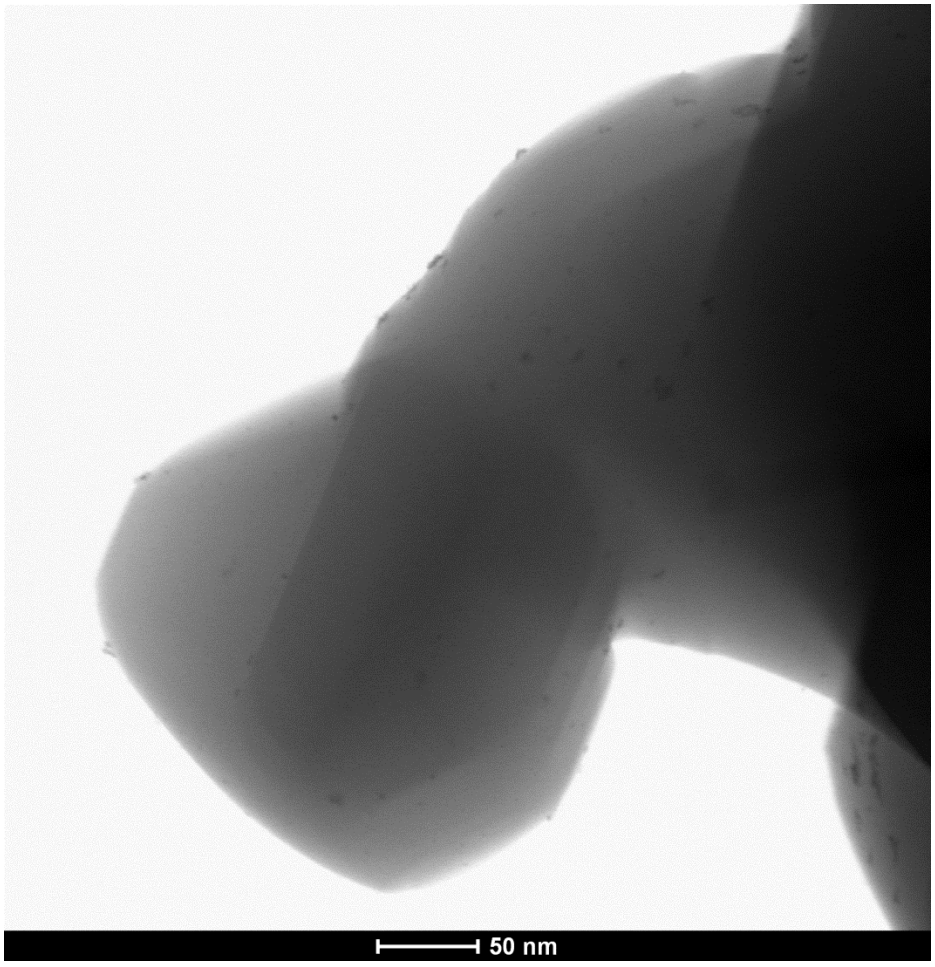

(a) Pt/CrTa-TiO_2(R)

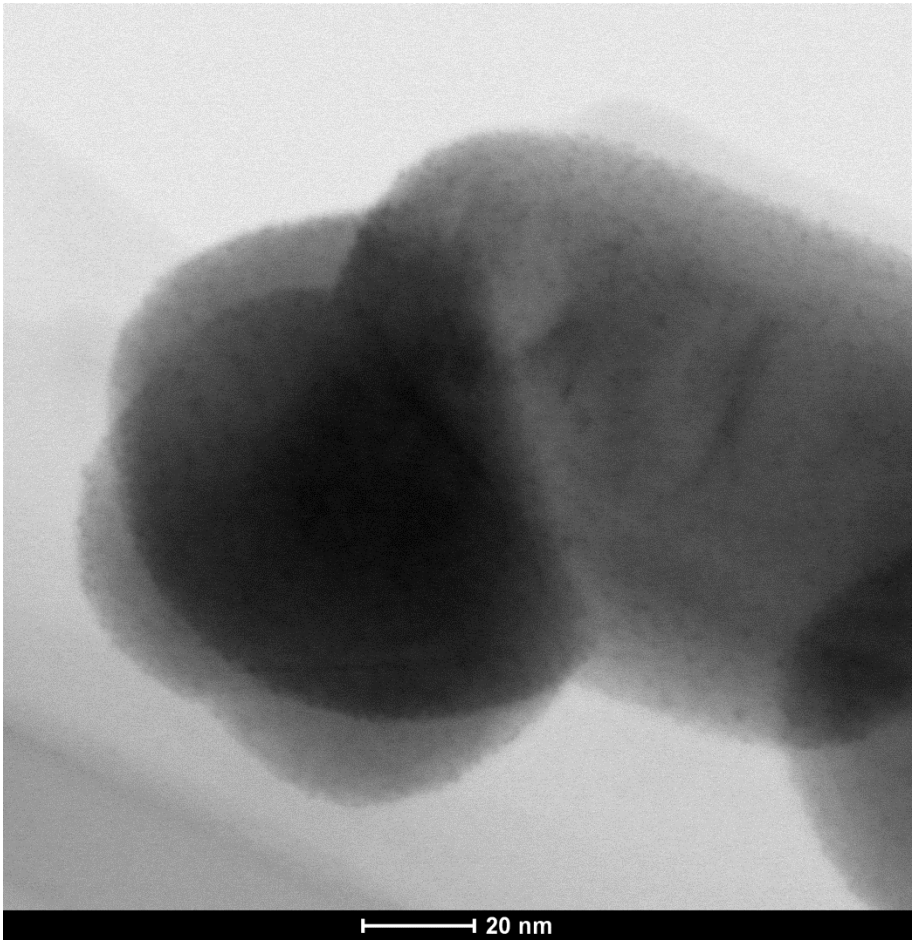

(b) Ru/Rh-STO

Fig.3.5 STEM images of (a) Pt/CrTa-TiO_2(R), (b) Ru/Rh-STO

From these STEM images, nanometer order of Pt on Cr,Ta-TiO_2 and Ru on Rh-STO could be observed. From these observations, we confirmed the deposition of Pt and Ru co-catalysts on Pt/Cr,Ta-TiO_2 and Ru/Rh-STO, respectively.

3.4.5 Brunauer-Emmett-Teller specific surface area

BET specific surface areas of CrTa-TiO_2(R) and Rh-STO were determined using a nitrogen adsorption apparatus. The equations which used to calculate specific surface area were described in chapter 2.4.4.

BET specific surface areas of Pt/CrTa-TiO_2(R) and Ru/Rh-STO were 1.43 m^2/g and 2.80 m^2/g, respectively. These results support the results of SEM that Cr,Ta-TiO_2(R) particle is larger than Rh-STO particle.

3.4.6 X-ray photoelectron spectroscopy

XPS of Cr,Ta-TiO_2(R), TiO_2(R), Rh-STO, and $SrTiO_3$ were measured and the results are shown in figure 3.6. All peaks were corrected by C1s peaks as 284.5 eV.

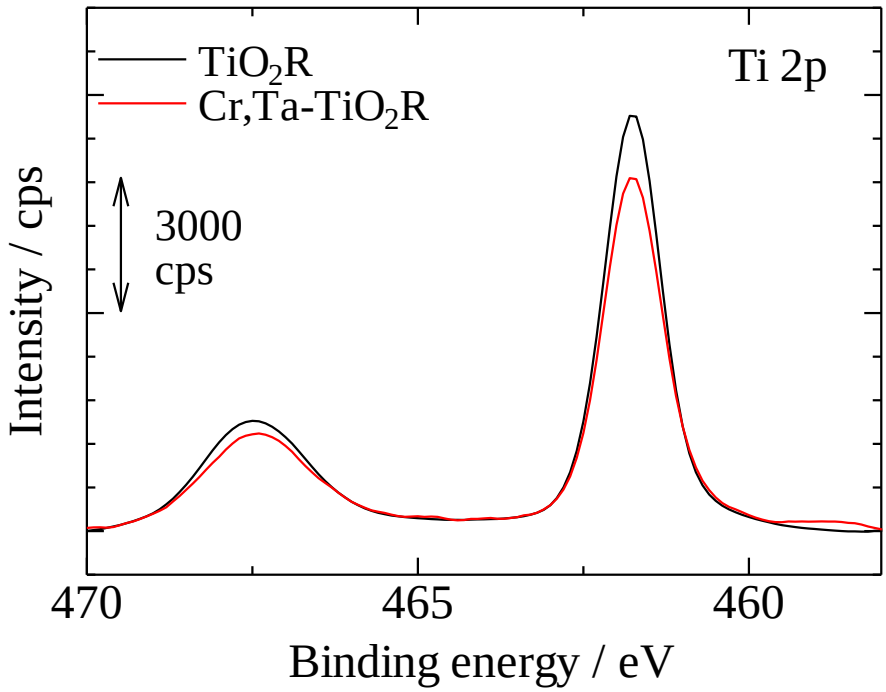

(a) Ti 2p peaks of TiO_2 based samples

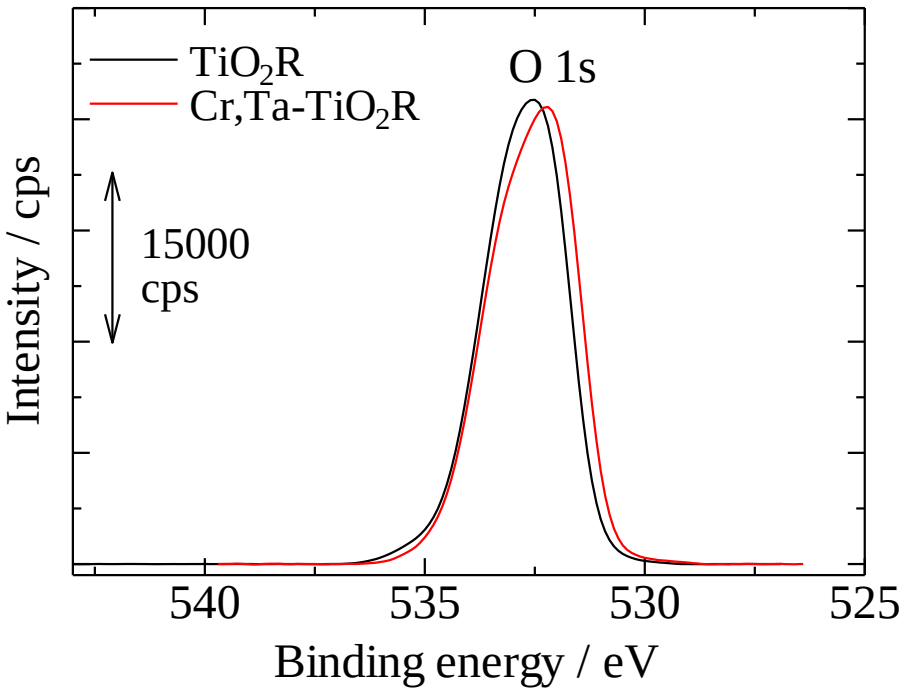

(b) O 1s peaks of TiO_2 based samples

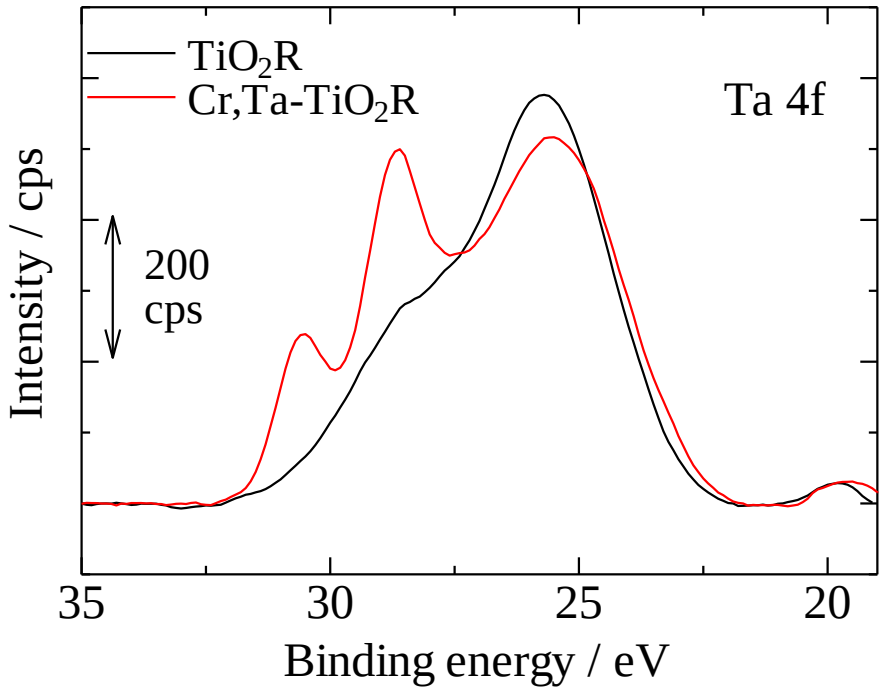

(c) Ta 4f peaks of TiO_2 based samples

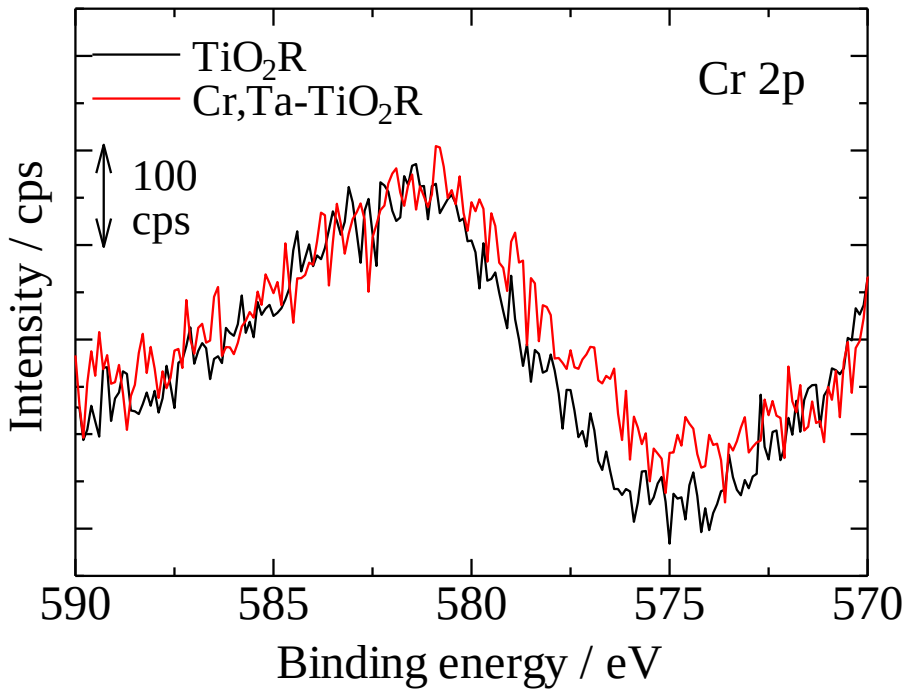

(d) Cr 2p peaks of TiO_2 based samples

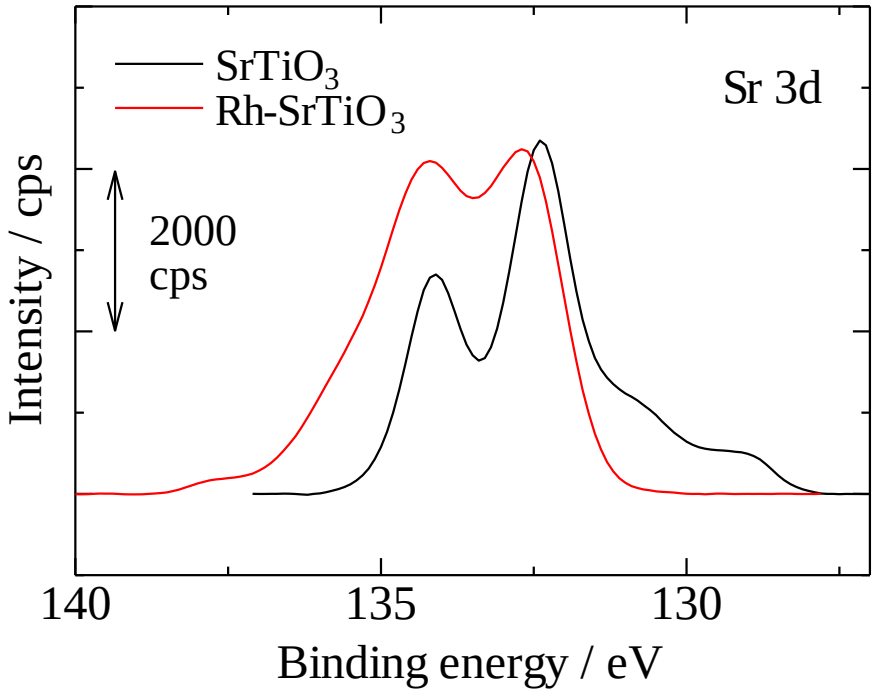

(e) Sr 3d peaks of $SrTiO_3$ based samples

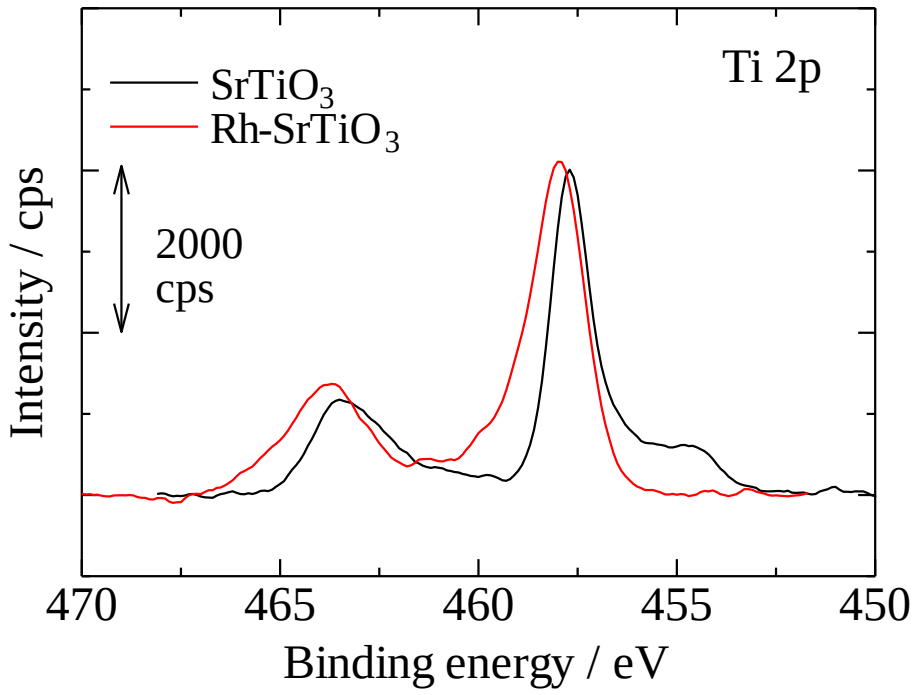

(f) Ti 2p peaks of $SrTiO_3$ based samples

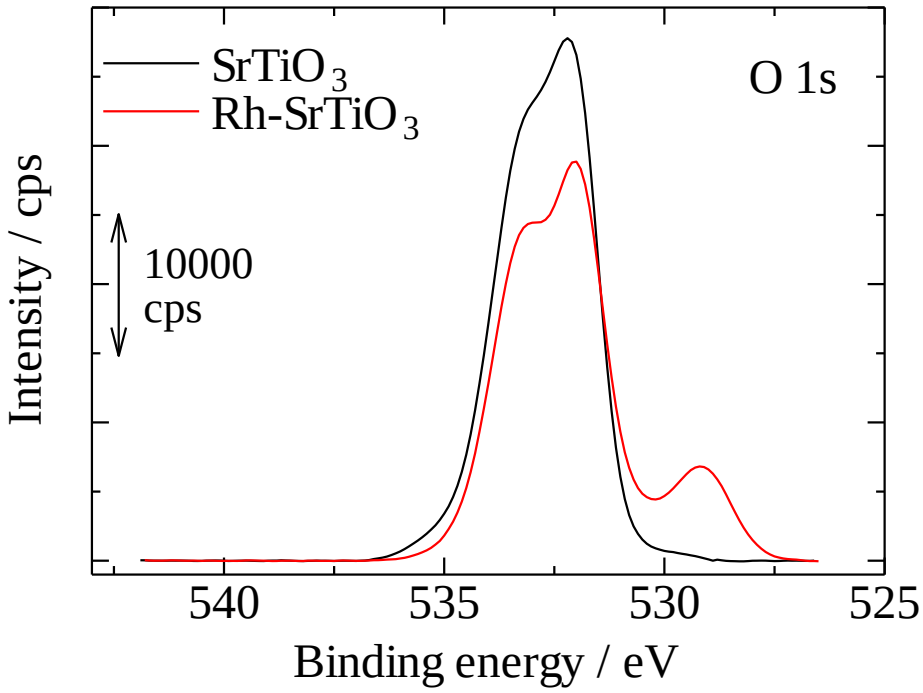

(g) O 1s peaks of $SrTiO_3$ based samples

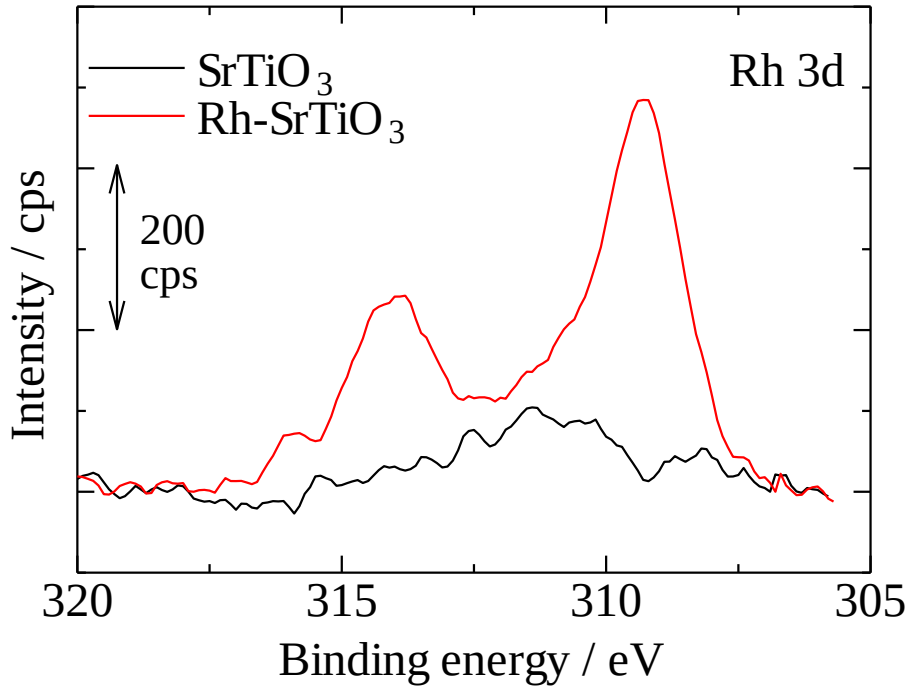

(h) Rh 3d peaks of $SrTiO_3$ based samples

Fig.3.6 XPS peaks of (a)(b)(c)(d) TiO_2 based samples and (e)(f)(g)(h) $SrTiO_3$ based samples

Figure 3.6(a)-3.6(d) show the spectra for the Ti 2p, O1s, Ta 4f, and Cr 2p orbitals, respectively, of the prepared TiO_2 and Cr,Ta-TiO_2 after calibration with the C 1s peak, derived from a conductive carbon-tape that had a binding energy of 284.5 eV. The spectra of Ti 2p of the prepared TiO_2 and Cr,Ta-TiO_2 were quite similar without any shoulder or peak at lower binding energy side (Figure 3.6(a)). Thus, the valency of Ti was 4+ in the prepared TiO_2 and Cr,Ta-TiO_2 [6-7]. The Cr 2p peaks derived from Cr3+ (Cr 2p3/2 at 576.9 eV and Cr2p1/2 at 587.0 eV [6]) and Ta 4f peaks from Ta5+ (Ta 4f7/2 at 26 eV and Ta 4f5/2 at 28 eV [8]) were observed only in Cr,Ta-TiO_2 as shown in Figure 3.6(c) and Figure 3.6(d), respectively. In Figure 3.6(b), the O 1s spectra are shown, however, they contain the spectra originated from the carbon tape. So, we are unable to discuss the valency of O and oxygen defects from these spectra. However, we consider that the prepared TiO_2 and Cr,Ta-TiO_2 do not have much oxygen defects because both of them contain Ti as Ti4+ and Cr,Ta-TiO_2 has Cr and Ta as Cr3+ and

Ta5+.

Figure 3.6 (e)-(h) show the spectra for the Sr 3d, Ti 2p, O1s, and Rh 3d orbitals, respectively, of the prepared $SrTiO_3$ and Rh-STO after calibration with the C 1s peak similarly. The Sr 3d spectrum peak positions (Sr3d5/2 at 132 eV and Sr 3d3/2 at 134 eV [9]) were quite similar both the prepared $SrTiO_3$ and Rh-STO. However, the spectrum shape of Rh-STO was different from reference of $SrTiO_3$ (Figure 3.6(e)). According to Ehre et al., the Sr 3d spectrum peak positions shift to higher energy region when $SrTiO_3$ becomes amorphous [9]. So, the Sr-O bonding in Rh-STO would be looser than that in $SrTiO_3$. As for Ti 2p, Rh-STO had shoulders at higher energy side (Figure 3.6(f)), indicating the existence of the structure similar to Ti_3O_5 [10]. So, the oxygen defects were presumably incorporated in Rh-STO. The Rh3d peaks were observed only in Rh-STO as shown in Figure 3.6(h). In Figure 3.6(g), the observed O 1s spectra contain those originated from the carbon tape. So, we are unable to discuss the valency of O and oxygen defects from these spectra. However, as mentioned above, Rh-STO possibly contains oxygen defects.

3.4.7 X-ray fluorescence

Elemental analyses by XRF were carried out and results are shown in Figure 3.7.

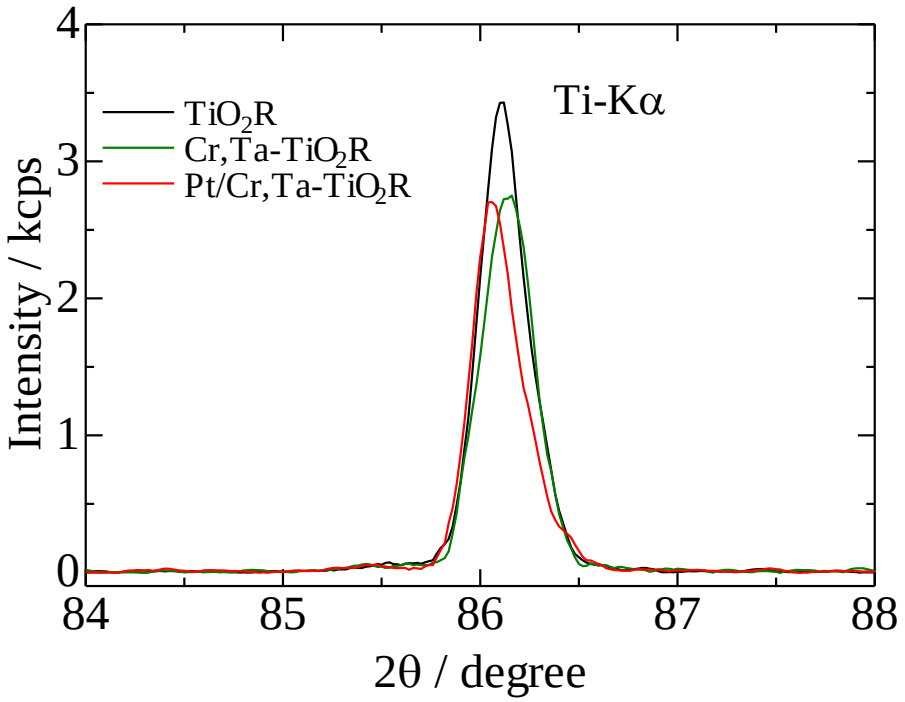

(a) Ti-Ka peaks of TiO_2 based samples

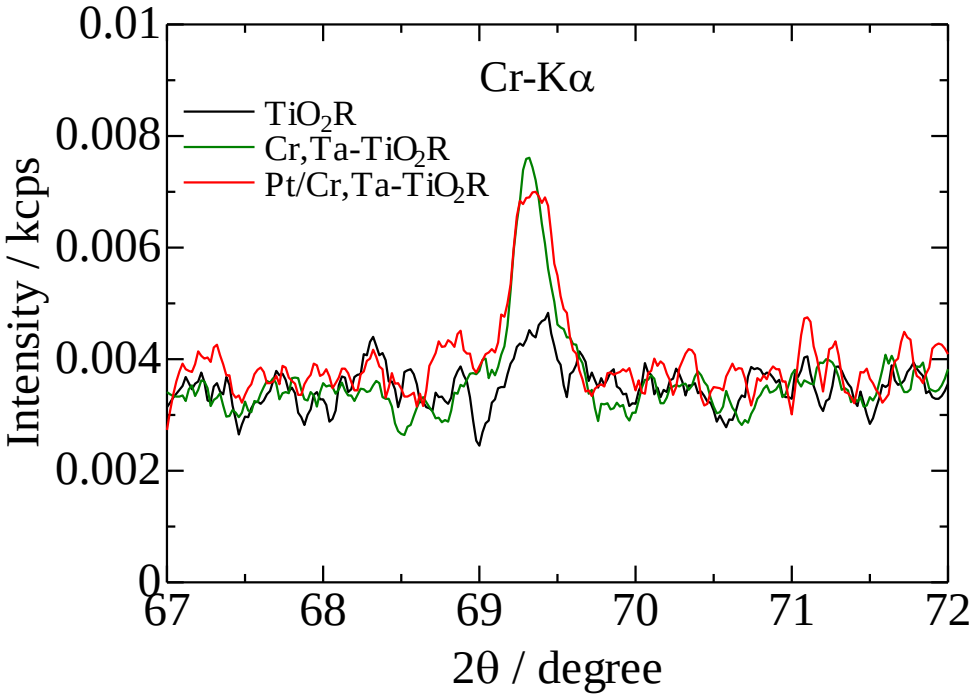

(b) Cr-Ka peaks of TiO_2 based samples

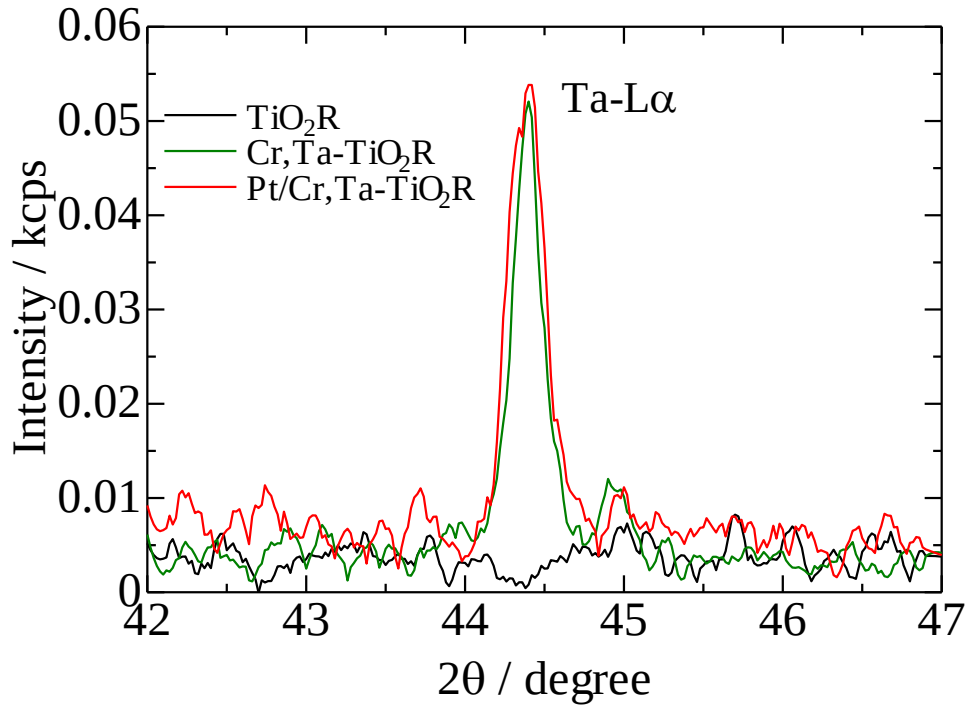

(c) Ta-La peaks of TiO_2 based samples

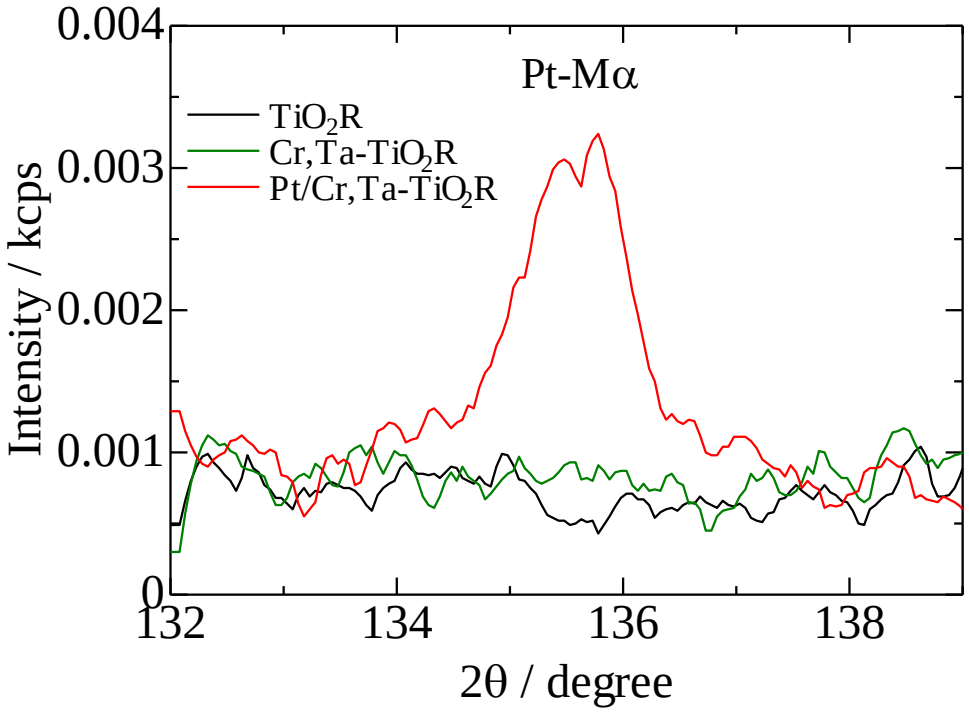

(d) Pt-Ma peaks of TiO_2 based samples

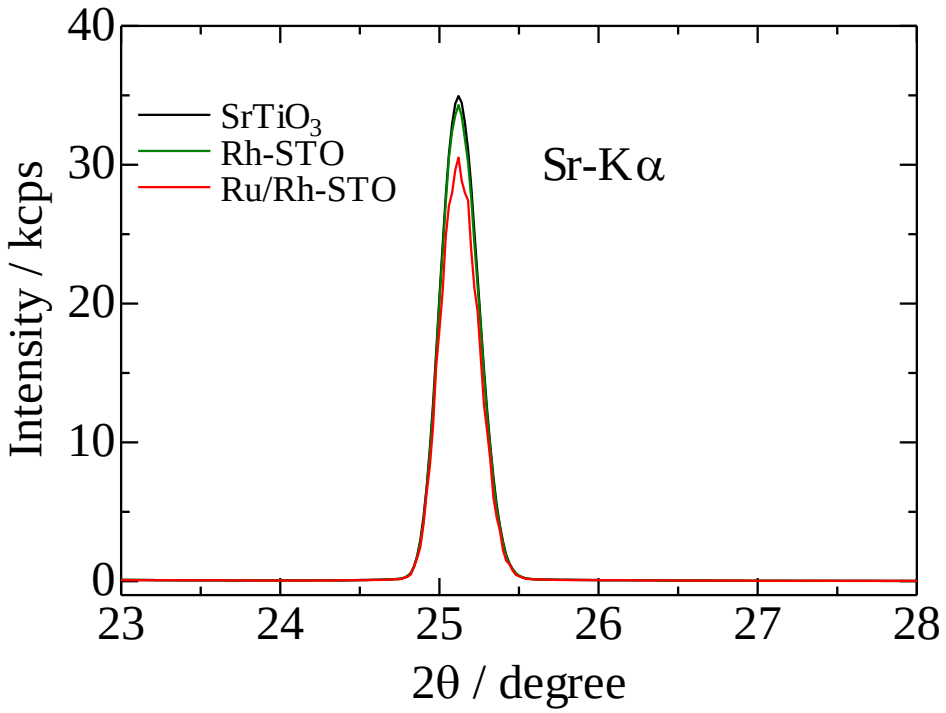

(e) Sr-Ka peaks of $SrTiO_3$ based samples

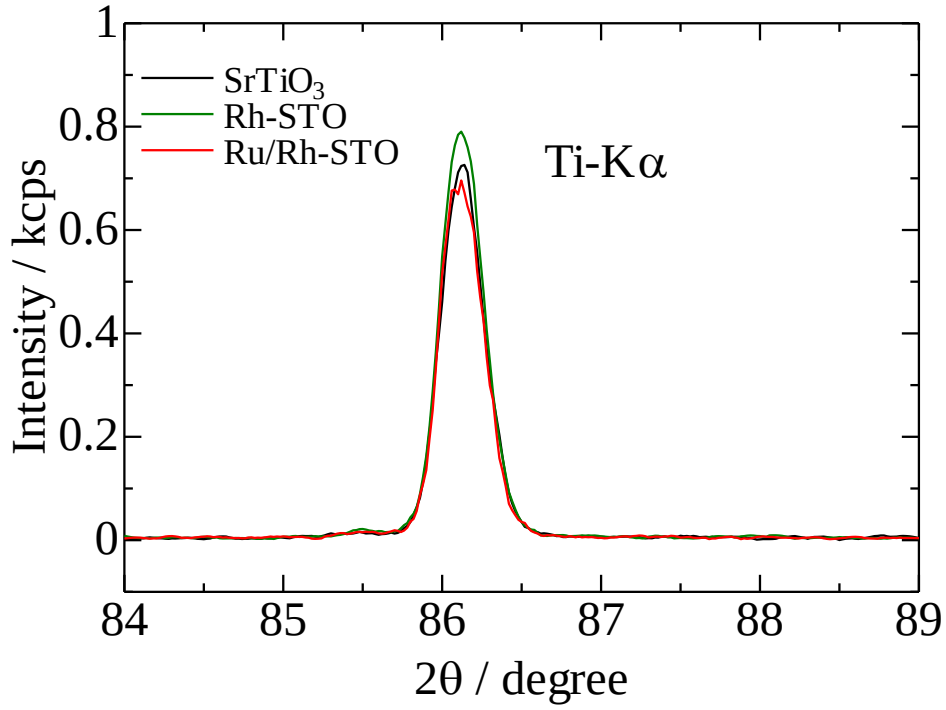

(f) Ti-Ka peaks of $SrTiO_3$ based samples

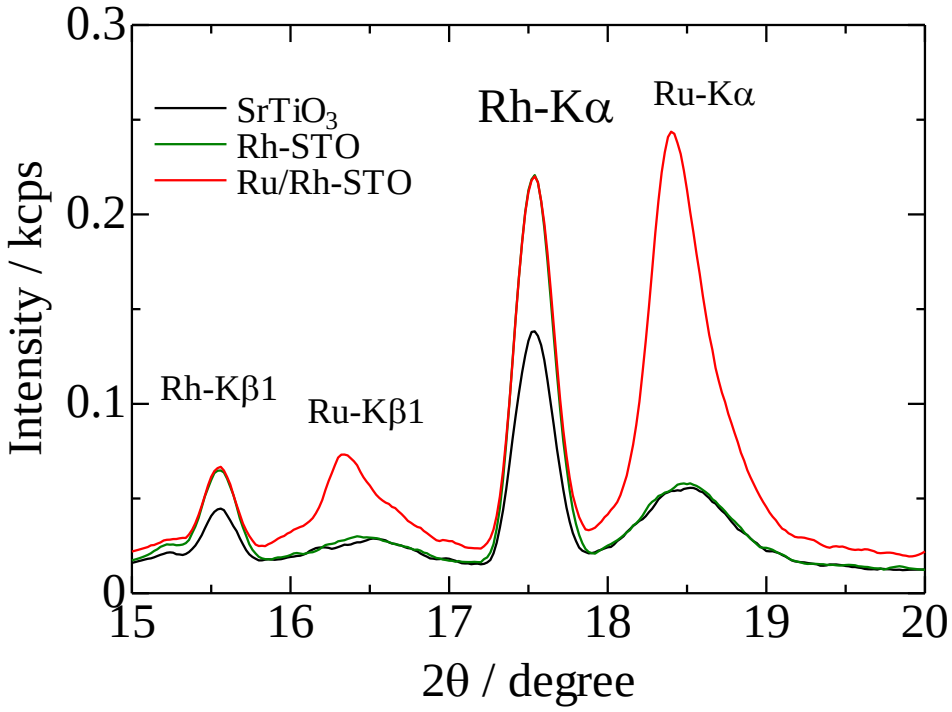

(g) Rh-Ka peaks of $SrTiO_3$ based samples

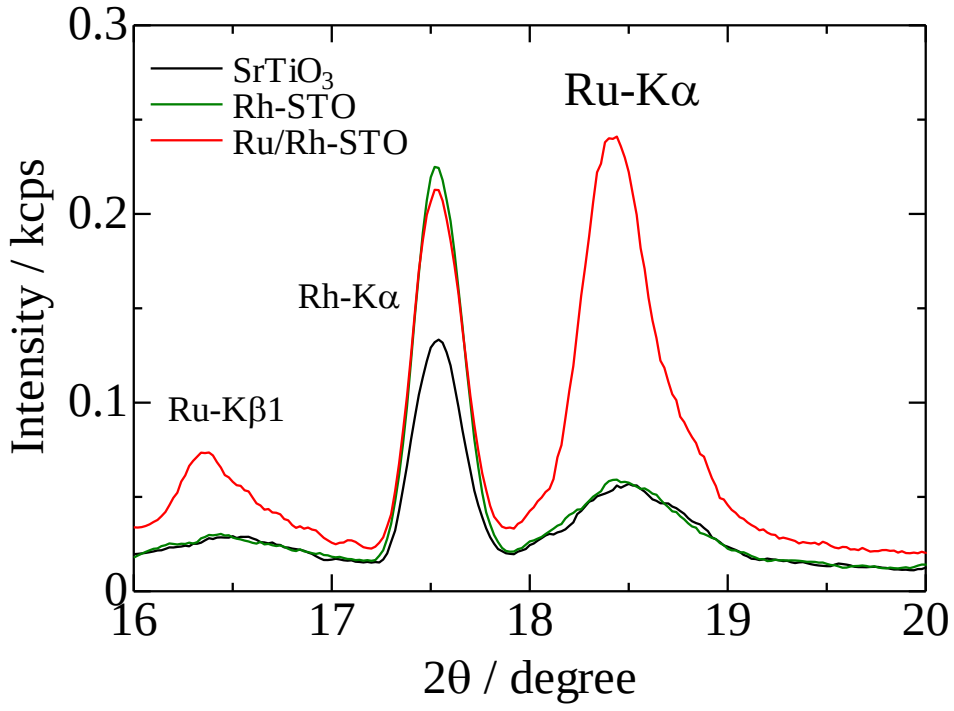

(h) Ru-Ka peaks of $SrTiO_3$ based samples

Fig.3.7 XRF peaks of (a)(b)(c)(d) Pt/Cr,Ta-TiO_2(R) and (e)(f)(g)(h) Ru/Rh-STO.

According to these XRF results, the molar ratios of Ti : Cr : Ta in Pt/Cr,Ta-TiO_2(R) was 0.9944 : 0.0016 : 0.0040. Notably, this molar ratio was not consistent with the starting ratios used in the preparation of the photocatalyst. This discrepancy could be explained by difference of the solubility of Ti, Cr and Ta in aqueous solution under hydrothermal conditions. The molar fraction of Pt relative to Cr,Ta-TiO_2 was also indicated 1×10^{-4}. In contrast, Tte molar ratios of Sr : Ti : Rh in Rh/Rh-STO was 0.4924 : 0.4933 : 0.0143 nearly equal to the starting fractions used in the preparation. The Ru amount relative to Rh-STO was observed to be 1×10^{-2}.

3.4.8 Half reactions

Hydrogen evolution reaction of Ru/Rh-STO using I^- as sacrificial agent and oxygen evolution reaction of Pt/Cr,Ta-TiO_2(R) using IO_3^- as sacrificial agent were measured under visible light irradiation. Here, sample amount of these reactions were 60 mg each, sacrificial solution: 10 mL each, irradiated light: LED420 nm.

The results shown in figure 3.8 indicate hydrogen and oxygen were generated linearly. Then Z-scheme system was constructed using these prepared samples.

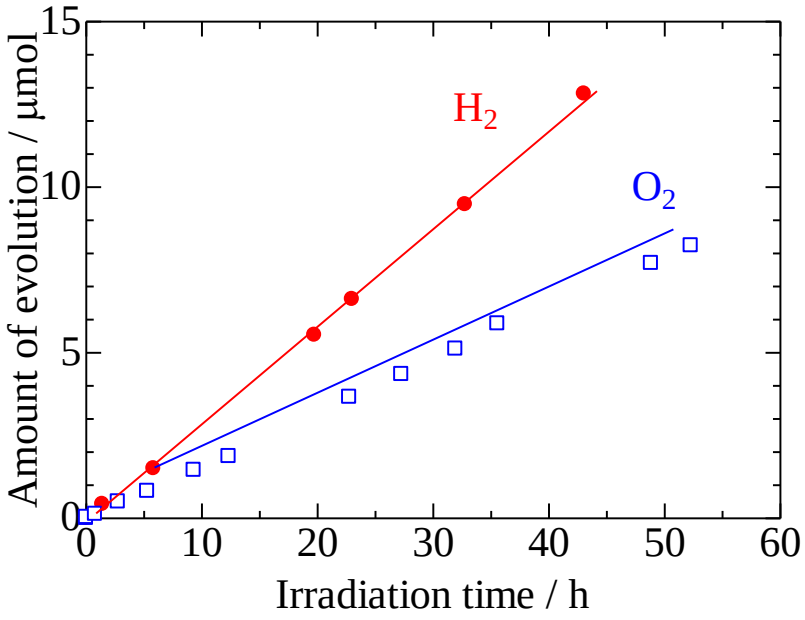

Fig.3.8 Half reactions of Pt/Cr,Ta-TiO_2(R) (O_2 evolution) and Ru/Rh-STO (H_2 evolution)

3.4.9 Water splitting reaction

The results of water splitting reaction of constructed Z-scheme system is shown in Figure 3.9. The experimental condition was shown in below. H_2-evolution sample was 10 mg, O_2-evolution sample was 50 mg, redox solution: I^-/IO_3^-, light source was LED420 nm

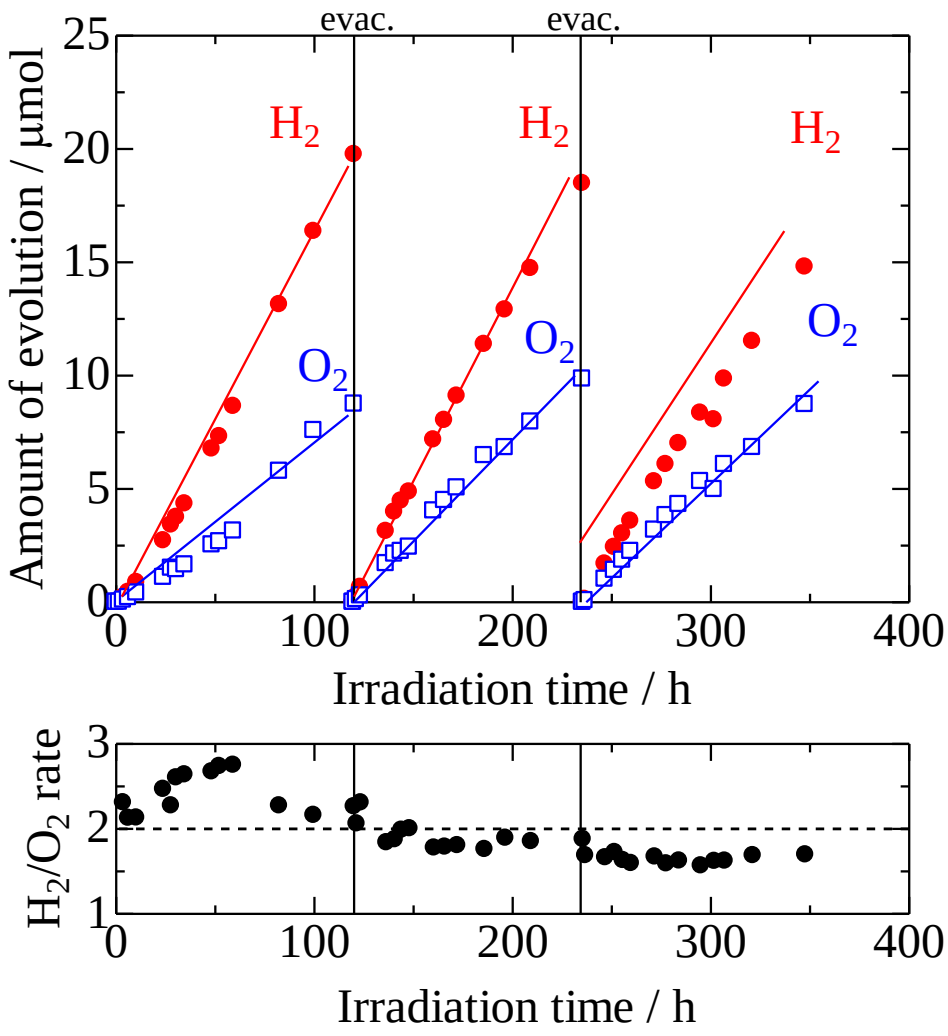

Fig.3.9 Water splitting reaction

From that figure, hydrogen and oxygen were generated simultaneously and stoichiometry. However, in 3rd cycle hydrogen evolution was slightly decreased

compared to 1st and 2nd cycle, the reason was estimated to the falling away of Ru co-catalyst.

According to our previous study, Ru on hydrogen evolution photocatalyst Rh-STO works as hydrogen evolution site. [2] Therefore, turn over number of this reaction was calculated in below equation. And the number was over 1, thus this reaction proceeded catalytically.

$$\mathrm{TON} = \frac{\text{product amount}}{\text{Reaction site}} = \frac{\text{hydrogen evolution amount}}{\text{Ruthenium amount}} \cong 100$$

Also turn over frequency (TOF) was calculated in below equation.

$$\mathrm{TOF\ (h)} = \frac{\text{Reaction site}}{\text{Reaction rate}} = \frac{\text{Ruthenium amount}}{\text{hydrogen evolution rate}} \cong 3.2$$

Apparent Quantum Efficiency (AQE) was calculated by following equation.

$$\mathrm{AQE\ of}\ H_2\ (\%) = \frac{2 \times \text{Hydrogen evolution rate}}{\text{incident photon rate}} \times 100$$

$$\cong 0.35\ (\%)$$

$$\mathrm{AQE\ of}\ O_2\ (\%) = \frac{4 \times \text{Oxygen evolution rate}}{\text{incident photon rate}} \times 100$$

$$\cong 0.38\ (\%)$$

3.5 short summary

Hydrogen and Oxygen were generated simultaneously and stoichiometry with good reproducibility. Therefore we also archived our objective to construct Z-scheme system using stable oxides. And water splitting activity of new constructed Z-scheme system was improved compared to my previous study which discussed chapter 2.

References

[1] R. Konta, T. Ishii, A. Kudo, *J. Phys. Chem. B*, **108**, 8992 (2004)

[2] S. Hara, M. Yoshimizu, S. Tanigawa, L. Ni, B. Ohtani, H. Irie, *J. Phys. Chem. C*, **116**, 17458 (2012)

[3] S. Tanigawa, H. Irie, *App. Catal. B*, **180**, 1 (2016)

[4] T. Umebayashi, T. Yamaki, H. Itoh, K. Asai, *J. Phys. Chem. Solids*, **63**, 1909 (2002)

[5] R.D. Shannon, C.T. Prewitt, *Acta Crystallogr. Sect. B*, **25**, 925 (1969)

[6] S.N.R Inturi, T. Boningari, M. Suidan, P.G. Smirniotis, *J. Phys. Chem. C*, **118**, 231 (2014)

[7] Y. Gönüllü, A.A. Haidry, B. Saruhan, *Sens. Actuators B*, **217**, 78 (2015)

[8] K. Obata, H. Irie, K. Hashimoto, *Chem. Phys.*, **339**, 124 (2007)

[9] D. Ehre, H, Cohen, V. Lyahovitskaya, I. Lubomirsky, *Phys. Rev. B*, **77**, 184106 (2008)

[10] J.F. Moulder, W.F. Stickle, P.E. Sobol, K.D. Bomben, L. Chastain, R.C. King Jr., Handbook of X-Ray Photoelectron Spectroscopy. Physical Electronics Inc., Chanhassen (1995)

4. Conclusion

4.1 Conclusion

Isolated mini-band was formed above valence band in Cr, Ta co-doped TiO_2(A), and below conduction band in Cr, Ta co-doped TiO_2(R). Cr, Ta co-doped TiO_2(A) and Cr, Ta co-doped TiO_2(R) served as hydrogen- and oxygen-evolution photocatalysts, respectively. Constructing Z-scheme system by these TiO_2 based hydrogen- and oxygen-evolution photocatalysts, stoichiometric amounts of hydrogen and oxygen were generated simultaneously under visible light irradiation. We confirmed the overall water-splitting reaction by using isotope labeled-water ($H_2{}^{18}O$). From the present system, isotopic oxygen was generated when the visible light was irradiated. Therefore, photocatalytic overall water splitting using only titanium dioxide based photocatalyts was achieved. However, in comparison with the activity of oxygen evolution over Cr, Ta co-doped TiO_2(R) and that of hydrogen evolution over Cr, Ta co-doped TiO_2(A), lower activity for hydrogen evolution was observed, which we considered the bottleneck of water splitting efficiency. Therefore, to improve water splitting activity, new hydrogen evolution stable oxide photocatalyst was investigated.

Kudo et al., reported Rh doped strontium titanate as a hydrogen evolution photocatalyst, and this oxide showed high hydrogen evolution activity in our previous study. [1-2] Then we constructed Z-scheme system using TiO_2 based photocatalyst and $SrTiO_3$ based photocatalyst to improve water splitting activity under visible light irradiation. From the Z-scheme system, hydrogen and oxygen was generated stoichiometry and repeatedly. Additionally, the water splitting activity of the new constructed Z-scheme system was improved about 100 times higher than that of previously constructed system composed of only titanium dioxide in chapter 2. [3]

In summary, hydrogen- and oxygen-evolution photocatalysts among stable oxides, titanium dioxide and strontium titanate, were prepared and overall water-splitting under visible light irradiation was accomplished.

4.2 Perspective

Both, Cr, Ta- co-doped TiO_2(R) and Rh-doped $SrTiO_3$ samples showed activity of half reaction of water up to around 520nm of visible light. Therefore overall water-splitting tests using longer wavelength needs to be performed. Furthermore, we have recently reported an all solid-state two-step overall water-splitting photocatalyst, in which the H_2- and O_2-evolution photocatalysts were connected via silver [5]. In that system, "pure" water could be split without a redox mediator. Therefore, silver inserted Cr,Ta-TiO_2(R) and Rh-STO Z-scheme system will be constructed for overall water splitting under visible light irradiation with pure water (Figure 4.1). This system may be advantageous for industrial and practical applications, as no chemicals are required as redox mediators. In addition, we are trying to improve oxygen evolution activity by depositing oxygen evolution co-catalyst, such as CoOx on oxygen-evolution photocatalyst.

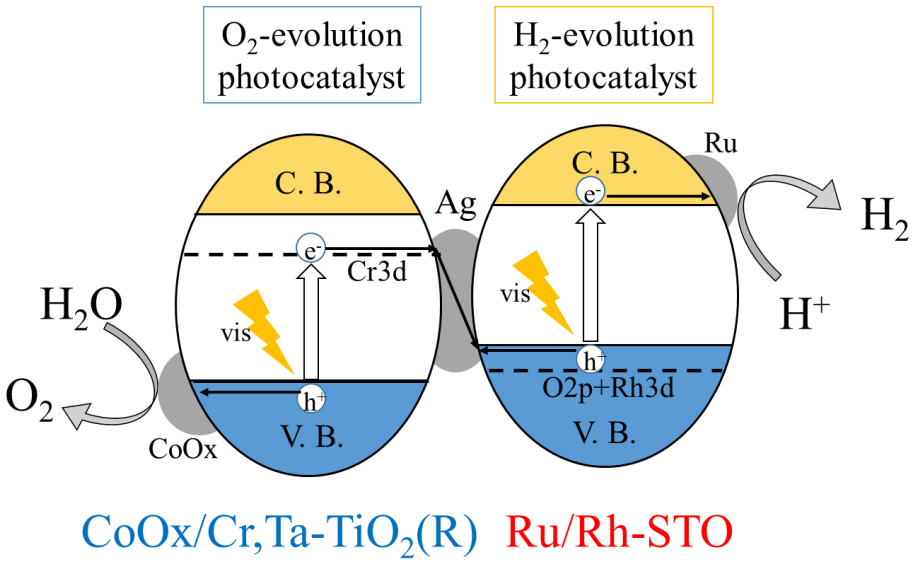

Fig.4.1 silver inserted Z-scheme system

References

[1] R. Konta, T. Ishii, A. Kudo, *J. Phys. Chem. B*, **108**, 8992 (2004)

[2] S. Hara, M. Yoshimizu, S. Tanigawa, L. Ni, B. Ohtani, H. Irie, *J. Phys. Chem. C*, **116**, 17458 (2012)

[3] S. Tanigawa, H. Irie, *App. Catal. B*, **180**, 1 (2016)

[4] S. Tanigawa, T. Takashima, H. Irie, *J. Mater. Sci. Chem. Eng*. **5**, 129 (2017)

[5] R. Kobayashi, S. Tanigawa, T. Takashima, B. Ohtani, H. Irie, *J. Phys. Chem. C*, 118, 22450(2014)

Acknowledgement

I would like to great thank to my supervisor Prof. Dr. Irie. I'm grateful to Prof. Dr. Komiyama for useful discussion, Prof. Dr. Bahneman and his laboratory members at university of hannover for helping laser flash photolysis measurement. I express grateful thank to the program for Leading Graduated Schools. I acknowledge the work of past and present members of our laboratory. At last, I would like to thank to my family.

List of publication

S. Hara, S. Tanigawa, H. Irie et al., “Hydrogen and Oxygen Evolution Photocatalysts Synthesized from Strontium Titanate by Controlled Doping and Their Performance in Two-Step Overall Water Splitting under Visible Light”, *J. Phys. Chem. C*, 116, 17485(2012)

R. Kobayashi, S. Tanigawa, H. Irie et al., “Silver-Inserted Heterojunction Photocatalysts for Z-Scheme Overall Pure-Water Splitting under Visible-Light Irradiation”, *J. Phys. Chem. C*, 118, 22450(2014)

S. Tanigawa, H. Irie, “Visible-light-sensitive two-step overall water-splitting based on bandstructure control of titanium dioxide”, *Appl. Catal. B*, 180, 1(2016)

S. Tanigawa, T. Takashima, H. Irie, “Enhanced Visible-Light-Sensitive Two-Step Overall Water-Splitting Based on Band Structure Controls of Titanium Dioxide and Strontium Titanate” *J. Mater. Sci. Chem. Eng*. accepted

Participated conference

S. Tanigawa, H. Irie, “Two-step excitation system for water-splitting using titanium oxide”, 19th International Conference on Conversion and Storage of Solar Energy, 2012/7/29 - 8/3, Pasadena, U.S.A. (Poster Presentation)

S. Tanigawa, H. Irie, 「酸化チタンを用いた２段階励起水分解システムの構築」第 2 回 JACI/GSC シンポジウム, 2013 年 6 月 6-7 日、大阪　（ポスター発表）

S. Tanigawa, H. Irie, “Two-step overall water-splitting system composed of only titanium dioxide”, International Workshop on Green Energy Conversion 2013, 2013/9/2 – 4, Nagano, Japan (Poster Presentation)

S. Tanigawa, H. Irie, “Two-step excitation Z-scheme system for overall water-splitting under visible light using titanium oxide”, The 6th Asia-Pacific Congress on Catalysis 2013/10/13 – 17, Taipei, Taiwan (Poster Presentation)

S. Tanigawa, H. Irie, 「酸化チタンを用いた可視光二段階励起完全水分解システムの構築」第 3 回 JACI/GSC シンポジウム, 2014 年 5 月 22-23 日、東京　（ポ

スター発表）

S. Tanigawa, H. Irie, “Two-Step Excitation System for Overall Water-Splitting under Visible Light Using Only Titanium Oxide”, 20th International Conference on Conversion and Storage of Solar Energy, 2014/7/27 - 8/1, Berlin, German (Poster Presentation)

S. Tanigawa, H. Irie, “Hydrogen and Oxygen Evolution Photocatalysts Synthesized from Titania by Controlled Doping and Their Performance in Two-Step Overall Water Splitting under Visible Light”, International Workshop on Green Energy Conversion 2014, 2014/8/25 – 27, Nagano, Japan (Oral Presentation)

S. Tanigawa, H. Irie, “Photocatalytic water-splitting activity of chromium and tantalum co-doped titanium dioxide”, The 20th China-Japan Bilateral Symposium on Intelligent Electrophotonic Materials and Molecular Electronics (SIEME’20) 2014, 2014/9/21 – 24, Chengdu, China (Poster Presentation)

S. Tanigawa, H. Irie, “Two step overall water-splitting system consisted of stable oxides”, 21th International Conference on Conversion and Storage of Solar Energy, 2016/7/25 - 7/29, St. Petersburg, Russia (Poster Presentation)

S. Tanigawa, H. Irie, “TWO-STEP OVERALL-WATER-SPLITTING SYSTEM CONSISTED OF TITANIUM DIOXIDE AND STRONTIUM TITATANE” International Workshop on Green Energy Conversion 2016, 2016/8/31 –9/2, Nagano, Japan (Poster Presentation)

S. Tanigawa, H. Irie, “Solar Hydrogen Production via Two-Step Overall Water-Splitting System Consisting of Stable Oxides” Honda Y-E-S forum 2016, 2016/11/19, Tokyo, Japan (Poster Presentation and short Oral Presentation)